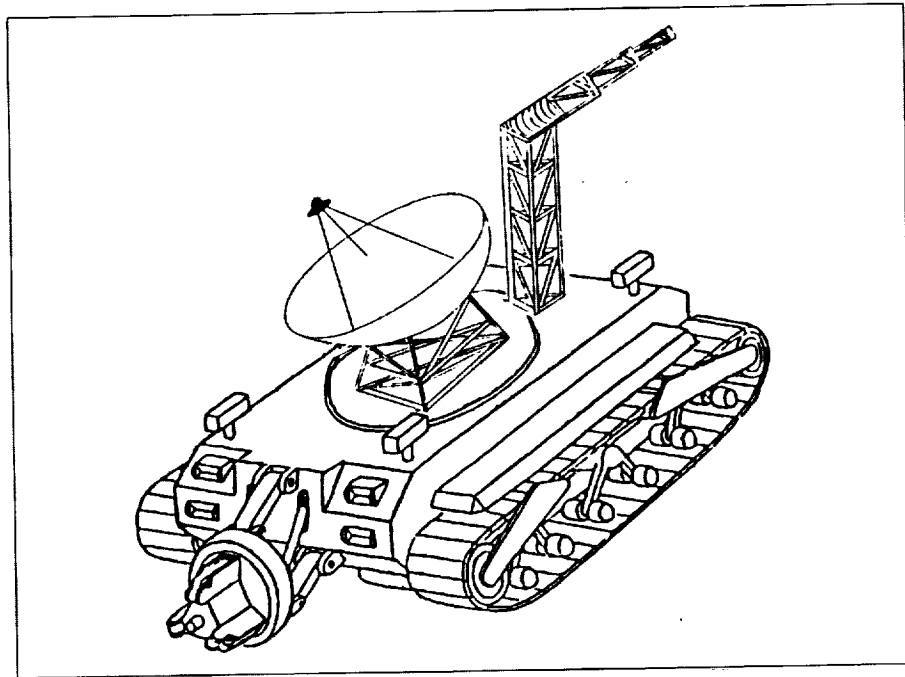


NASA/USRA
 ADVANCED DESIGN PROGRAM
 OLD DOMINION UNIVERSITY
 1989 - 1990



DESIGN OF AN AUTONOMOUS
 LUNAR CONSTRUCTION UTILITY VEHICLE

(NASA-CR-186832) DESIGN OF AN AUTONOMOUS
 LUNAR CONSTRUCTION UTILITY VEHICLE (Old
 Dominion Univ.) 168 p CSCL 13T

N90-26330

Unclas
 G3/37 0294999

ABSTRACT

In order to prepare a site for a manned lunar base, an autonomously operated construction vehicle is necessary. In this report, a Lunar Construction Utility Vehicle (LCUV), which utilizes interchangeable construction implements, has been designed conceptually. Some elements of the machine have been studied in greater detail and are the focus of this report.

Design of an elastic loop track system has advanced to the testing stage. A standard coupling device has been designed to insure a proper connection between the different construction tools and the LCUV. Autonomous control of the track drive motors has been simulated successfully through the use of a joystick and computer interface. A study of hydrogen-oxygen fuel cells has produced estimates of reactant and product size requirements and identified multi-layer insulation techniques. Research on a 100 kW heat rejection system has determined that it is necessary to house a radiator panel on a utility trailer. The impact of a 720 hr use cycle has produced a very large logistical support lien which requires further study.

ACKNOWLEDGEMENTS

The Lunar Construction Utility Vehicle is a project in which senior mechanical engineering students at Old Dominion University participated. Their accomplishments and the support of USRA should be noted.

Dr. Robert L. Ash Department chairman and USRA project advisor
Dr. Mason Chew Class instructor
Iain Dixon Teaching assistant and editor of this report

Autonomous Coupling Group

Dan Nelms
Robert Marshall
Ken Cowen
Anton Largiader
Chris Kannan
Murat Bengi

Heat Rejection Group

Rick Boothe
Tim Sivertson
Leal Boyd
Kevin Gentry
Tara Henderson
Dexter Tugbang
Patrick Vick

Track Testing Group

Brian Jones
Todd Lackey
Bill Groeninger

Control System Group

Thomas Young
Robert Arguelles
Leonard Heyman

Power Supply Group

Jim Henderson
Mehran Ghofrani
Steven Stapura
Robert Santa-Maria

The help of Tony Coulson, Rachelle Bentley, and Richard Faulkenberry should also be acknowledged.

TABLE OF CONTENTS

Table of Contents	iii
List of Figures	v
List of Tables	vii
Introduction	1
1.0 Autonomous Coupling Device	2
1.1 Assumptions	2
1.2 Coupler Design	3
1.2.1 Location of Coupler	3
1.2.2 Single Point Design	4
1.2.3 Three Point Design	5
1.3 Load Analysis	7
1.4 Materials	8
1.5 Tool Acquisition	10
1.6 Tool Types	15
1.7 Future Work	15
2.0 Track Construction and Testing	19
2.1 Loop Design	20
2.1.1 Track Material	20
2.1.2 Loop Bonding	23
2.1.3 Gear Belt Bonding	25
2.2 Telemetry Box	25
2.3 Pivot Plate	27
2.4 Chassis Connection	29
2.5 Testing Procedures	38
3.0 Control System	39
3.1 System Constraints	40
3.2 Control System Research	40
3.2.1 Feedback Device	40
3.2.2 Navigation Command Input Device	40
3.2.3 Motor Coordination System	40
3.3 Hardware Development	43
3.3.1 Motors/Tachometers	43
3.3.2 Lead - Lag Compensation	48
3.3.3 Joystick	48
3.3.4 D/A & A/D Converter	48
3.3.5 Programmable Amplifiers	48
3.4 Software Development	50
3.4.1 Joystick Program Code	50
3.4.2 Controller Programming	52
3.4.3 D/A & A/D Conversion Drivers	53
3.5 Design Problems and Solutions	54
3.5.1 Four Motor Design	54
3.5.2 Motor/Tachometer Characteristics	54
3.5.3 Assumptions about the LCUV	54

4.0	Power Supply	56
4.1	Fuel Cell Operation	57
4.1.1	Power Output	59
4.1.2	Mass Flowrate Determination	60
4.1.3	Heat Generation	61
4.2	Hydrogen, Oxygen, and Water Tanks	65
4.2.1	Multi-Layer Radiation Insulation	66
4.2.2	Tank Sizing	68
4.3	Heat Exchange System	71
4.3.1	Assumptions	72
4.3.2	Design Advantages	72
4.3.3	Heat Transfer Analysis	73
4.3.4	Materials	77
4.3.5	Problems and Solutions	77
4.4	Electrical and Control Systems	78
4.4.1	Temperature Control	78
4.4.2	Pressure Control	81
4.4.3	Current and Voltage Considerations	83
5.0	Heat Rejection System Carriage & Structure	85
5.1	Assumptions and Constraints	85
5.2	Carriage Configuration	85
5.3	Locomotion System	86
5.4	Telescoping Structure	90
5.4.1	Maximum Elongation and Loading	94
5.4.2	Structure	94
5.4.3	Materials	95
5.4.4	Sliding Mechanism	96
5.4.5	Thermal Problems	98
5.5	Fluid Lines	98
5.5.1	Design Concepts	99
5.5.2	Fluid Line Connections	106
5.6	Power Lines	106
6.0	Heat Rejection System Radiator	107
6.1	Assumptions	107
6.2	Radiator Sizing Program	107
6.3	Radiator Design	109
6.4	Radiator Orientation	115
6.5	Materials	115
6.6	Radiator Coating	117
6.7	Radiator Mounting	119
6.8	Radiator Shading	120
6.9	Radiator Cleaning	120
6.10	Refrigerants	124
6.11	Power Supply	126
6.12	Pump and Piping System Design	127
7.0	Conclusions	132
8.0	References	133
9.0	Appendicies	136

LIST OF FIGURES

Figure 1.1	Coupling Mounted to the LCUV	3
Figure 1.2	Single Point Coupling Design	4
Figure 1.3	Autonomous Coupling Design	6
Figure 1.4	Composite Properties	10
Figure 1.5	Fracture Toughness vs. Yield Strength for Various Composite Materials	11
Figure 1.6	Ultimate Tensile Strength Temperature Dependence for Composite Materials	11
Figure 1.7	Coupling Target Area	12
Figure 1.8	Separated Quick-Disconnect Coupling	14
Figure 1.9	Quick-Disconnect Coupling Engaged	14
Figure 1.10	LCUV Dozer Blade	16
Figure 1.11	LCUV Grader Implement	16
Figure 1.12	Backhoe	17
Figure 1.13	LCUV Hoist Mechanism	18
Figure 2.1	Elastic Loop Mobility System (ELMS)	19
Figure 2.2	Equation Parameters	21
Figure 2.3	Milled Connection	24
Figure 2.4	Assembly of Elastic Loop Track System	26
Figure 2.5	Telemetry Unit	27
Figure 2.6	Pivot Plate	28
Figure 2.7	Shaft Collar	29
Figure 2.8	Vertical Force Absorbing Connection System	30
Figure 2.9	Track Rotation Relative to Chassis	31
Figure 2.10	LCUV with Strut System	31
Figure 2.11	Detail of Strut	32
Figure 2.12	Suspension Incorporating a Torsion Spring	33
Figure 2.13	Frictional Damper	34
Figure 2.14	Manual Load Leveling Device	35
Figure 2.15	Autonomous Load Leveling System	37
Figure 3.1	NCS-LCS Interface Logic Scheme	39
Figure 3.2	Analog Control System	41
Figure 3.3	Motor Controller Diagram	42
Figure 3.4	Tachometer Voltage Signal Response	44
Figure 3.5	Manual Testing Diagram	45
Figure 3.6	System Gain and Phase Shift	46
Figure 3.7	System Gain (HP Dynamic Analyzer)	47
Figure 3.8	Root Locus of System Transfer Function	49
Figure 3.9	Joystick Command Mapping	50
Figure 3.10	Motor Response Characteristics	55
Figure 4.1	Fuel Cell Reaction Sequence	58
Figure 4.2	Schematic of Electro-Chemical Process	58
Figure 4.3	Schematic Showing Three Stacks of Eight Fuel Cells	59
Figure 4.4	Flowrate to Power Relationship	62
Figure 4.5	Control Volume of Fuel Cell	63
Figure 4.6	Power and Heat Output vs. Fuel Flowrate	64
Figure 4.7	Fluid Flow and Thermodynamic States	65

Figure 4.8	Multi-Layer Insulation	67
Figure 4.9	Hydrogen Boil-Off Rate	68
Figure 4.10	Oxygen Boil-Off Rate	70
Figure 4.11	Heat Exchanger	74
Figure 4.12	Oxygen Heat Transfer to Mass Flowrate Comparison ..	75
Figure 4.13	Hydrogen Heat Transfer to Mass Flowrate Comparison.	76
Figure 4.14	System Control Requirements	79
Figure 4.15	Fuel Cell Control	80
Figure 4.16	Reactant Tank Monitoring System	82
Figure 4.17	Power Transfer System Elements	84
Figure 5.1	Top Sectional View of the Heat Rejection System ...	87
Figure 5.2	Wheel Based Locomotion Systems	89
Figure 5.3	Deployable/Retractable Truss	91
Figure 5.4	Sleeved Beam Structure Design	93
Figure 5.5	Box Truss Bay of Ladder	95
Figure 5.6	Slide Pad Locations	97
Figure 5.7	Detail of Slide Pad	97
Figure 5.8	Flexible Fluid Lines Beneath Truss	100
Figure 5.9	Reeling System for Flexible Hose and Power Lines ..	101
Figure 5.10	Truss and Telescoping Tube Location	102
Figure 5.11	Telescoping Fluid Tube Housing	103
Figure 5.12	Truss and Swivel Joint Connections	104
Figure 6.0	External Loads on Radiator	108
Figure 6.1	Radiator Size vs. Fluid Return Temperature	110
Figure 6.2	Radiator Size vs. Fluid Return Temperature	110
Figure 6.3	Radiator Size vs. Angle of the Sun (Zinc Oxide Coating)	111
Figure 6.3	Radiator Size vs. Angle of the Sun (Silverized Teflon Coating)	111
Figure 6.6	Radiator Size vs. Angle of the Sun	112
Figure 6.7	Radiator Size vs. Angle of the Sun	112
Figure 6.8	Radiator Being Deployed	113
Figure 6.9	Basic Radiator Configuration	114
Figure 6.10	End View of Radiator	115
Figure 6.11	Radiator Positioning	116
Figure 6.12	Evaporation Rates	117
Figure 6.13	Silverized Teflon Absorptance	118
Figure 6.14	Conceptual Design of Ground Shading	121
Figure 6.15	Conceptual Design of Radiator Shading	122
Figure 6.16	Ground Shading System	125
Figure 6.17	Double Acting Piston Pump	127
Figure 6.18	In Line Axial Flow Centrifugal Pump	128
Figure 6.19	Conceptual Pump Design	129

LIST OF TABLES

Table 1.1	Properties of Metals	9
Table 1.2	Composite Matrix Properties	9
Table 5.1	Lunar Soil Data	88
Table 5.2	Properties of 6061 Aluminum	95
Table 5.3	Properties of 2014 Aluminum	96
Table 6.1	Surface Coating Properties	117
Table 6.2	Surface Coating Exposure Effects	119
Table 6.3	Lunar Temperature Variations	124
Table 6.4	Freezing and Boiling Points for Various Fluids	124

INTRODUCTION

President George Bush has made human missions to the moon and Mars national goals. He has directed the National Aeronautics and Space Administration to develop the necessary technologies and planning which will ultimately lead to permanent bases on the moon and Mars. A lunar base will likely evolve first because of its relative closeness to Earth. Regardless of the evolution, initial construction of these bases will rely on autonomous and tele-operated construction vehicles to reduce hazards to humans.

A rugged and reliable construction vehicle which is capable of a range of construction tasks is needed. Old Dominion University has investigated a Lunar Construction Utility Vehicle (LCUV) during the last two years as part of the USRA program. This vehicle is designed to perform several construction tasks by autonomously interchanging tools. The evolution of the LCUV has proceeded from a conceptual design of the overall system to a more detailed design of the coupling system for interchangeable construction implements, power generation trade off studies, heat rejection system design, control system strategies, and tracked locomotion design refinements. The report which follows is a current overview of the LCUV design.

1.0 AUTONOMOUS COUPLING DEVICE

One of the major purposes of the LCUV is to prepare a lunar base site for construction. To complete this task, several different operations need to be completed. However, it is advantageous to use one type of vehicle for many job descriptions so that the number of machines on the moon is minimized. It is therefore necessary to have a vehicle (the LCUV) which is able to interchange tools for specified functions. To do so, a standard coupling device is needed for proper connection between the tools and the LCUV.

Since the LCUV will be operated autonomously, in the early stages, a foolproof method of aligning the coupling to the tools is necessary. Also, the coupling must have the ability to provide electrical power and fluid coolant lines to the implements.

1.1 ASSUMPTIONS

In order to analyze the coupling, to select suitable materials, and to determine the factor of safety, the loads on the coupling had to be assumed. To determine these forces, certain key assumptions had to be made about the implements.

The maximum vertical upward force was assumed to be caused by the LCUV itself. The upward force, under extreme circumstances, may be equal to one half the weight of the LCUV. This would occur when the backhoe is pressed into the lunar soil to the point where the front of the LCUV raises up.

The maximum horizontal force exerted on the coupling was assumed to be caused by the operation of the backhoe also. It was assumed that the backhoe implement would have extendable legs to provide stability and help support the vertical component of the lift. However, a maximum horizontal tensile load of 40,500 N has been assumed.

The maximum forward and aft force was assumed to be caused by the pulling or pushing of a grader blade. Although 2 meters is typical for terrestrial grader blades, the 3 meter width of the LCUV necessitated a grader blade length of 3.2 meters. This would put the tip of the blade at the side of the LCUV when the blade is at a 20 degree angle.

The assumed maximum resulting forces were used in the Load Analysis section. Because the forces resulting from the grader blade operation are significantly higher than any other operation, only the grading operation is covered in the impact analysis, and the factor of safety is applied to the grading operation. The maximum force resulting from the grader blade was the determining factor in positioning the coupling points.

1.2 COUPLER DESIGN

1.2.1 Location of Coupler

The original design of the LCUV recommended using a robotic arm mounted on the top of the body to manipulate the tools (Reference 1). The design presented here anticipates mounting the coupling directly onto the body of the LCUV as shown in Figure 1.1. The main advantage of having the coupling mounted at the end of a robotic arm is because the arm would most likely have a finer degree of control than the vehicle itself. Coupling to the arm could simplify the mating of the LCUV with the implements significantly. However, the high arm strength required and the need to provide, fluid, electrical, and mechanical power connections to the coupled implements makes the coupling of tools directly to the LCUV more feasible. The mounting of the coupling to the body of the LCUV is a more failsafe design since failure of the robotic arm would render the LCUV useless.

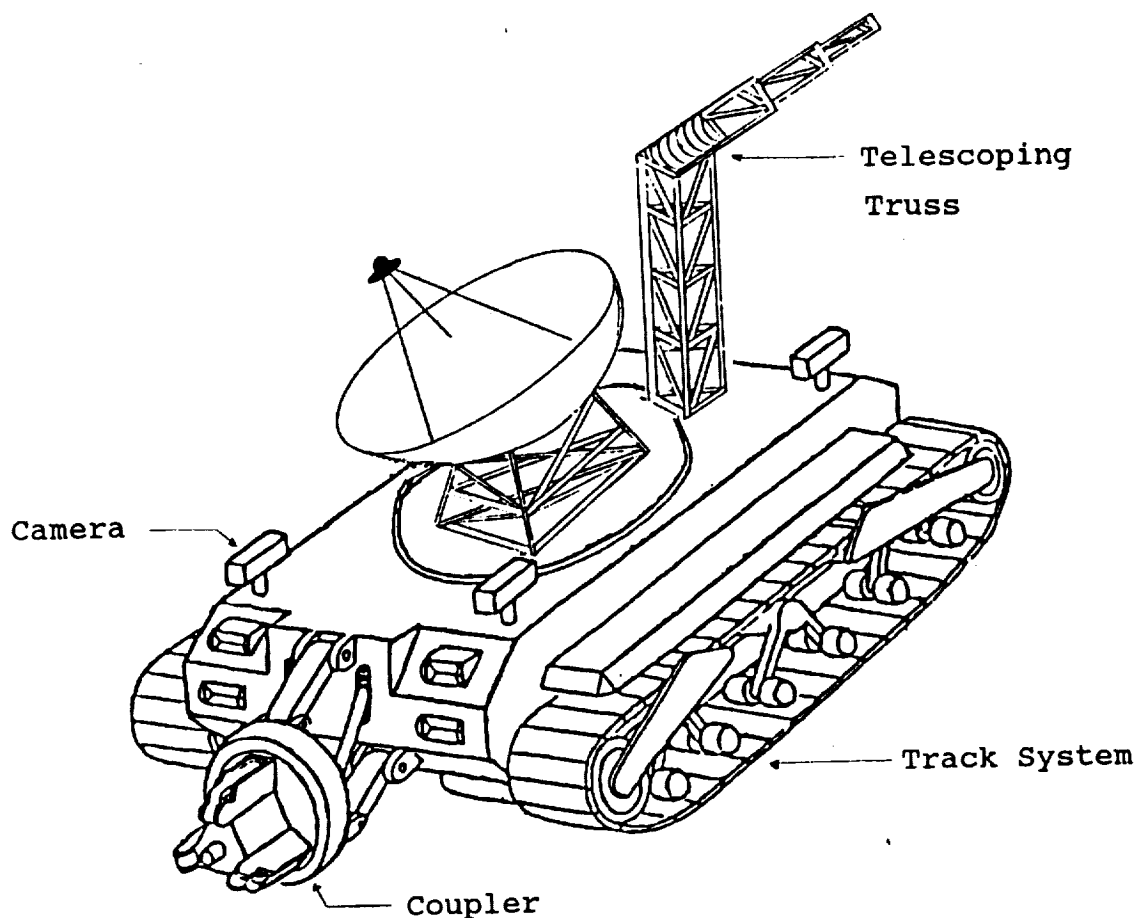


Figure 1.1 Coupling mounted to the LCUV

1.2.2 Single Point Design

Figure 1.2 shows the starting point for the coupling design. This one-point connection consisted of a tapered shaft which would be inserted into a socket and locked by pins which extended outward. This design was simple and readily lent itself to automatic engagement. In fact several methods of engagement were considered, including cams, springs, and power screws. After careful analysis it was determined that such a one point hitch had a fatal flaw. A single-point coupling would have a very low resistance to torque loading. Since any lifting operations at extended distances (such as lifting a habitation module) or grading operations generate high torque loads, this approach was abandoned.

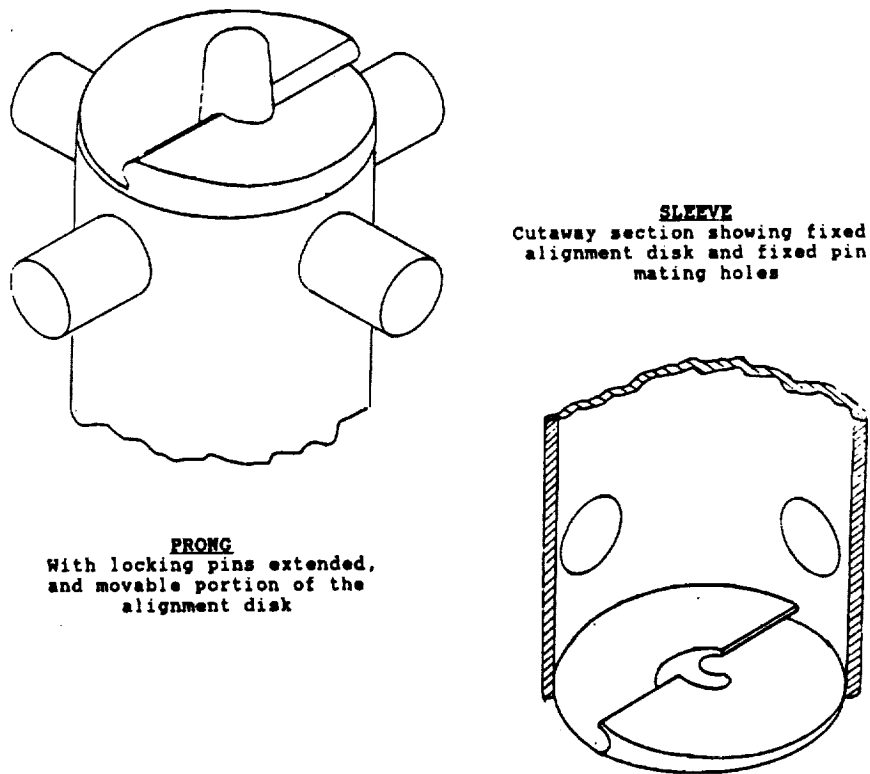


Figure 1.2 Single Point Coupling Design

The failure of the one point connection led to cylindrical and box shaped connections. The main disadvantages of these designs were not as obvious as the one point connection but each had problems that caused them to be discarded.

1.2.3 Three Point Design

The coupling device presented here is based upon the three-point hitch configuration which is used extensively in agricultural implements (see Figure 1.3). There exists a somewhat autonomous arrangement of the three-point hitch which is known as the quick-connect coupler. This coupler enables the use of a single attachment point for the expedient utilization of many different farm implements in an autonomous manner. However, this configuration does not lend itself to a fully automatic implementation scheme. Considerable manual assistance is needed to fully engage the tool implements. Thus the three-point configuration was modified to facilitate autonomous acquisition and retrieval of the tool implements.

It is important to note that most farm implements are pulled rather than pushed. Initially it was assumed the coupling would be mounted to the robotic mechanical arm. However, after consideration of the dynamic and static loadings which will occur, it was decided that resulting reaction forces and torques would be too great for similar robotic arms using present technology. Therefore, it is anticipated that the coupler is to be mounted on the front of the LCUV and pulling operations are accomplished by operating the LCUV in reverse.

The receiving end of the coupling is located on the tool implement itself. The receiving end consists basically of a shell-like triangular box. The face of the box is open to facilitate the insertion of the locking mechanism. This mechanism (which is located on the LCUV) looks similar to the three-point hitch configuration which was described earlier. At the end of each point are locking arms which, when in the receiving position, are inserted into the open end of the box. Each of the three arms will be driven by worm gears. Worm gears were chosen over linkages because of their ability to move the arms through greater angles. The ability to move the arms greater than 180 degrees is necessary to allow for greater tolerances. The coupling device will be adjusted vertically by three movable arms attached to the LCUV. Each arm will be connected directly to the case which houses the corresponding coupling arm. The coupling will be able to rotate about the fore-and-aft axis to facilitate coupling and tool movement. After the three locking levers are inserted into the box, they rotate outward and around the outside of the box, grasping pins at the outermost corners of the box on the implement. As they swing around, they pull the implement into position and then they are locked into position by a solenoid operated locking device. Provisions can be made for connecting cooling fluid, data and mechanical power lines to the implement via connections within the implement box. This method of transmission is explained later in this report. A picture of the coupling as it would look on the LCUV is shown in Figure 1.1.

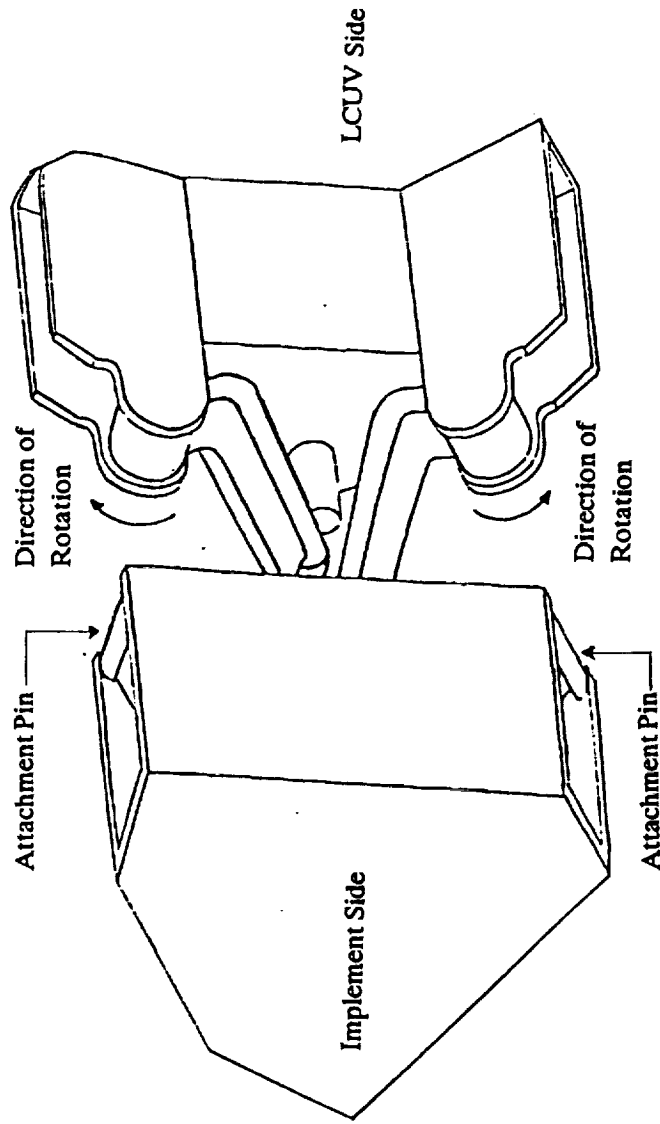


Figure 1.3 Autonomous Coupling Design

1.3 LOAD ANALYSIS

The important task of estimating the applied forces and determining what the stresses on the coupling components that will result from the forces is explained in this section. The following assumptions/decisions were made about the load situation:

1. Worst-case load scenario would come from either the hoist or grader blade configuration.
2. Theory suggests that failure is most likely to occur at interface of coupling halves (namely the pin-locking bar arrangement).
3. Of the above interfaces the pin was deemed to have the highest chance of failure.
4. The lifting hoist would be self-supported on three legs arranged in triangular fashion.
5. The worst-case load scenario for the hoist would be supporting the habitation module as a free weight.
6. The worst-case load scenario for the grader blade would be a sudden deceleration of the LCUV from its maximum speed of 0.2 meters/second to a complete stop due to an impact with an imbedded obstruction.
7. The pin load situation would be considered as one subjected to pure shear due to the area/length ratio of the pin.

Consider the situation of the hoist operation. It is commonly known that a crane with an extended load is in jeopardy of overturning, especially if other instability factors are present such as uneven terrain. Thus the configuration is prescribed with a tripod base connected to a centrally located machined hub. The machine hub is connected to the coupling device via the implement receiving box. The boom would be ten meters in length at a forty-five degree angle. It would have the ability to raise the six meter wide habitation module a distance of two meters above the lunar surface. The subsequent torque generated would be approximately 281 kN m. This moment is transferred to the coupling device via the one and one-half meter cantilever beam that is determined as the distance from the mid-point of the machine hub to the coupling interface. Due to the large bending moment that the couple would impart, it was decided that a reinforcing brace in the form of a third leg was required. It was determined that even if the coupling were built strong enough to withstand the load, the LCUV would tip over. This determination was based on a maximum LCUV mass of 15,000 kg (which could double in the final design), the habitation module mass of 19,490 kg and the LCUV dimensions of

3 m by 3 m (Reference 1). For this reason it was concluded that habitation module transport must be done by lifting the modules onto a dolly using a free standing hoist. This leg design would be part of the actual implement design which was not an objective of this project.

This led the investigation to the worst-case load scenario anticipated as part of the coupling design. The LCUV is specified as having a maximum straight-line velocity of 0.2 meters/sec due to the concern over the three-second communications delay (Reference 1). The anticipated loading would entail the grader blade being towed behind the LCUV in a manner similar to terrestrial agricultural applications. If the blade strikes an embedded impediment located near the lunar surface the dynamic inertial load, in addition to draw-bar pull capabilities, would create a critical load. That load is due to the magnitude of the force in conjunction with the impact force caused by the sudden deceleration of the LCUV.

For the purposes of calculating this maximum impact load it is assumed that the LCUV would go from its maximum speed of 0.2 m/s to a complete stop in 0.1 seconds. This would add an impact load of 37,400 N to the maximum draw-bar pull of 40,500 N.

The maximum stress was determined to be on the pins where the coupling is attached. Treating the stress on the pin as if it were double shear (Reference 2), the required pin diameter is:

$$d = 2 \left(\frac{F_n}{S_{ut}\pi} \right)^{1/2} \quad (1.1)$$

The required pin size was determined to be 37.2 mm under these conditions.

1.4 MATERIALS

Material selection for the coupling is very important. Due to the extreme environmental conditions encountered on the moon, materials considered appropriate on earth would prove to be unacceptable for similar lunar applications. The materials which have been considered are in two categories: metals and fibrous composites. The composites are divided further into metal-matrix and polymer matrix families (Reference 3).

According to Reference 3 the mechanical and thermophysical properties of the candidate aerospace-grade materials are well documented. In general, they exhibit moderate strength and stiffness and good radiation resistance. Table 1.1 is a summary of

the mechanical and physical properties for some metals. In the past, titanium has been a leading contender for high-tech applications (Reference 3). However, due to its brittleness at low temperatures and its susceptibility to radiation and sublimation, titanium is not considered ideal for this application (Reference 4).

Two distinguishing characteristics of the metals family are that they are homogeneous and isotropic; their properties are neither a function of position nor direction. Composites, on the other hand, have some directional properties which can be varied to suit the application. A list of typical composite matrix properties are shown in Table 1.2 (Reference 3).

Table 1.1 Properties of Metals

MATERIAL	E (Mpsi)	F _{ut} (kpsi)	DENSITY (lb/in ³)
Aluminum	10.5	70.0	0.100
Titanium	16.0	160.0	0.160
Steel	29.0	260.0	0.283
Invar	20.5	65.0	0.291
Beryllium	42.5	44.0	0.066

Table 1.2 Composite Matrix Properties

Material	Temperature Use From To	(°F)	Glass Transition Temp. (°F)	Space Radiation Resistance	Density (lb/in ³)
Thermosetting Epoxy	-250	300	350	Good	0.040
Thermoplastic Acrylic	-250	175	250	Questionable	0.043
Polysulfone	-250	275	370	Very Good	0.045
Cross linked	-250	300	370	Very Good	0.045
Polymide	-250	600	700	Excellent	0.054
Metallic Aluminum	-250	350	-	Excellent	0.10
Magnesium	-250	425	-	Excellent	0.06

Due to the excellent resistance to radiation and the appropriate working temperature range, metal matrix composites appeared most promising and were subject to further investigation. Because of its resistance to sublimation, aluminum was chosen as the matrix.

Properties to be taken into consideration when selecting an aluminum composite are stiffness, toughness, and tensile properties. Major improvements in strength and elevated temperature stability can be achieved by strengthening the material with incoherent dispersoids. Figure 1.4 shows the corresponding dependence of the composite's properties, and Figure 1.5 (Reference 5) shows the fracture toughness and yield strength. After considering the data shown, the best material was considered to be the 6061-T6 with silicon and carbon fibers. Figure 1.6 shows the temperature dependence of the ultimate tensile strength for many composites (Reference 5). From this figure, a value of 500 MPa for the ultimate tensile strength was chosen to be used in the stress analysis.

Further steps can be taken to reduce sublimation and radiation damage to the selected material. Polymeric coatings are being developed which provide short-term protection; although no long-term protective coating is currently available, research is continuing (Reference 4).

1.5 TOOL ACQUISITION

It was determined that a simple camera/rangefinder arrangement would adequately permit a remote operator from earth to visually acquire a tool and then position the LCUV to engage the desired tool. The simplicity of the coupling design permits this targeting scheme to be sufficient for obtaining tools. Originally there was concern that the three-second communication delay between the earth and the lunar surface would demand a complicated system which would be capable of minute changes in position in order to perform tool implement acquisition. This coupling design incorporates large tolerances between the mating sections, which are reduced when the grasping arms close.

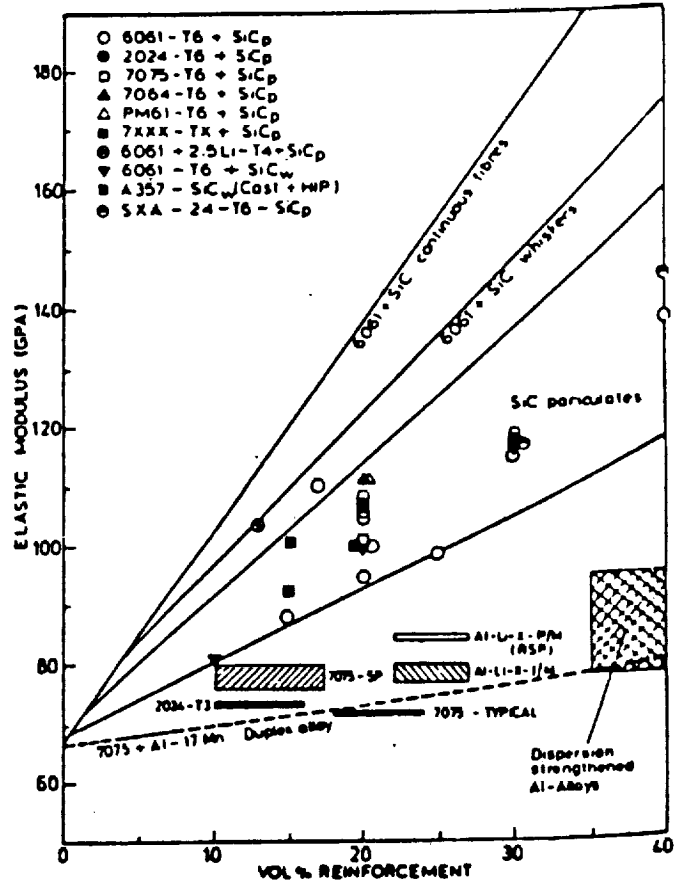


Figure 1.4 Composite Properties

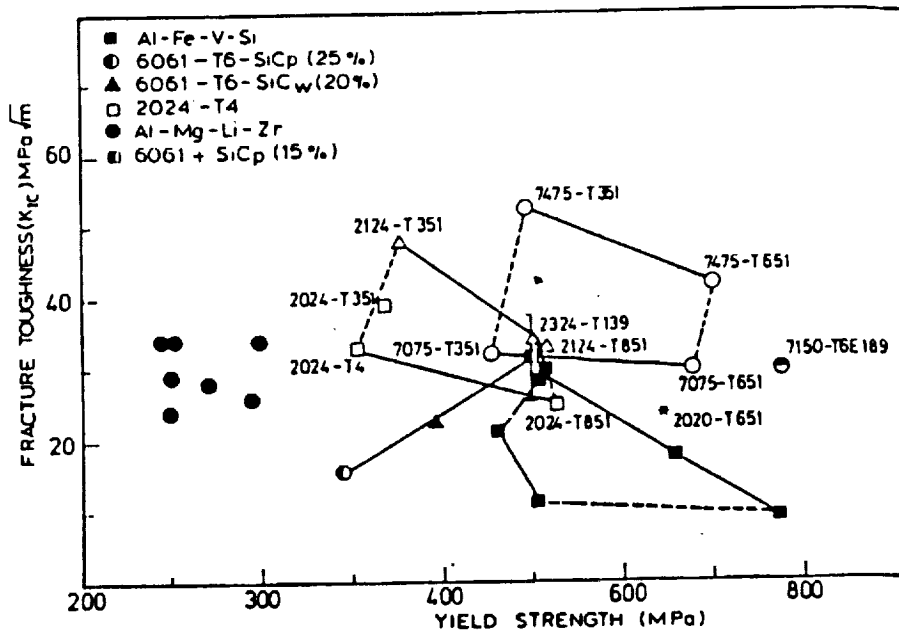


Figure 1.5 Fracture Toughness vs. Yield Strength for various Composite Materials

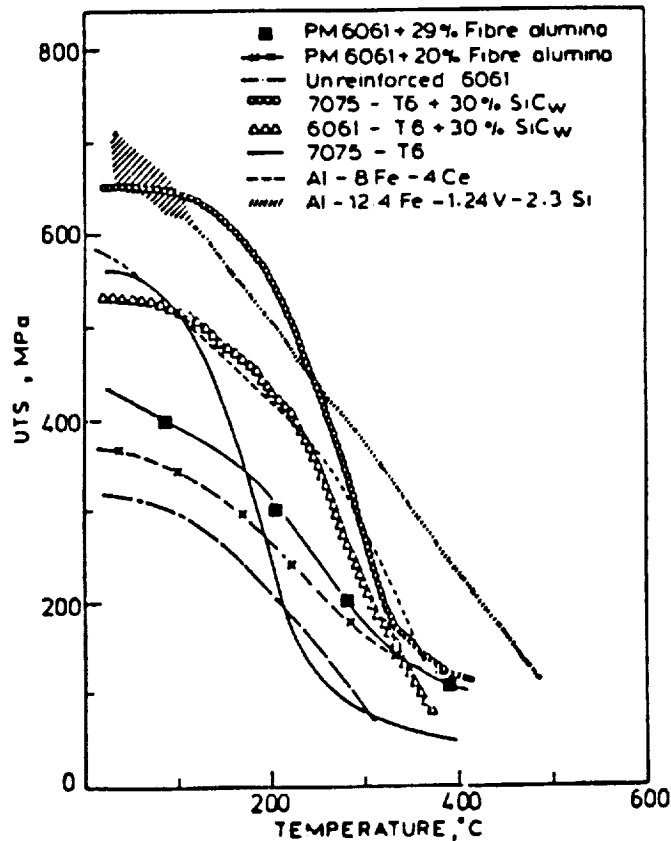


Figure 1.6 Ultimate Tensile Strength Temperature Dependence for Composite Materials

The camera/rangefinder arrangement would incorporate a specialized camera configuration coupled with a laser rangefinder. The requirements for the camera as defined in Reference 1 are:

- Automatic focus
- Two degrees of freedom
- Wide angle
- Continuous, simultaneous and individual camera operation
- Automatic aperture adjustment

This is considered to be the optimum camera configuration for the required LCUV operation in close proximity to the coupling. Although, the harsh lunar environment will certainly require significant material and durability modifications, most of the required technology is available presently. The rangefinder configuration was deemed to be one which utilizes a laser beam to determine the relative position of the LCUV. The laser rangefinder is extremely accurate. The laser rangefinder transmits a beam of light at its intended point of reference and then measures the time which elapsed until the light wave returns. This information coupled with knowledge of the wave speed is used to determine the distance from the LCUV to a specified tool. The reason the laser is able to achieve accurate measurement is because the laser light beam is concentrated and does not diffract (Reference 1).

The anticipated alignment tolerance for successful coupling is going to be a function of the coupling dimensions and the power that can be delivered to the arms of the coupling. Using a one meter per side equilateral triangle, the target area for successful coupling is estimated to be the circled area as shown in Figure 1.7.

This 57 cm diameter circle in the center of the coupling should be adequate for coupling. To control the LCUV with the three second time delay the LCUV speed should be no more than 0.12 m/s. Although this is a relatively slow rate of speed, it is 60% of LCUV's top rated

0.2 m/s. A possible method for minimizing the arm torque required to couple with an implement, would be to use an internal grid of sensors within each of the locking bars. This network will be connected to the LCUV's central processing unit. The feedback

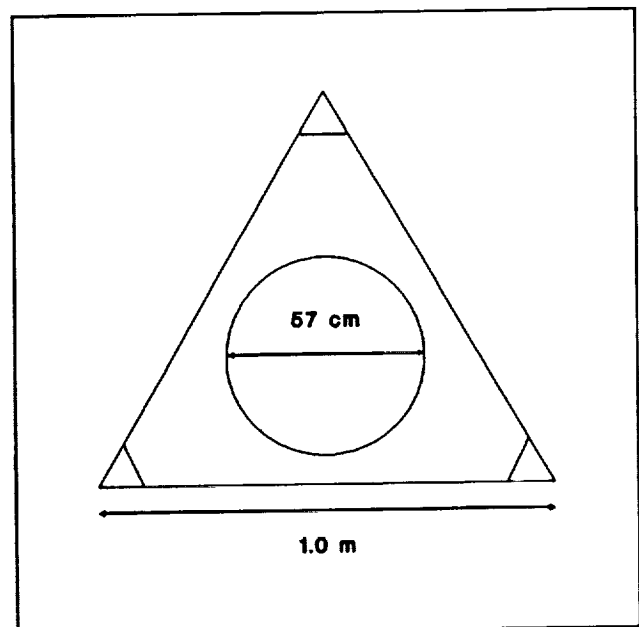


Figure 1.7 Coupling Target Area

received could be interpreted in the form of corrective commands that would be transmitted to the mechanisms.

The coupling will be outfitted with mechanical aids to assist in correcting misalignments. A "bull" gear arrangement will be used to correct angular misalignments. Bars attached to the coupling at the hitch points and parallel to both the centerline and baseline of the LCUV will be employed to raise the coupling vertically, via a power screw, to allow for discrepancies in height (y-direction). With such devices, the coupling will have the ability to allow (approximately) a vertical misalignment of 18 centimeters and maximum angular displacement of 58 degrees.

Another original design consideration pertaining to tool acquisition was the need for a tool bin which could be used to store the tool implements while they were not being used. Incorporated in this tool bin would be an indexing scheme that would permit easy access to the tools.

One avenue that was considered, was to use an arrangement similar to that of a pen plotter or numerically-controlled milling machine or drill press. The LCUV would be positioned at the same location each time it needed to acquire a tool implement. Some means of communication between the LCUV and the tool bin would be necessary so that rotation of the tool bin could position the desired tool implement directly in front of the LCUV. These different schemes were pursued at length until it became evident that the required size and configuration of implements implied that these schemes were inappropriate. The problem of what type of structure would support the tool implements could be solved by introducing the idea of free standing implements. The only structure anticipated to be needed is one to protect the tool implements from the effects of solar radiation.

The tool implements can be designed to be free standing entities without the requirement of external support during coupling/decoupling operations and periods of storage. Some of these implements have additional motors and controllers so that extra degrees of freedom are available. Thus power, data, and coolant must be supplied to the implements from the LCUV. Since the tools are interchangeable, then the power, data, and coolant lines must be able to be disconnected. Therefore, an interface is conceptualized which resembles a Quick-Disconnect coupler. It is to be located centrally on the coupling device and it will mate with a female socket on the implement receiving box. NASA has commissioned and received such an interface that can be modified which may be suitable for this purpose. The figures below show United States Patent number 3,656,781 which was invented by Thomas O. Paine, Allan R. McDougal, and Douglas P. Davis (Reference 6). Figure 1.8 shows the Quick-Disconnect coupling separated into its male and female components. Figure 1.9 shows the Quick Disconnect coupling in its fully engaged position. This coupling was designed

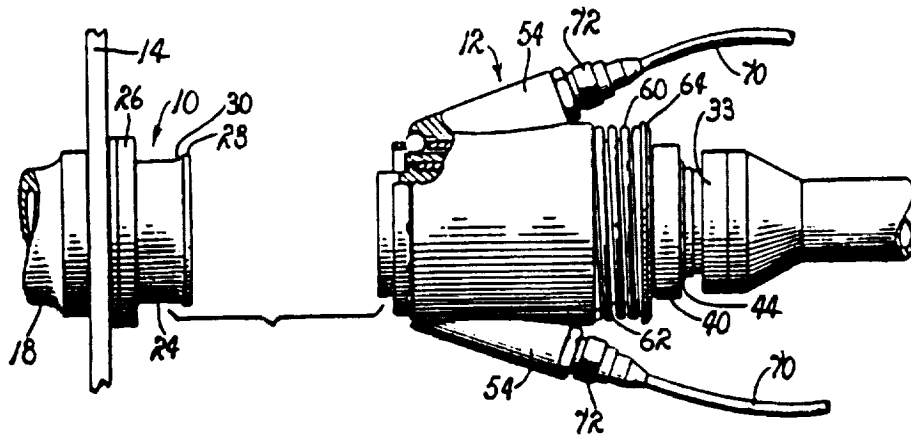


Figure 1.8 Separated Quick-Disconnect Coupling

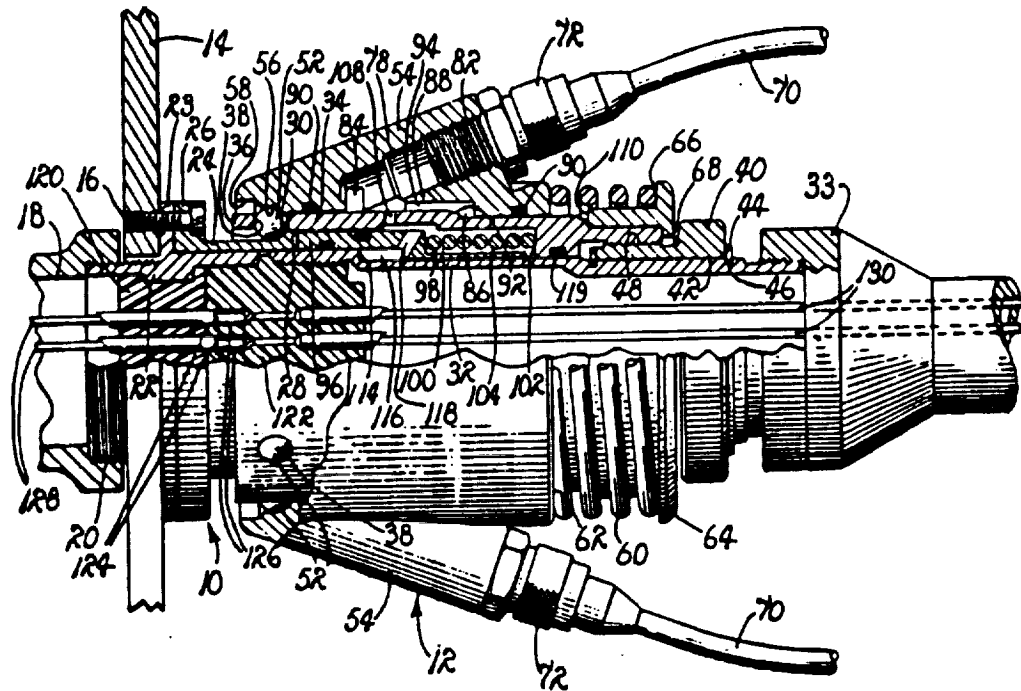


Figure 1.9 Quick-Disconnect Coupling Engaged

as a solution to solve technological problems incurred in umbilical-type connections. With further investigation, this design may be the start of an appropriate power connection lead.

1.6 TOOL TYPES

To complete the job tasks outlined in the operation requirements of the LCUV, multiple types of tools are needed. The LCUV will use four types of implements. The types of tools are a dozer blade, grader, backhoe, and hoist.

The dozer is a blade mounted on the front of the LCUV which will be used for excavating and pushing regolith over short distances. This will allow the LCUV to scrape long sections of lunar top soil off of the surface (Reference 7). The grader is used to make relatively precise leveling of top soil. The backhoe is particularly suited to tasks such as trenching and excavating. The hoist will be used primarily for loading and unloading the habitation module (Reference 8). These tools can be seen in Figures 1.10 through 1.13.

1.7 FUTURE WORK

Although a viable coupling design has been proposed there is still much work to be done. The future work falls into two broad categories.

First, the conceptual work still remains to be completed. This includes such subjects as the actual implement design, the design of the tool bin, the selection of suitable fluid, electrical and power transmission, protective boots to prevent dust contamination, and the finalization of the navigation/rangefinding system. Also, data on the effects of extreme temperature cycling on materials (for prevention of sublimation) is not fully understood.

Second, the iterative nature of the design process necessitates a continuous review of the present design. As discussed in the **Assumptions** section of this report, all forces used in the analysis are still tentative. These forces were based on the preliminary LCUV traction, weight, speed, and the assumed tool functions and dimensions. As noted in the **Load Analysis** section, dimensioning and orienting the coupling is a subject that is well suited for an optimization study.

Also much of the conceptual plan for accomplishing certain tasks is based on the anticipated LCUV configuration. Specifically, the radiator system and tethering system for transfer of cooling fluid. These ongoing design challenges could easily demand significant modifications to the present coupling design. As the plans for these areas of the LCUV operating environment become more definite the coupling design will become more stable.

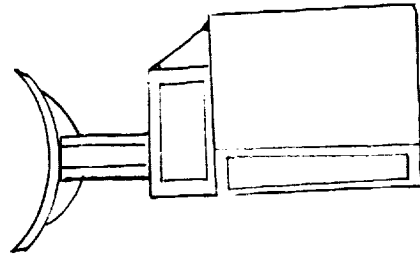


Figure 1.10 LCUV Dozer Blade

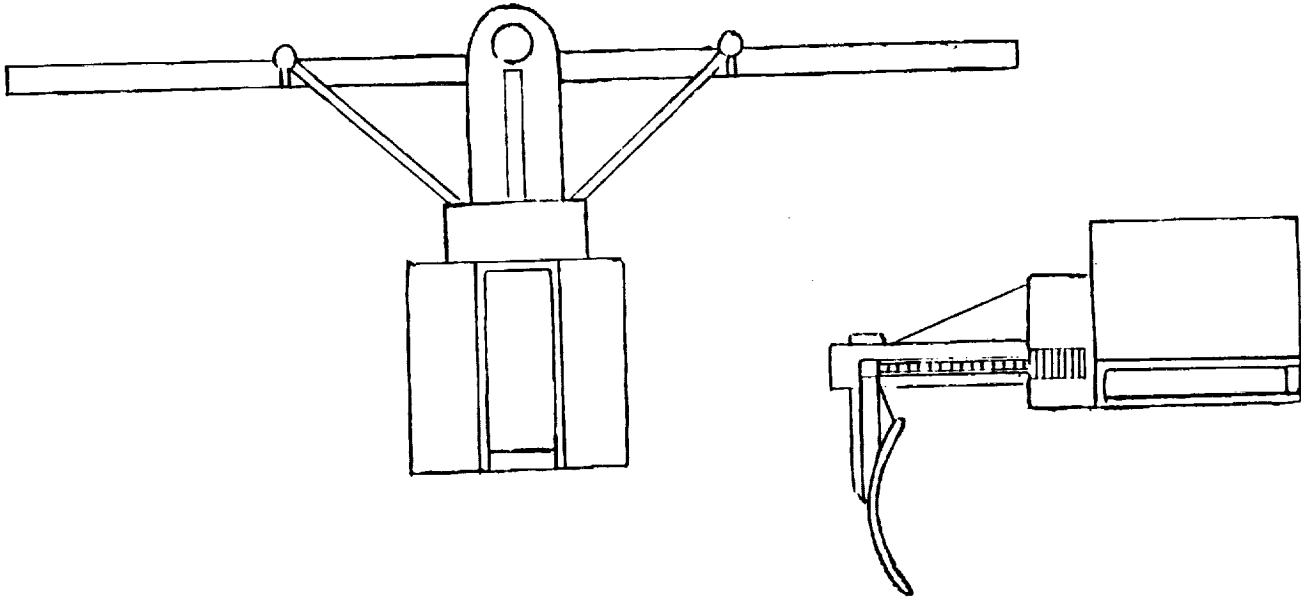


Figure 1.11 LCUV Grader Implement

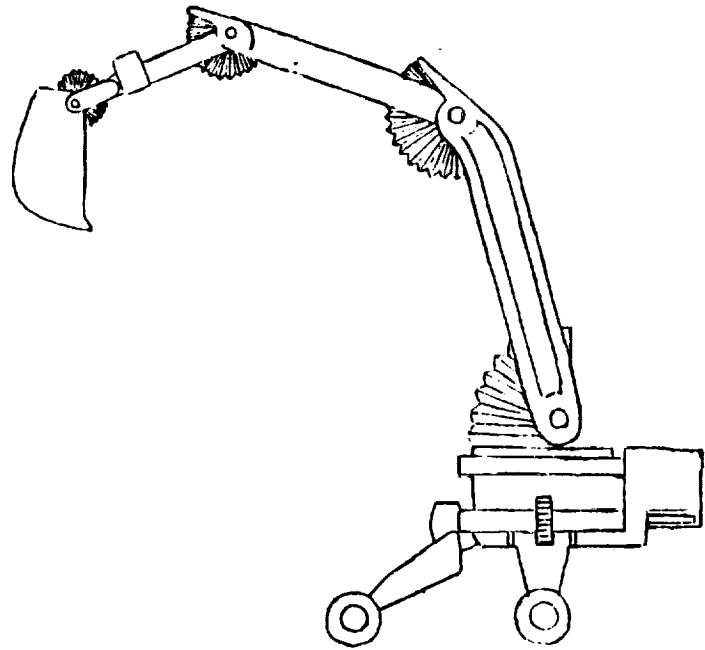
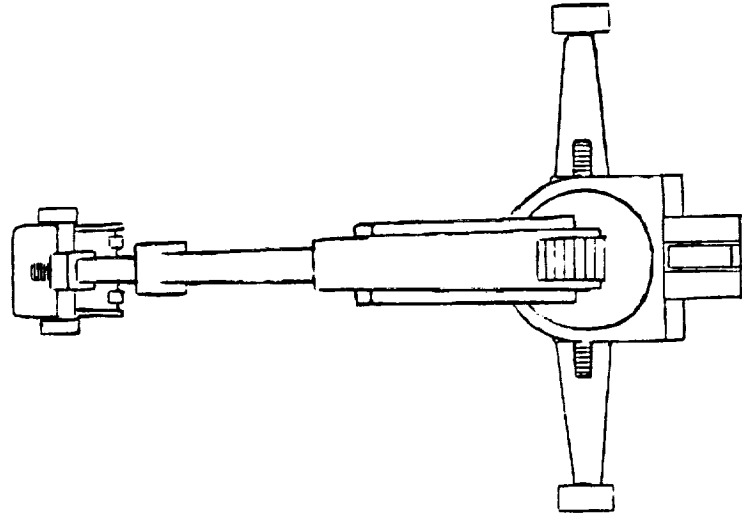


Figure 1.12 Backhoe (Top and Side Views)

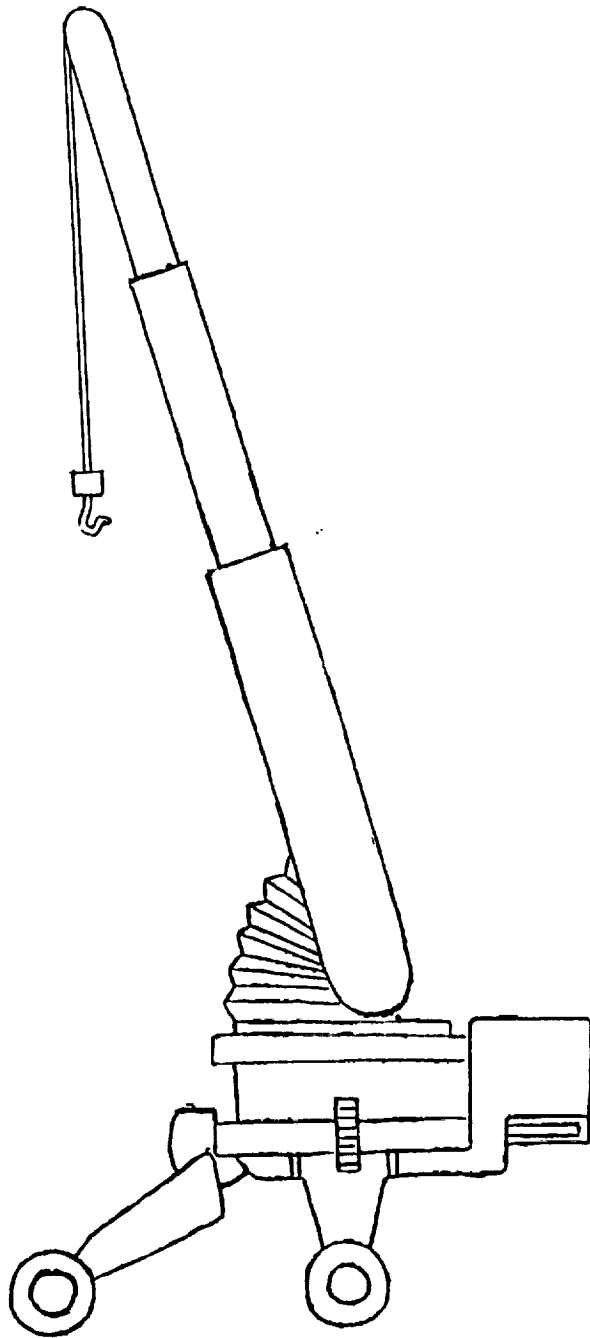


Figure 1.13 LCUV Hoist Mechanism

2.0 TRACK CONSTRUCTION AND TESTING

The Elastic Loop Mobility System (ELMS) was designed originally by Lockheed Missiles and Space Company (Reference 9) in the early seventies for use on a Mars Explorer (see Figure 2.1). The elastic loop system utilizes a continuous track that is designed to deflect when loaded. The advantages of the elastic loop system arise from this ability to deflect and by its simple design. As the load on the track is increased, the deflection of the track will result in a greater contact area with the ground thus increasing the traction of the LCUV. Probably the most important advantage of the ELMS is the built-in shock absorption provided by the track deflection. The track acts like a spring when it deflects, eliminating the need for a complicated suspension system. The simple track design uses few moving parts, a prime objective for a unmanned vehicle in the harsh lunar environment. The conceptual design for the LCUV elastic loop system was completed during the Fall 1989 by T. Coulson and P. Stiles (see reference 10 for details). However, a large amount of mechanical design remained before any construction or testing could begin. Some design areas that needed to be addressed were:

- Loop Design
- Telemetry Box Design
- Pivot Plate Construction
- Chassis Connection
- Testing Procedures

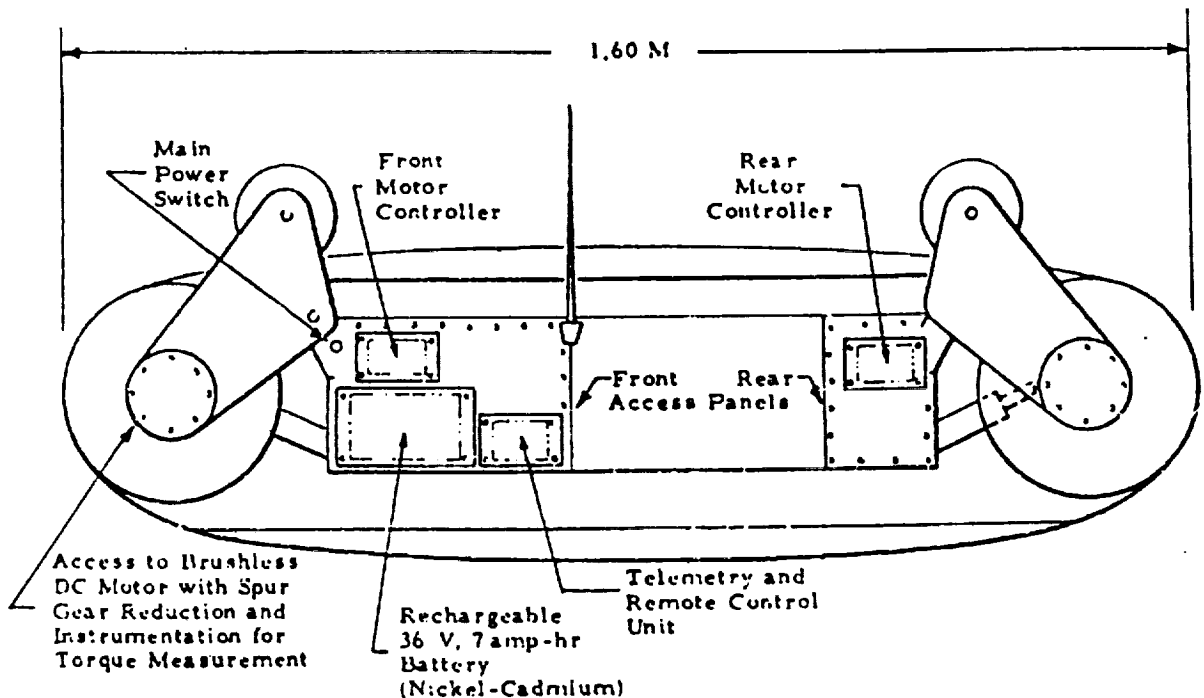


Figure 2.1 Elastic Loop Mobility System, ELMS (Lockheed)

The construction of one loop, so that the mechanism of the ELMS can be tested, has been completed. Evaluation of this first loop revealed some problems that were not addressed in the initial stages of construction. Once the first loop has been debugged, a second loop can be constructed to take advantage of the modified plans. A preliminary conceptual design for the chassis connection has also been completed but work has not begun in the construction of this connection. Once construction of the connection system is completed the tracks can be attached to the LCUV chassis and testing can begin.

2.1 LOOP DESIGN

The most important element of the ELMS is the track loop. The loop is the determining factor of whether or not the track will roll. The design areas addressed were: determination of the material type for the loop; determination of the method of bonding the material into a loop; and determination of a way to bond a gear belt on the inside of the loop.

2.1.1 Track Material

The first major design problem faced by the traction testing and evaluation group was to find a material that could be used as a temporary loop that would enable the group to evaluate and test a prototype. The material must be rigid enough to support the LCUV prototype as well as provide suspension. This proved to be more difficult than was assumed initially.

The rigidity of the loop is an essential part of the design of the tracks. The rigidness of the track determines how much the track will deflect under a given load, and using this value the proper material and material thickness can be determined. Rigidity is defined as the modulus of elasticity, E , times the area moment of inertia of the cross section ($I=wt^3/12$) of the loop (Reference 9). However, in the calculations to follow, the thickness t will be determined by varying the value of Et^3 .

Another area that must be examined is the failure of the loop at its maximum bending stress. At this point the stress due to the bending of the material exceeds the material's yield strength and causes it to deform permanently. This would move the loop out of the elastic region and defeat the purpose of using the loop as a suspension device.

To calculate the required value of rigidity, equations derived in the July 1972 Lockheed Technical Report (Reference 9) were used. That study related the bending rigidity B to the loading and to a number of geometric parameters.

$$B = \frac{F}{\pi b (K_b)^2} \left[1 - \frac{K_q + \nu (K_b - K_q)}{K_b} \right]^{-1} \quad (2.1)$$

where:

$F = 50$ lb	Max. Load
$b = 8$ in	Width
$K_q = .075$ radian/in	Unloaded Curvature
$K_b = .180$ radian/in	Loaded Curvature
$\nu = .3$	Poisson's Ratio (steel)

A schematic representation is shown in Figure 2.2.

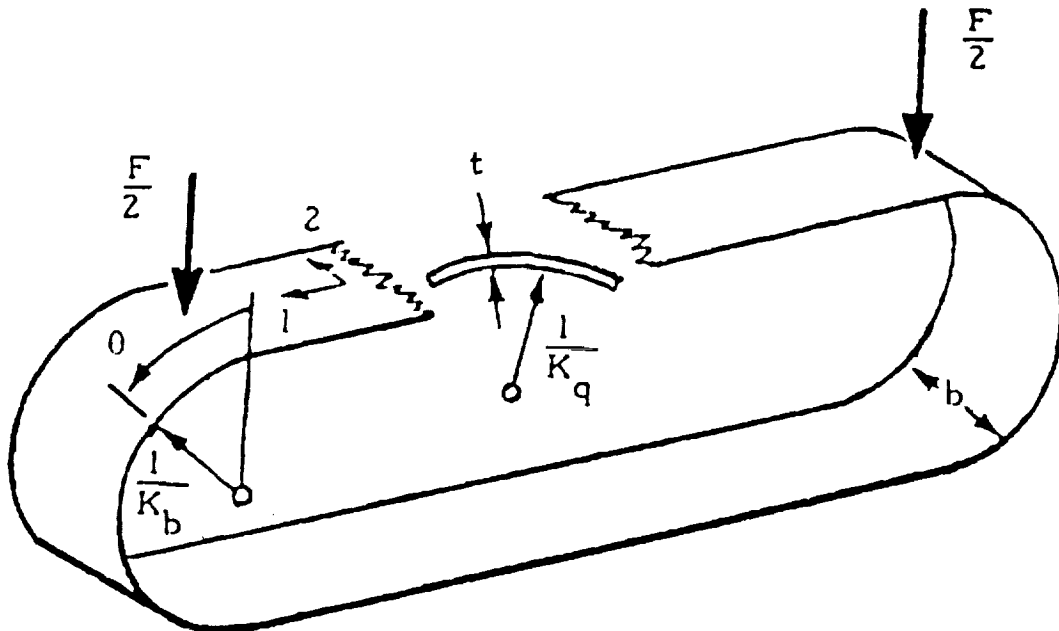


Figure 2.2 Equation Parameters

This equation used the loaded and unloaded curvatures along with the moment of inertia, modulus of elasticity and Poisson's ratio to determine the force that must be applied to create the loaded shape. The unloaded curvature, K_q , was calculated assuming the loop was made perfectly circular, and the loaded curvature, K_b , was determined from the fact that at maximum load the loop would be bent at least one quarter of the way around the drive drum. This leads to $K_b = 1/r$ where r is the radius of the drum. From here, the modulus of the loop material can be determined as a function of the thickness t .

$$Et^3 - 12B(1 - \nu^2) \quad (2.2)$$

which yields:

$$Et^3-1149 \quad (2.3)$$

This relation can be used to determine the required thickness of a specific material with modulus E.

The Lockheed report (Reference 9) also developed estimates of the bending moment and stress that would occur due to the load as:

$$M_{ij} = B[(1-\nu)K_b + \nu\delta_{ij}K_b] \quad (2.4)$$

and

$$\sigma_{ij} = \frac{6}{t^2 M_{ij}} \quad (2.5)$$

This yields a maximum value of:

$$\sigma = \frac{152}{t^2} \quad (2.6)$$

Using Equations 2.3 and 2.6, a variety of materials were investigated to determine if they could be used. First the modulus of elasticity was used to find the required thickness, and then the maximum stress was found and compared to the material's yield strength.

Many different types of metals and metal alloys have been tested using this procedure and a list of qualifying metals was produced. Most of the metals that qualified were high strength steels with yield strengths above 200 kpsi. However, steel at that strength is scarce and rarely, if ever, comes in 20 gauge sheets as required by Equation 2.3.

The next step was to try plastics. Many plastics have much lower moduli compared to steels, and this allows for a greater thickness which leads to a lower maximum bending stress occurring in the material; which makes them well suited for this purpose. Some technical literature that was obtained from D. Thornes at Read/Cadillac Plastics and B. Inman at AIN Plastics, in Norfolk Virginia, became very helpful in the selection of a plastic sheet that could be used to make the loop.

To find an appropriate material, the plastics discussed in the literature were evaluated using the same method used for steels. All the plastics in the literature had approximately the same modulus of rigidity: 300 kpsi. This led to a thickness of about 0.125 inches and a maximum stress at around 7,000 psi. Almost all of the plastics qualified except for some of the brittle materials

such as polycarbonate and acrylic. Nylon 6/6 was selected because of its availability, resistance to abrasion, resiliency, and low weight. Unfortunately, after examining the Nylon it was found that it was too brittle when bent and would most likely break at the high bending stresses that would occur when it was formed into a small loop.

After consulting with D. Blount, a chemical engineer specializing in plastics, polyethylene was chosen for further evaluation because it is relatively inexpensive and highly obtainable. Specifically, a sheet of type I PVC and high density polyethylene was examined and used. The PVC was favored because of its high resistance to abrasion; this was a major concern with the polyethylene.

After forming the materials into loops, it was determined that the polyethylene was rigid enough to carry both drive drums, and would return very slowly to its original circular shape after a large deflection. This is a desirable material property that may help damp the vibrations in the track; however, the return time for the polyethylene was much too large; it took several seconds for the loop to return to its original shape.

The 1/8 inch PVC seemed to work well, but the loop was not quite rigid enough to hold up both drive drums. On the other hand the loop did return quickly and was also light-weight and very durable. To remedy the rigidity problem, the thickness of the plastic loop was increased to 3/16 inch. This small 1/16 inch increase in thickness raises the rigidity of the loop a great deal. This can be observed from the fact that the moment of inertia, $I=bt^3/12$, increases as a cubic function of the thickness. This was proven experimentally by observing only a moderate deflection under the load of the track components. Therefore, a 3/16 inch thick type I PVC was selected as the track material.

2.1.2 Loop Bonding

Another area of concern in the design of the loop is how it can be bonded. The plastic is obtained in 4 by 8 foot sheets. It is then cut into 8 inch wide by 7½ foot long strips. Problems were incurred when attempting to bond a strip into a continuous loop. Three methods of bonding were tried: epoxying, riveting, and welding.

Initially it was thought that epoxies could be used, but there were none that were strong enough. When the loop was to be glued, the joining surfaces were made at an angle to reduce the stress across the bond (see Figure 2.3). This was effective in making a stronger bond; however, the rigidity increased over a larger area. This increase in rigidity was not what was originally expected

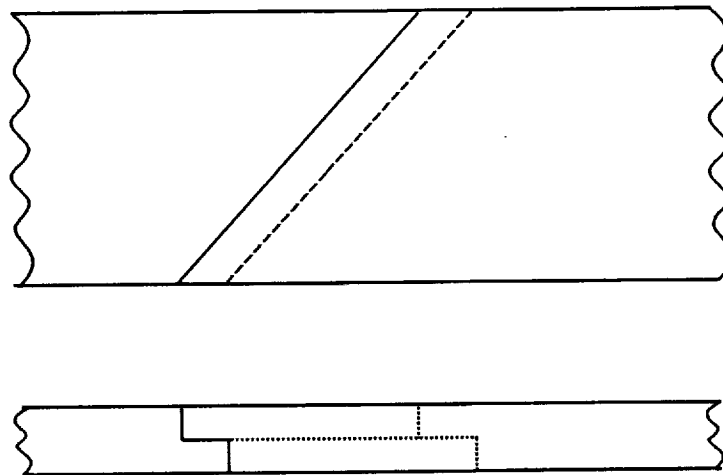


Figure 2.3 Milled Connection

for the angled joint. It was assumed that the rigidity would be lowered. Also in the vicinity of the bond, the stress caused a large deformation of the plastic.

To assure a definite bond in the loop, rivets were installed. However, this caused even larger stress concentrations than what was observed with the epoxied surfaces. The deformation was to the point where the plastic began to fail.

Fortunately PVC can be welded. It is welded by heating the two mating surfaces and melting in a bead of PVC between them. The welded bond formed is about 85% of the initial tensile strength of that material (Reference 11). In this case, the resulting bond is strong enough to be bent into a 5.5 inch radius.

When the welded loop was constructed, the same angled joint was used. The increase in rigidity in the area of the bond caused problems in the prototype. The welded joint actually increased in rigidity, thus it is possible that the loop could be welded straight across. This would greatly decrease the size of the rigid area, and reduce the effort required by the motors to bend that portion of the loop. It is suggested that this type of weld be considered in the future.

2.1.3 Gear Belt Bonding

In order for the drive drums to have positive traction on the inside of the loop, gear slots were machined on the drive drums and a gear belt was to be mounted on the inside of the loop. However, a problem was encountered when an attempt was made to bond the belt to the loop. Initially it was thought that the belt could be glued to the loop, but in order to do this, the inner diameter of the loop must match exactly the outer diameter of the drive belt. It was decided that the belt be bolted to the loop so that it could be used in other loops to be tested in the future. Also, when the loop is deformed and/or rolled, a large shear force is created between the loop and belt that tends to make the belt slide against the loop. After the drive belt was bolted onto the inside of the loop, it became difficult to roll the loop when deformed because this sliding was prohibited, and often the bolts tore from the belt.

A possible solution to this problem is to cut slots into the loop so that the bolts are allowed to slide or to individually bolt or glue the teeth to the inside surface of the loop. It may also be possible to eliminate the teeth altogether by using friction to drive the belt. This could be done by installing stronger springs on the pivot plates and placing soft rubber sheeting on the inner surface of the loop and on the drive drums.

2.2 TELEMETRY BOX

The telemetry box (refer to Figure 2.4) is the mounting point for the pivot plates and the tensioners. The pivot plates and tensioners keep the drive drums in contact with the loop; therefore, they transmit large forces to the telemetry box. The telemetry box for the conceptual model built last year for the USRA conference was determined to be inadequate for a working model. The box was too large and not strong enough to withstand the loads to which it would be subjected. It was therefore redesigned and constructed.

The material used to construct the box was 1 x 1/8 in. aluminum angle welded at all joints (Figure 2.5). The two sides of the telemetry box were connected by screwing 1/8 x 8 in sheets of aluminum to the top and bottom of each side of the box.

The pivot plates had to be able to rotate freely about their pivot points on the telemetry box. Initially, ball bearings were to be press fitted into the pivot plates which would allow them to rotate about a fixed shaft. It was decided that ball bearings were not necessary and a bushing was used instead. A 3/4 in. teflon rod was cut into 1 in. sections through which a 5/16 in. bolt was inserted. This assembly was then bolted through holes in the sides of the telemetry box. This provided a smooth, slick surface about which the pivot plates could rotate.

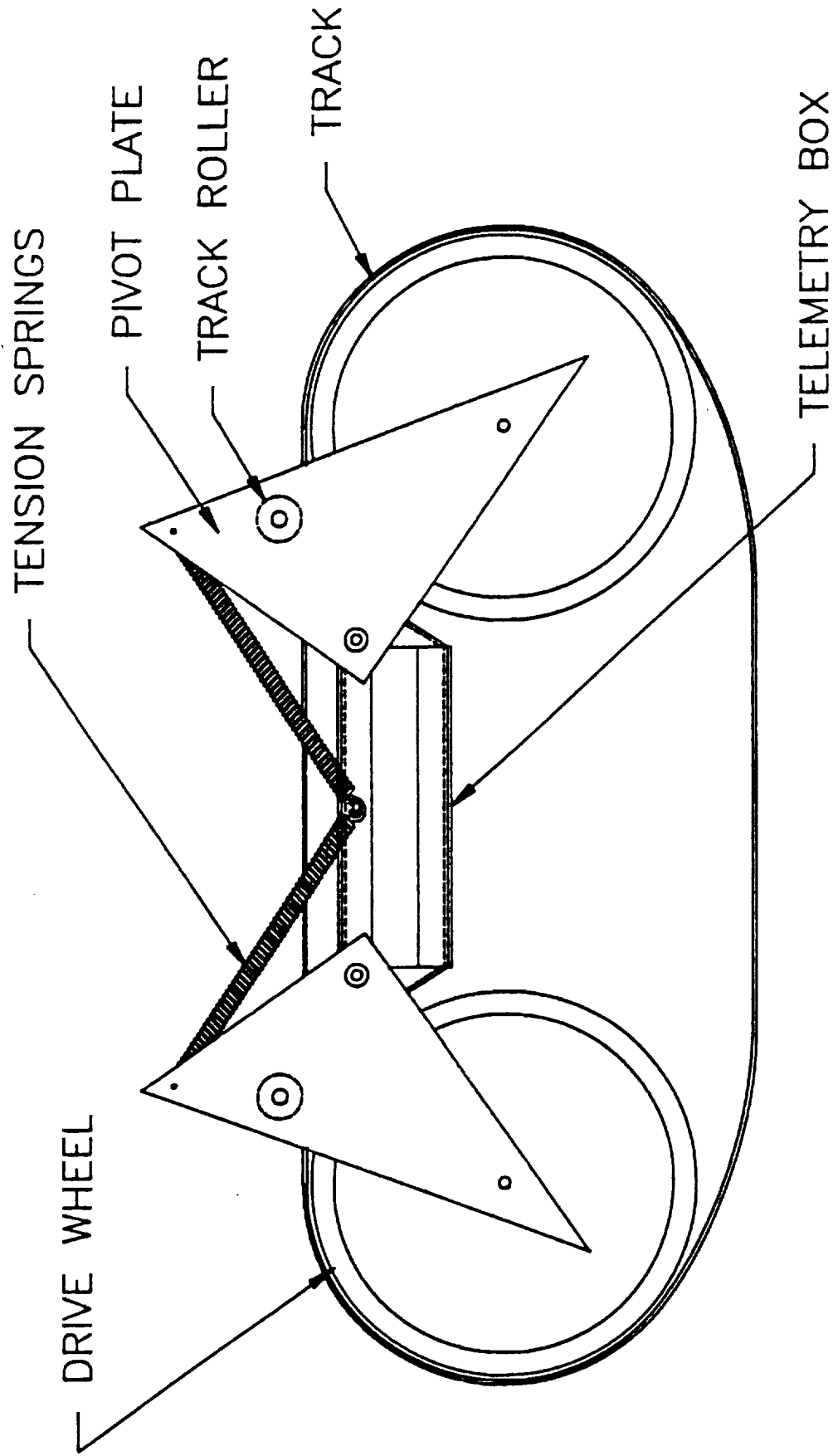


Figure 2.4 Assembly of Elastic Loop Track System

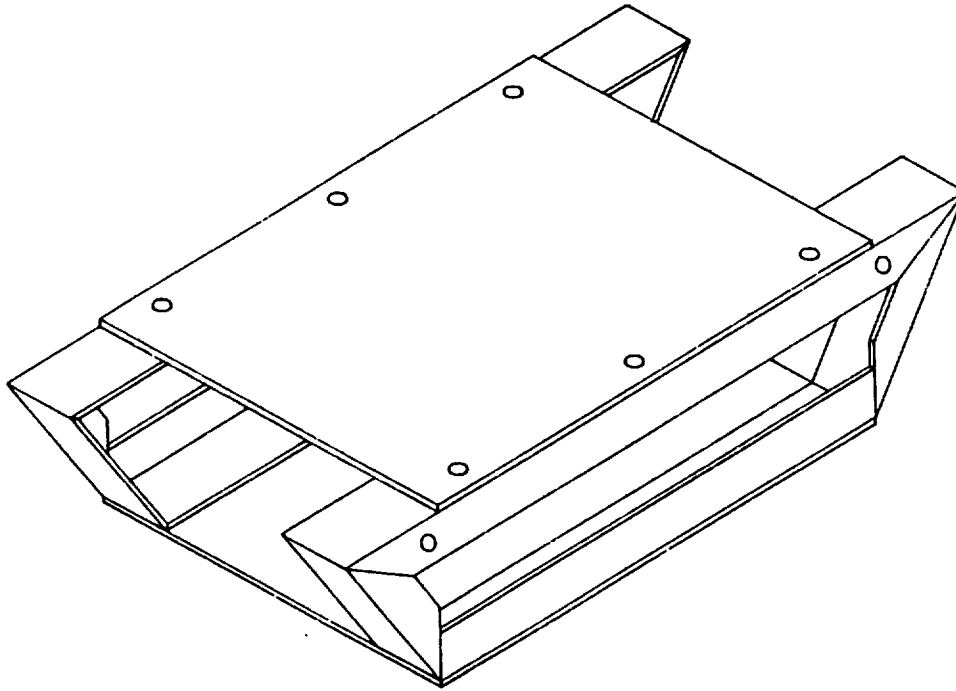


Figure 2.5 Telemetry Unit

2.3 PIVOT PLATE

The pivot plates are an important part of the ELMS. The drive drums and tensioning mechanism are both mounted to the pivot plates. Also a roller that helps to flatten the top of the track and support the weight of the LCUV is mounted to each pivot plate. The position of each of these components is critical to the overall ability of the mechanism to function properly.

The initial design was for the pivot plates to be constructed, of 1/8 in. thick aluminum, so that the position of the rollers, drive drum mounts, and the pivot points were all variable (Figure 2.6). Due to time considerations the pivot plates were constructed without the variable mounts. The mounting position for the drive drums, rollers, and pivot points were determined as accurately as possible, and the pivot plates were then constructed. The pivot point was set at a fixed position, and the drive drum and roller position were calculated relative to that point. After the loop was constructed and the ELMS assembled, the position of the rollers was found to be too close to the telemetry box and too far over the drive drum. The rollers must therefore be moved up and toward the center of the telemetry box. The design is presently being modified.

The tensioning mechanism is also mounted to the pivot plates. The conceptual design called for the mounting of a hydraulic compression strut from the bottom of the telemetry unit to the

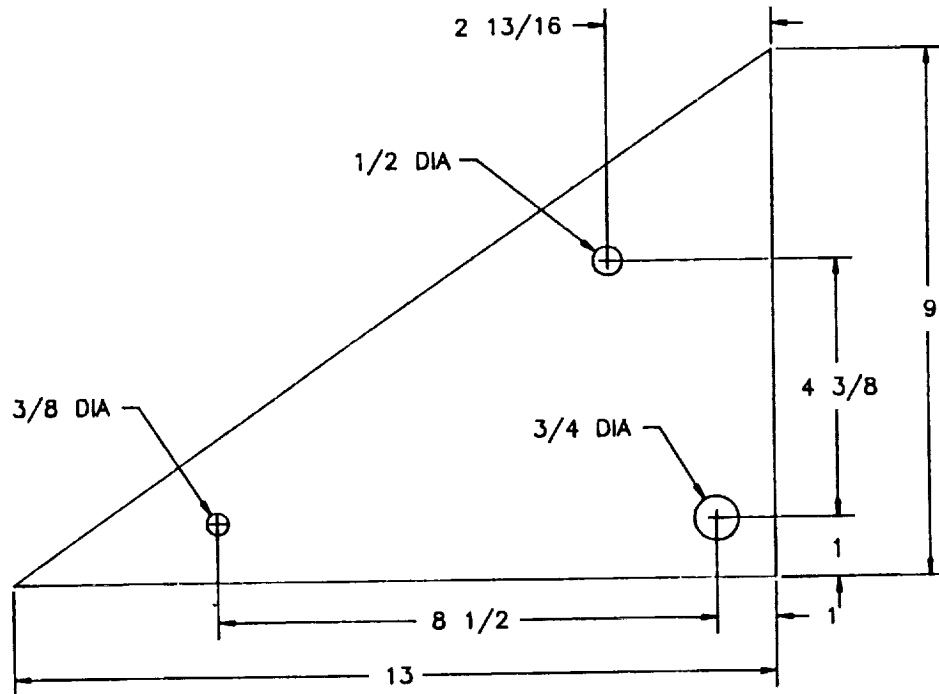
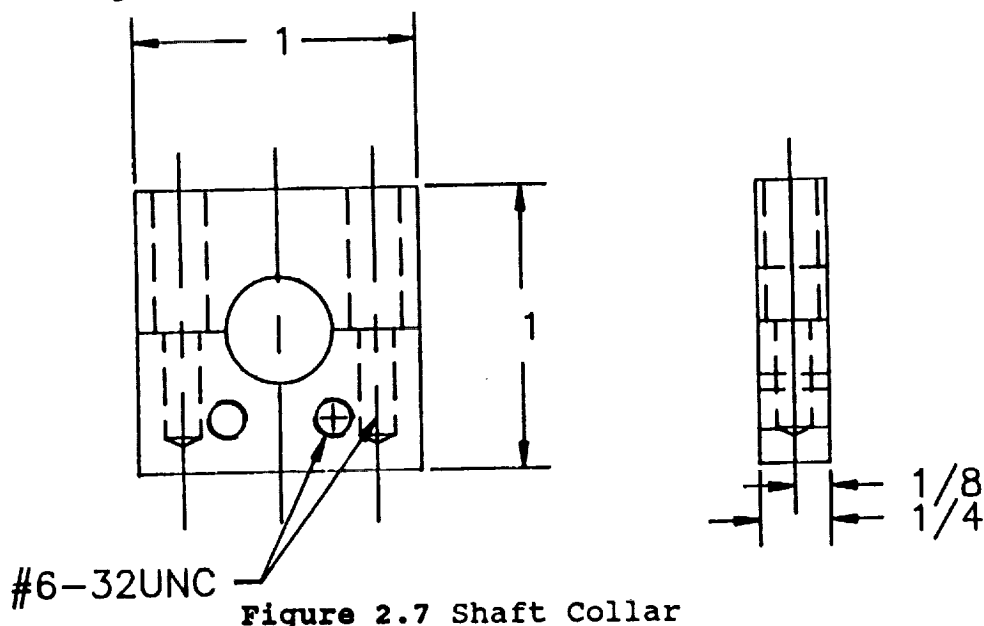


Figure 2.6 Pivot Plate

drive drum axle. Because a hydraulic strut cannot be used in a lunar environment, a new method of keeping tension on the track was developed. It was decided that a tension spring connected between the top of the front and rear pivot plates would provide enough tension on the loop. This design did not work; as one pivot plate would start to rotate and take up slack in the loop, the other would be pulled by the spring attached between the two and the entire telemetry unit would torque to one end of the track. The solution to this problem was to separate the pivot plates into two separate systems by mounting a tension spring from each pivot plate to the top of the telemetry box. This design works well but a turnbuckle should be added to each spring allowing tension on the loop to be adjustable. Presently, struts are being mounted between the telemetry unit and the bottom of the pivot plates. Through a kinematic analysis, this method seems to be more stable than using the springs alone.

The mounting of the drive drums to the pivot plates required a rotating shaft on one side of the drum and a fixed shaft on the other side. The rotating side of the drive drum required a ball bearing mounting. The pivot plates have not yet been bored for these bearings. The shaft on the other side of the drive drum is fixed to the outer casing of the drive motor, and it therefore must not be allowed to rotate. To fix the shaft a 1.5 x 1.5 x 3/16 in. aluminum block was formed into a two piece collar for the drive shaft (see Figure 2.7). The collar was fixed on the drive shaft and was drilled and bolted to the pivot plate. The torque requirements were underestimated and thus the shafts rotated in their collars. A set-screw machined in each collar solved this problem.

The rollers which ride on top of the track were designed to roll on brass bushings. The force on the rollers was found to be much greater than the initially calculated. It was decided that ball bearings were needed instead of bushings. Once the bearings are mounted they will greatly reduce the rolling resistance presented by the track rollers.



2.4 CHASSIS CONNECTION

A major design problem facing the track testing team is finding a means of connecting each track to the chassis of the LCUV. In addition to being operable in the lunar environment, the track design must perform certain other tasks. The first is to prevent the track from rotating into contact with the LCUV body. The second is to absorb a portion of the vertical forces encountered by each track as the LCUV travels over the rough lunar terrain. And finally, the chassis connection must have the ability to level loads as they are applied to the LCUV.

The LCUV 1989 Summer Report (Reference 1) labeled an initial chassis connection design as the Vertical Force "Absorbing" Connection System (V-FACS). The initial design of the V-FACS connection system is comprised of a shaft mounted horizontally through holes in connecting brackets mounted on both the chassis and the telemetry unit of the track. Figure 2.8 shows the orientation of the V-FACS system. Upon examining this figure, one will see that the V-FACS system operates in similar fashion as a hinge that connects a simple household door to it's frame.

The primary design flaw of the V-FACS system was it's inability to prevent the track from rotating into the chassis of the LCUV as seen in Figure 2.9. Rotation of the track creates a problem in

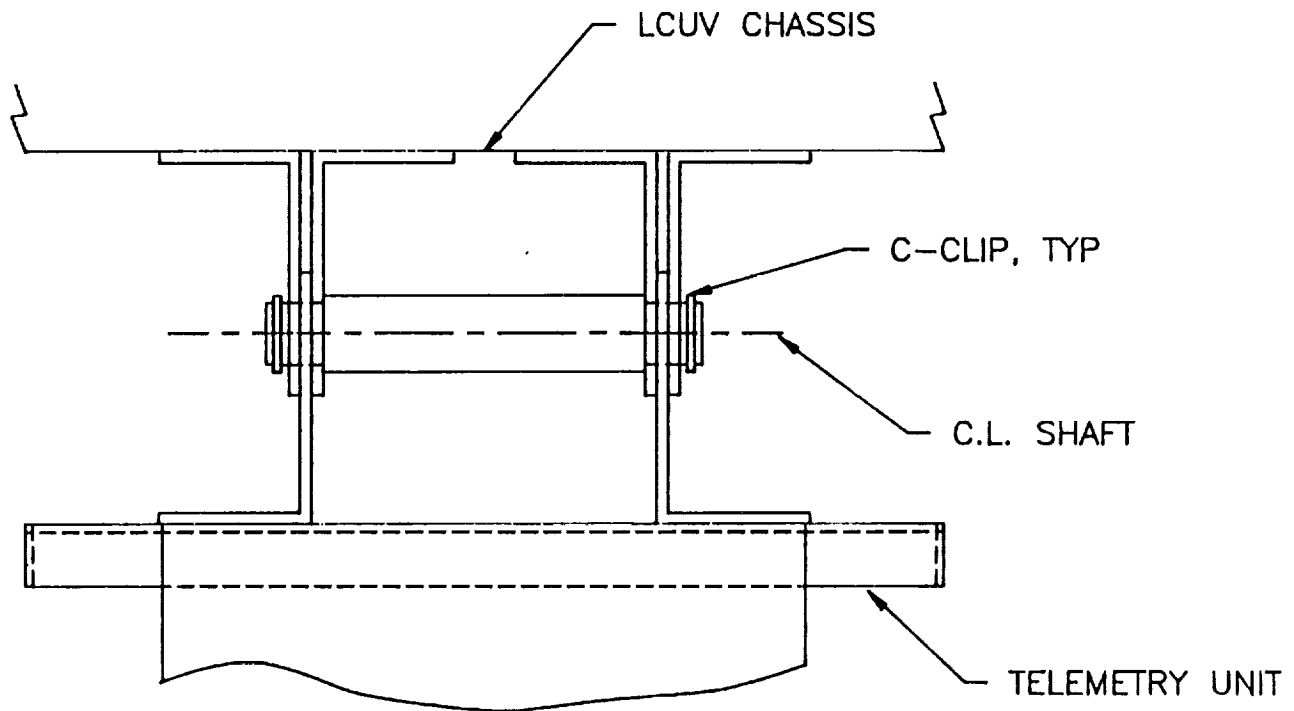


Figure 2.8 Vertical Force Absorbing Connection System

the total suspension of the LCUV. Without any means of preventing rotation, the ELMS track that is to be used in the LCUV design would be useless. Previous traction testing groups working on the LCUV conceived a rotation prevention system that included a strut mounted at an angle between the upper part of the LCUV chassis and the telemetry unit of the track. This type of strut assembly resembles the MacPherson strut incorporated into the suspension systems of many modern automobiles. Figure 2.10 shows this type of system.

The damping device to be used in this strut assembly is a frictional damping device coupled with a spring as shown in Figure 2.11. The frictional device was chosen since gas filled devices of this sort cannot be used in the lunar environment. The traction testing group has taken into consideration the initial design of

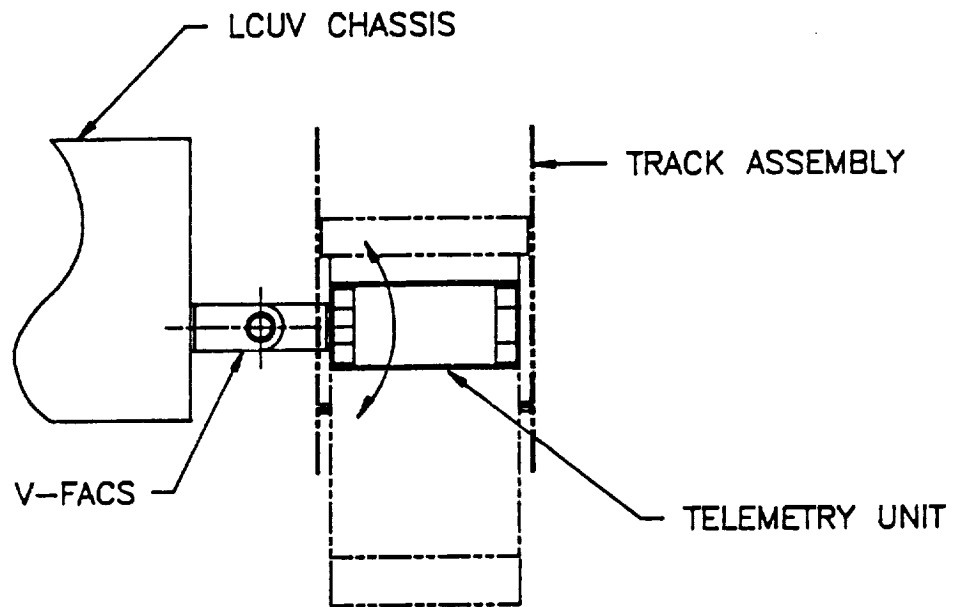


Figure 2.9 Track Rotation Relative to Chassis

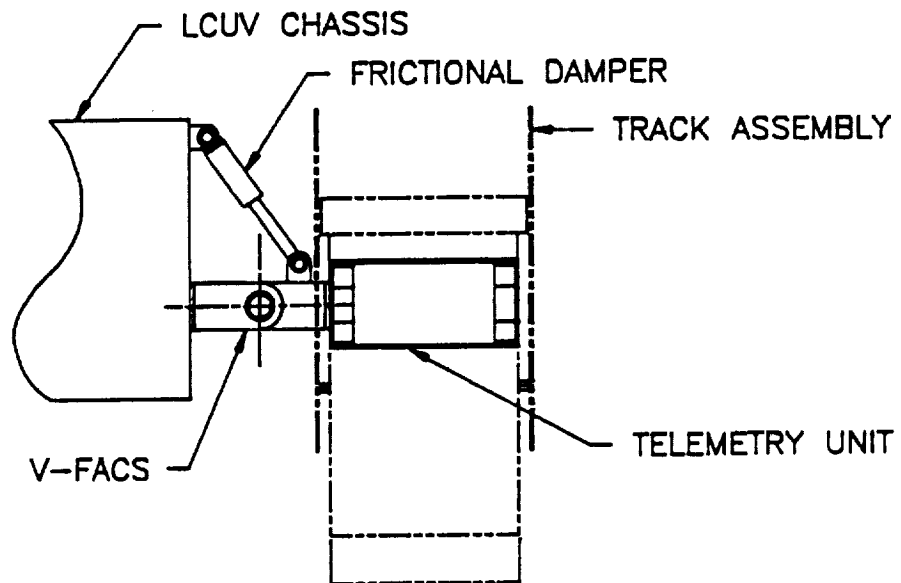


Figure 2.10 LCUV with Strut System

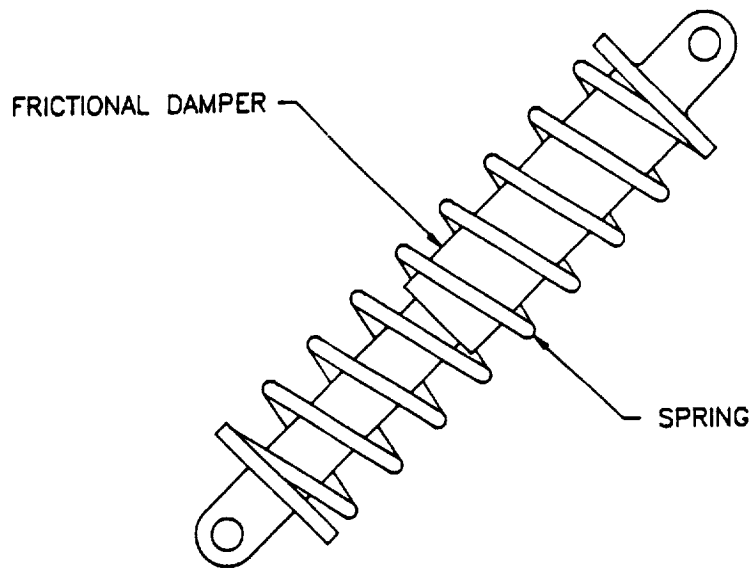


Figure 2.11 Detail of Strut

the rotation preventing strut as it was conceived. It was decided that it does not meet the required design needs. Although it is a sufficient means of suspension for application on the lunar surface, it does not meet the load leveling requirement.

In lieu of using the strut described previously as a prevention for rotation, a connection device incorporating torsion springs was devised. This device consists of brackets mounted on the chassis and telemetry unit in a similar manner as the original V-FACS system. A shaft will once again be mounted through holes within each of the brackets. To prevent rotation, torsion springs will be mounted between the inner and outer brackets toward the front and back of the connection system. Pins or C-clips applied on the outermost ends of the shaft will lock the shaft in position whereas pins or C-clips applied on the inner section of the shaft will prevent movement in the horizontal direction. A schematic drawing of this connection system is shown in Figure 2.12.

Initially, torsion springs were to be used alone in the chassis connection as described earlier; however, after further examination, two flaws in the design were revealed. First of all, there was no means of preventing the LCUV from "bouncing" as it travelled over the rough lunar terrain. Secondly, the track still had the ability to rotate in the chassis of the LCUV if the applied torque exceeded the resistance of the torsion spring. To remedy these problems a damping strut was added to the connection design. It is a frictional damping device intended to overcome the "bouncing" that would occur if the torsion springs were used alone and to act as a stopper as the track rotates toward the LCUV chassis. Although the new damping strut looks very much like the

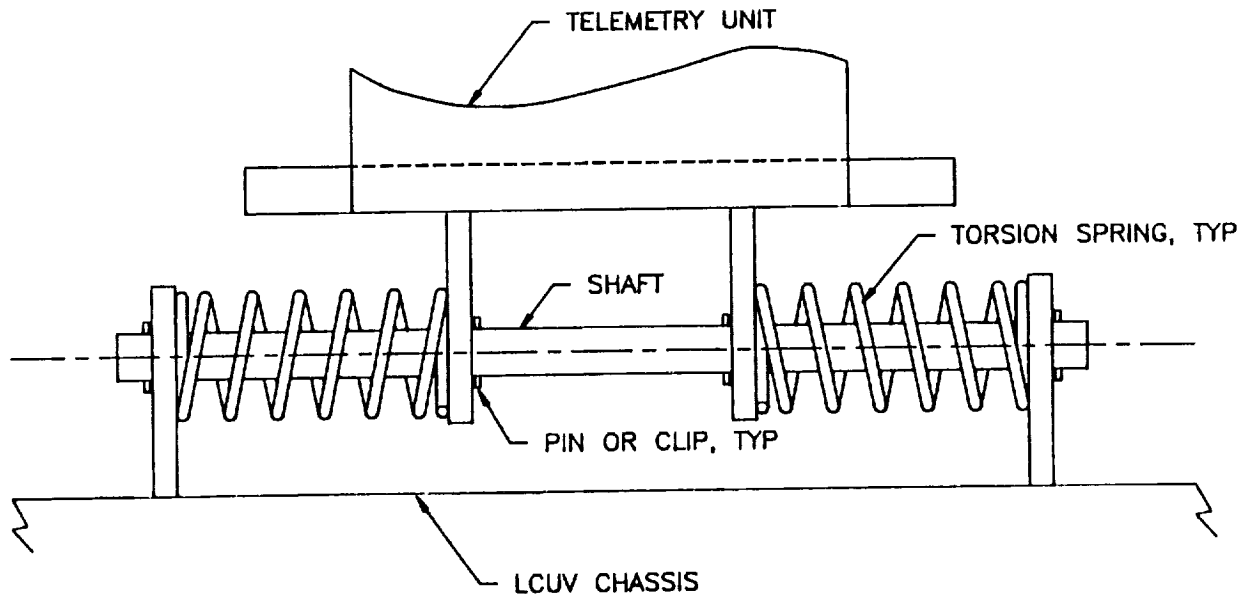


Figure 2.12 Suspension Incorporating a Torsion Spring

strut described earlier in this section and is to be mounted between the chassis and the track in the same way, it's only functions are to dampen the action of the springs and act as a stopper, not to absorb any of the vertical force the track may encounter.

The frictional damper consists of pads mounted on the inside of a cylinder with a plunger in contact with the pads within the inner diameter of the cylinder. A stopper ring has been included to inhibit extreme track rotation. A diagram of the device is shown in Figure 2.13. As the device is put to use, the thickness of the friction pads will reduce due to wear. To insure constant contact between the pads on the plunger, each pad will be spring loaded against the cylinder wall. A material for the friction pads has not been determined at this point but it is known that they must resist excessive wear and the extreme temperatures encountered in the lunar environment.

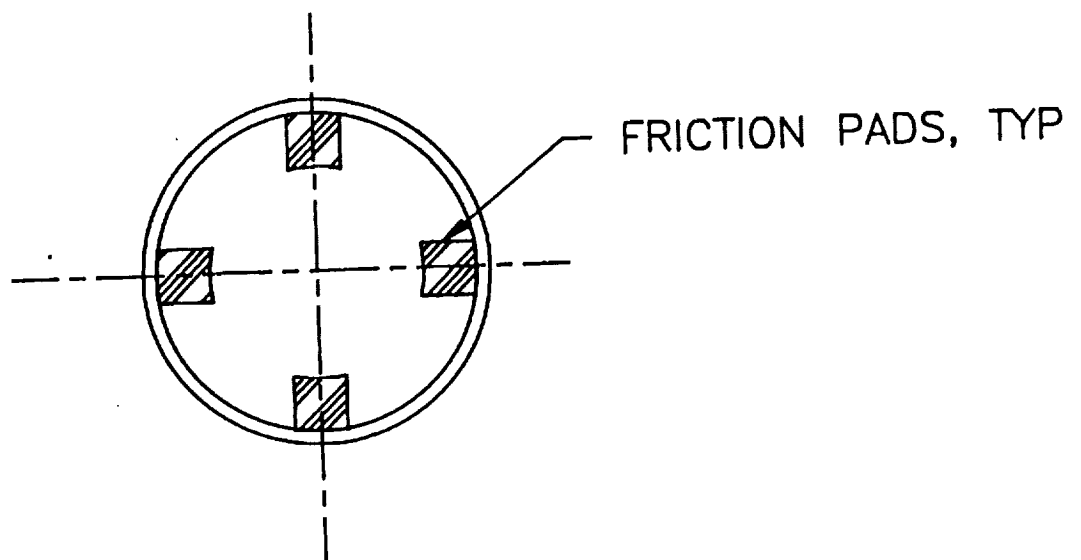
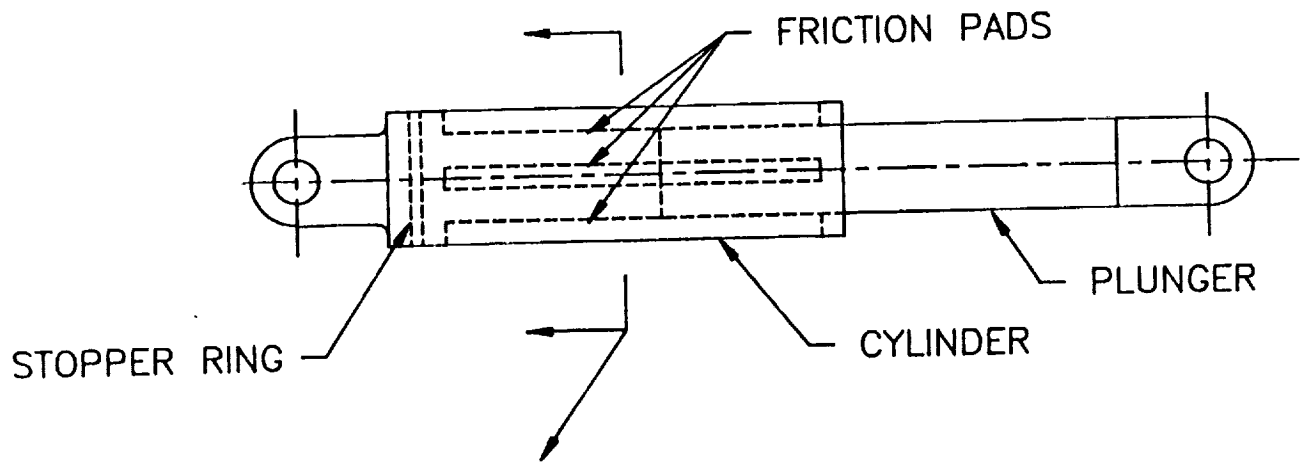


Figure 2.13 Frictional Damper

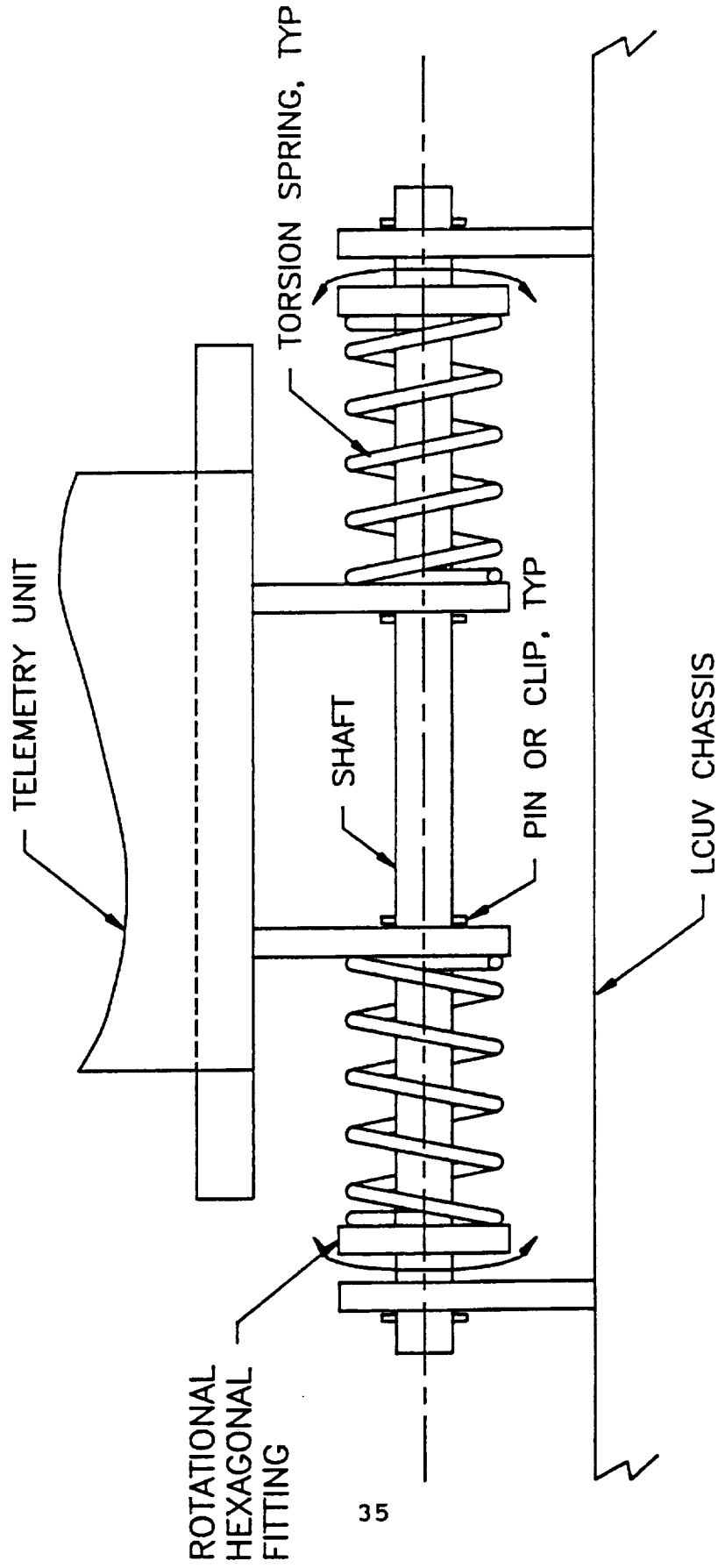


Figure 2.14 Manual Load Leveling Device

An added advantage of using the torsion spring connection system is it's ability to be used as a load leveler just by adding a few components. A diagram of the load leveler device designed by the traction testing team is shown in Figure 2.14. From the diagram one can see that each torsion spring is fixed to the inner brackets of the track's telemetry unit. At the opposite end of each spring is a hexagonal fitting with the ability to rotate freely around the horizontal shaft. By rotating the fitting, the number of turns of each spring is increased thus increasing the strength of each spring and it's ability to resist the applied torque when loaded. When the LCUV is unloaded, the springs are allowed to unwind bringing the LCUV back to it's resting level. The outer brackets slide outward so that an adjustment can be made. They slide inward to lock the fitting into hexagonal shaped holes in each bracket after the adjustment has taken place.

To accomplish the task of load leveling in an autonomous manner, it is necessary to find a means of winding the torsion springs. One method of winding would be to attach motors to the forward and rear ends of the horizontal shaft and in turn connect the motors to the hexagonal fittings by means of a separate hollow shaft. A limit switch is installed on the system to determine whether to wind or unwind the springs. Figure 2.15 shows the configuration of such a system.

Much of the chassis connection design has been completed thus far, but there is still some research to be done. One example is finding a material for the friction pads of the damper as stated previously. A more serious topic to be researched is the effects of cyclic loading on the life span of the torsion springs. In most cases, torsion springs are very practical to use as long as they are made to wind up during loading. In addition, torsion springs can operate at levels which equal or even exceed the yield strength of the material of which they are made because the residual stresses oppose the working stresses. Unfortunately, with the addition of the load leveling device, the springs in the system will be made to unwind as well as wind, so cyclic loading may be a problem.

Three additional areas of attention are left for the traction testing group to address when considering chassis connection. First, final dimensions must be obtained for the system. This may be done once the dimensions of the telemetry unit have been finalized and the amount of space to work with is known. Second, spring characteristics must be computed and a fabrication material chosen. Finally, the springs must be obtained and the connection system needs to be constructed.

Once the testing of the traction system begins, the torsion spring connection system can be evaluated and suggestions will be made on improving the design.

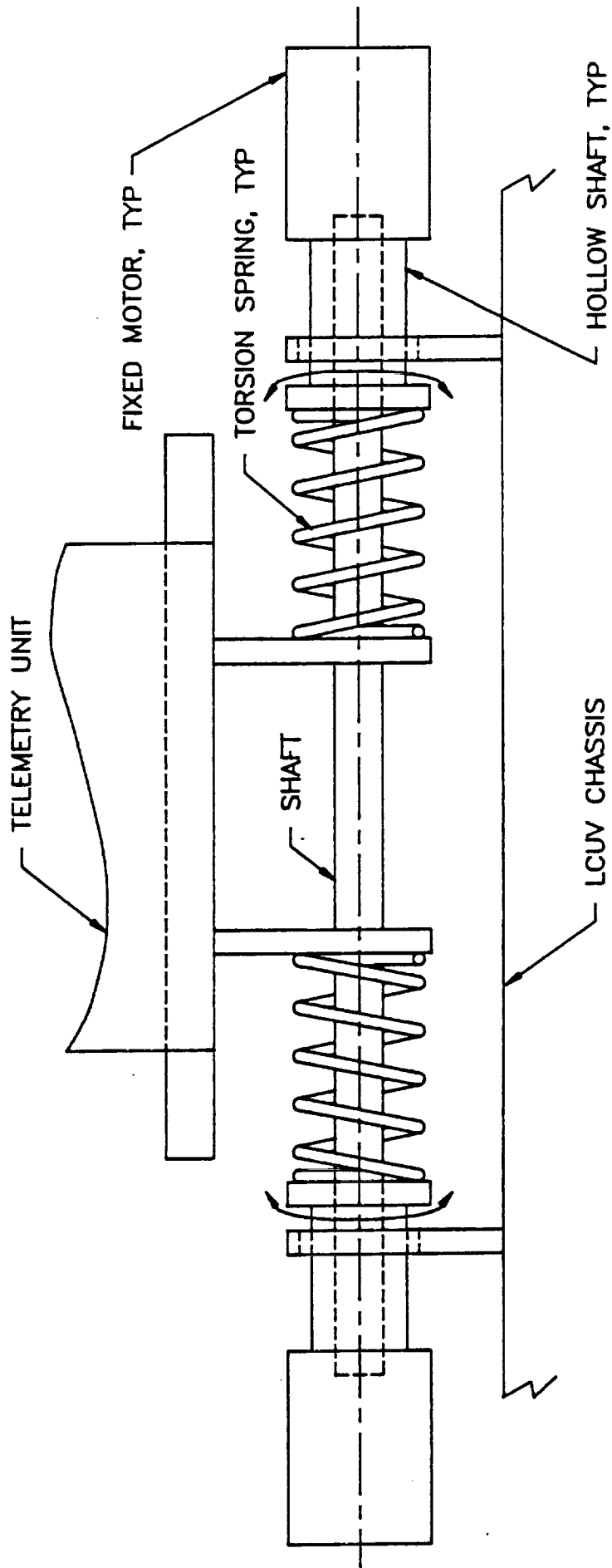


Figure 2.15 Autonomous Load Leveling System

2.5 TESTING PROCEDURES

Future work facing the track testing group is to thoroughly test the track design. Measuring and recording results during testing will enable the group to determine if the design is sufficient and to make suggestions on ways to improve the design in the areas of weakness.

Research has been conducted using a report submitted by Lockheed in 1972 (Reference 9). This report gives details on the design of an elastic loop mobility system and certain data that should be recorded when testing such a device. This track testing design team will base it's collection of data on this Lockheed report.

Data that are to be recorded are as follows:

- torque at loop/soil interface
- translational speed
- angular velocity of drums
- slip at the surface
- drawbar pull
- internal energy losses

By recording these data, the performance of the track design can be evaluated. An important part of the testing is visual observation. Visual testing is necessary to determine how the track will react to certain terrain and load applications.

At this point, the track testing group is considering various methods of testing the track design. It will be necessary to test the tracks in an environment that is similar to the lunar environment. Soil type and surface terrain are the two major conditions to be considered. The lunar soil consists mostly of silicate mineral fragments with more than 50% having a grain size of 0.075mm or less and 90% having a grain size of 1mm or less. The soil properties vary little throughout the entire area of the lunar surface. As for the surface terrain, slopes on the lunar surface range from 4 to 6 degrees for distances of up to 25m and are relatively constant in the plane areas. At mountainsides, slopes of up to 30 degrees are common. In addition to the slopes encountered on the lunar surface, obstacles such as rocks, ridges, uneven surfaces and depressions may be encountered (Reference 7).

It has been concluded that an enclosure consisting of sand would be an adequate testing facility for the tracks. A sandy environment was chosen because dry sand has properties similar to the soil on the lunar surface. It is also advantageous to use this material because it is inexpensive, readily available and easy to form into slopes and hills.

3.0 CONTROL SYSTEM

The research and development of an autonomous Lunar Construction Utility Vehicle requires a Locomotion Control System (LCS). The LCS is an integral part of the overall LCUV control system. This system is logically situated between the Navigation Control System (NCS) and the two drive motors.

In Figure 3.1, the top two blocks represent operations that occur on Earth. It is here that the tasks the LCUV must perform are generated. Once the list is generated, they are relayed to the LCUV via a data link, represented in Figure 3.1 as the jagged line connecting row 1 to row 2. The LCUV must store the list of operations, and send each operation to the proper control system. Should the instruction require the LCUV to move, it is sent to the NCS. The NCS then determines the LCUV's present location, and plots a course, around obstacles if necessary, to the required destination. This is then translated into a series of navigational instructions. For each specified length of time, the NCS sends the required speed and angular velocity to the LCS. The LCS interprets incoming data as movement of left and right motors. For each motor the desired response is compared to feedback and output voltage is adjusted.

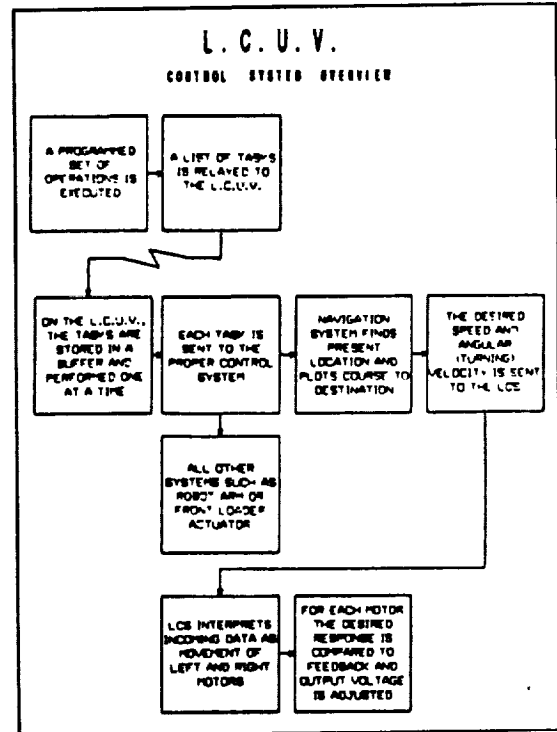


Figure 3.1 NCS - LCS INTERFACE LOGIC SCHEME

The purpose of the LCS is to ensure that the drive motors are performing as the NCS requires, i.e., each motor rotating at the specified angular velocity.

The LCS must operate under the harsh lunar environment to maintain the vehicle's autonomy of operation as efficiently and cost effectively as possible. The task of developing this control system is explained in this section. Also, the areas of command input, control mode, output mode and feedback measurement have been analyzed and modified. The project covers five major areas:

- System Constraints
- Control System Research
- Hardware Requirements
- Software Requirements
- Problems and Solutions

3.1 SYSTEM CONSTRAINTS

The limitations placed on the control system are listed below:

- 1) The main drive motors of the LCUV, having already been purchased, were inadequate for an advanced control system due to their non-linearity and high stiction.
- 2) The Keithley board, which houses the A/D and D/A converters, were easily saturated due to their low power limitations.
- 3) The tachometer mounts, which physically connected to the main drive motors, were large and, cumbersome. This prevented the direct implementation of the locomotion system on the LCUV.
- 4) The computer's relatively slow sampling rate restricts the controller's scanning ability, which slows response time considerably.

Some of these constraints were unknown until each component of the LCS was analyzed.

3.2 CONTROL SYSTEM RESEARCH

The effective development of this system required the full understanding of feedback and navigation command input devices, motor coordination systems and motor operational characteristics.

3.2.1 Feedback Device

The available options for feedback devices were tachometers, optical encoders, and resolvers (Reference 12). Tachometers were determined to be the foremost option. This decision was made in light of their low cost, high reliability, and ease of system implementation.

3.2.2 Navigation Command Input Device

The optimum simulator of the navigation controller input directives was determined to be a bi-axial linear analog input device, a common joystick. The problem of deciphering the stick position was examined. Please refer to Appendix A for the program code. Further discussion of this program code is made in the software development section.

3.2.3 Motor Coordination System

Fuzzy logic, analog control, and digital control were compared in order to determine the most appropriate method of motor control. The results are discussed below.

Fuzzy logic is a strictly digital implementation of the required control system. This realm of control uses pre-assigned "Look Up Tables". These tables are of the form of rough and fine speed control. The mentality behind fuzzy logic is as it's names conveys. Direct measurements of error and the change in error are made once through every controller cycle. These errors are then relayed onto the fuzzy logic control subroutine and compared to the values within the tables. Depending on a predetermined table resolution, it may be necessary to interpolate the fitting table values about the command input. Once the appropriate table values have been determined, a value for the necessary control effort is sent back to the signal dispensing region of the program subroutine. As the process error and it's change in error are minimized, the approach of fuzzy logic is mainly contingent on a fine control region. All fuzzy logic look-up tables are based and constructed on experimental results. It is imperative that these results be as accurate as humanly possible. Any error in experimentation will have disastrous results in the control effort. The factors of time and resource availability rendered this option inadequate. Yet, the use of a fuzzy logic controller is not out of the question. The ground work for the LCUV control system has been reached. Further efforts in control system development may open the door to this attractive and high speed alternative.

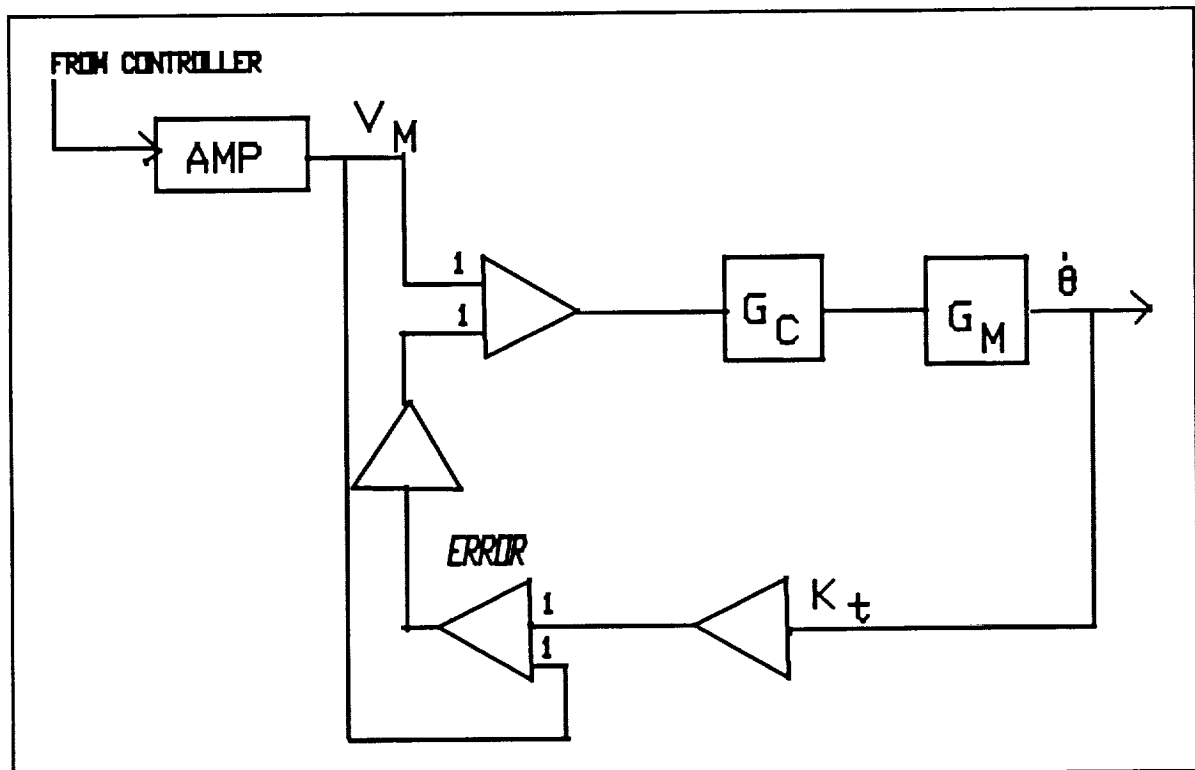


Figure 3.2 Analog Control System

Analog systems are frequently used in the arena of control systems. This style of control is centered around operational amplifiers for the tasks of supplying the necessary gains, along with the processes of proportional, derivative and/or integral control. With the use of easily constructed op-amp circuits, a cost effective control circuit is realizable. The once proposed control circuit diagram is available in Figure 3.2. Many problems arise in the implementation of analog control systems. The first and most important problem encountered was the system's sensitivity to external interference. Electromagnetic interference made the system behave in a manner which was not satisfactory. Improper gains occurred and the control process was greatly inhibited. The existence of such a problem rendered this system useless. After all, the controller under consideration is to operate under harsh lunar electromagnetic disturbances.

The use of digital control was determined to be the best in accuracy, versatility and cost effectiveness. For the purposes of the project and the availability of the equipment, a standard 286 based personal computer interfaced with a Keithley 570 D/A and A/D conversion board was used as the primary control hardware. A visual representation of the control model is available in Figure 3.3.

The primary source of navigational information is provided from a joystick. The joystick information is scanned by the computer and the control software operates from this information in the following manner:

- 1) Joystick information is scanned by the computer.
- 2) This information is then translated into the desired angular velocity of each motor.
- 3) The desired angular velocity is then transferred onto the Keithley Board and sent to each respective motor in terms of voltage.
- 4) Once this voltage has reached the motors, they rotate at a specific angular velocity, thus rotating the tachometers mounted

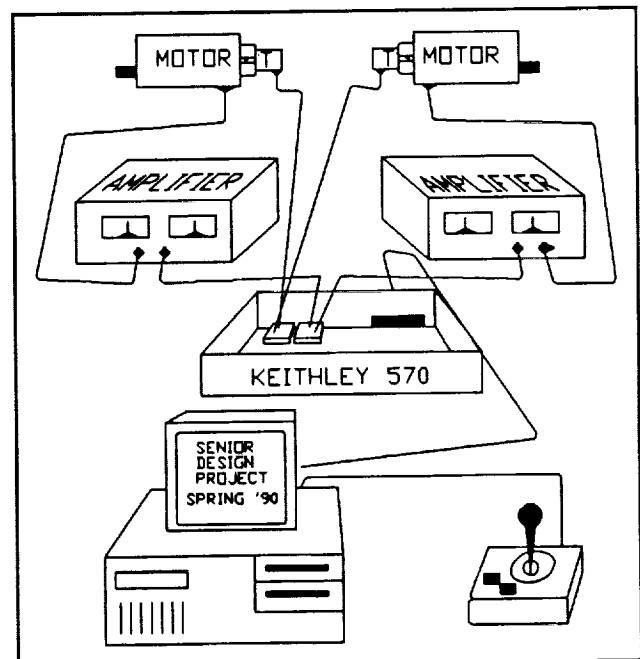


Figure 3.3 Motor Controller Diagram

on the drive shaft of each motor.

- 5) The rotation of each tachometer causes them to create a voltage.
- 6) This voltage is then input to the computer via the Keithley board.
- 7) The relationship between angular velocity and voltage is linear. This relationship is described by Equation 3.1 for a tachometer.

$$\omega = \frac{\text{Voltage}}{K_t} \rightarrow K_t = .022 \quad (3.1)$$

- 8) Thus, the computer has the values of the desired angular velocity and the actual angular velocity. The control error is then calculated. The error is the difference between these two values.
- 9) The control effort, u , is then determined from the error reading found by the computer. This effort is determined through the relationship presented in Equation 3.2.

$$U = K_p \cdot e \quad ; e = (\omega_{desired} - \omega_{actual}) \quad (3.2)$$

- 10) Step 3 is resumed by the control program until there is no error or until the computer receives new navigational information. In which event the processor would start with step 1.

3.3 HARDWARE DEVELOPMENT

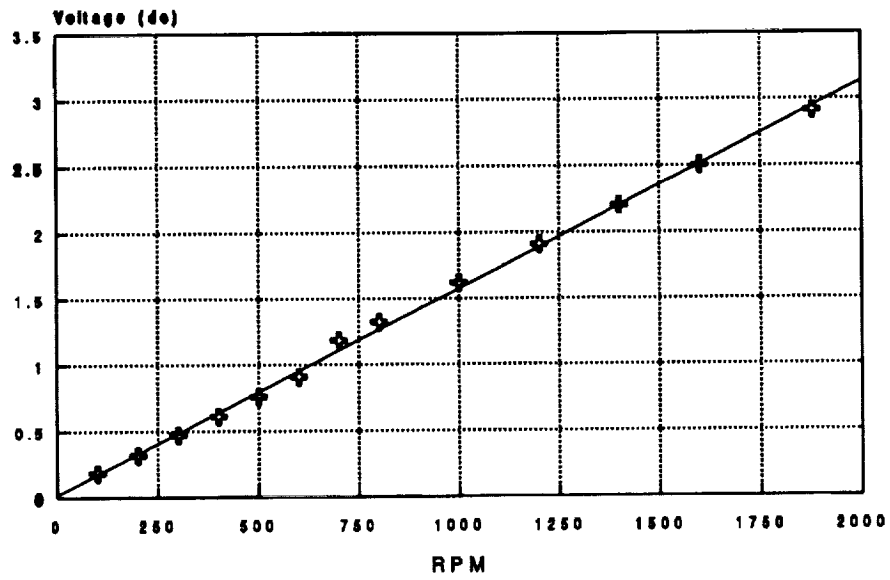
The hardware development aspect of this project includes incorporation of motors, feedback devices, and logic circuitry. These elements and their linkages were developed conceptually within the constraints of the present design of the LCUV.

3.3.1 Motors / Tachometers

The design of the LCUV control system revolves around two main drive motors. The two motors proposed for use in the LCUV are variable speed and reversible. Each motor is capable of 70 in-lb of torque at 36 volts. This high end torque is achieved by a 48.3:1 gear reduction system.

The angular velocity of each motor is a vital element of information for the LCS. This information feedback is to be represented by a voltage reading rendered by a tachometer connected to the rotor of the main motor. There exists a linear

Right Motor



Left Motor

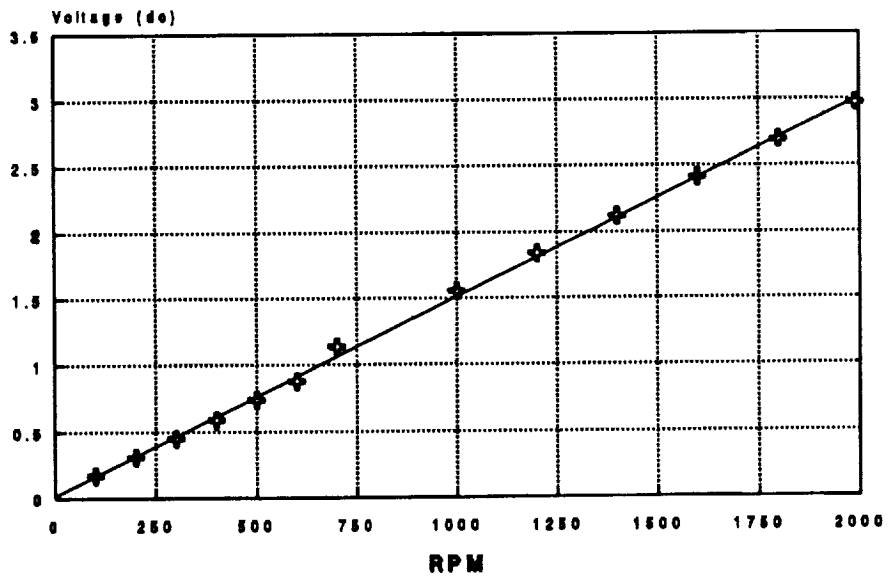


Figure 3.4 Tachometer Voltage Signal Response

proportionality between the tachometer output voltage and the drive shaft angular velocity as seen in Figure 3.4. Therefore, this instrument is a reliable feedback device. The proportionality of tachometer voltage versus it's angular velocity is clearly visible in Equation 3.1.

The completion of the task of tachometer mounting was followed by determination of the motor's transfer function. The plant transfer function was determined to be:

$$G(S) = \frac{177.3}{(S+36.61) \cdot (S+11.89)} \quad (3.3)$$

This testing involved two methods of experimental data retrieval. First, the motor-tachometer system was tested manually, as depicted in Figure 3.5. The motor was fed a sinusoidal input voltage at varying frequencies but at constant amplitude. The tachometer output signal was then monitored and compared to the original signal. Upon completion of this experimental procedure, the phase shift and gain for varying frequencies was obtained. Bode plots were then created based on experimentally determined information. The theoretical bode plot is shown in Figure 3.6. The results rendered by this experimental procedure are highly unreliable due to external interference and noise. As a result, the data rendered were useless to the project and so a better source for this information was required. The solution to this dilemma is the Hewlett-Packard Dynamic Analyzer.

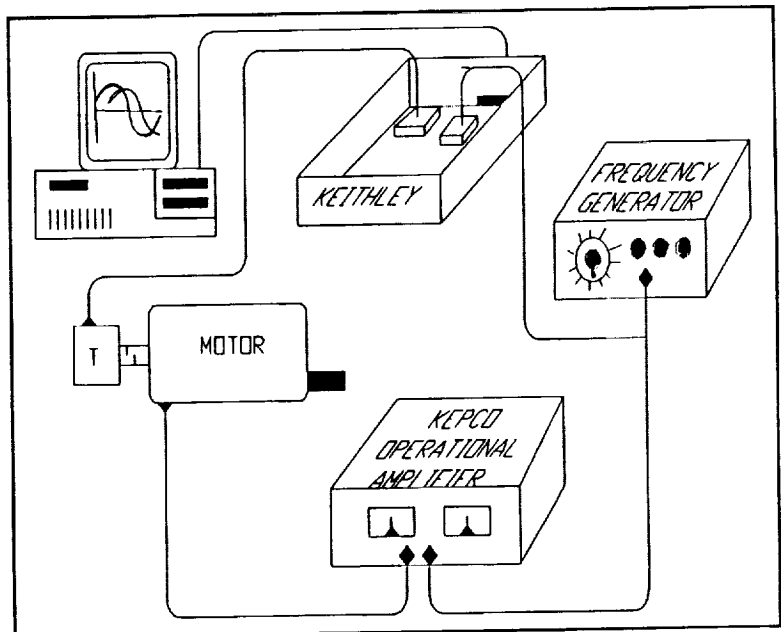


Figure 3.5 Manual Testing Diagram

This machine has the built in capabilities of noise filtering and signal discrimination circuitry. The results determined by the HP Dynamic Analyzer are also in the form of Bode Plots. This plot is available in Figure 3.7.

The primary concern of any control system designer is the stability of the plant at hand. System stability is best determined through a root locus plot. The motor transfer function root locus plot is shown in Figure 3.8. The system is definitely

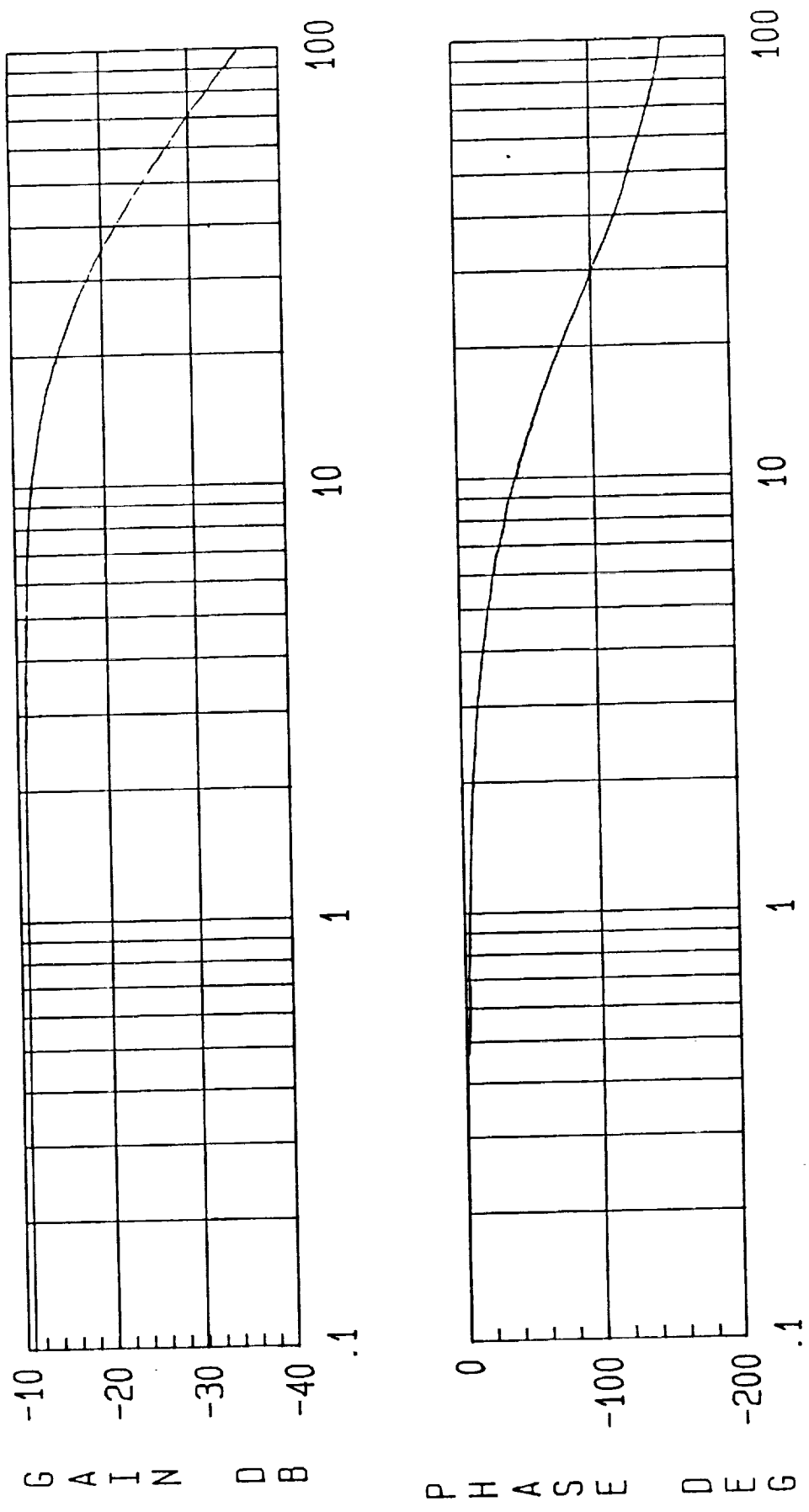


Figure 3.6 System Gain

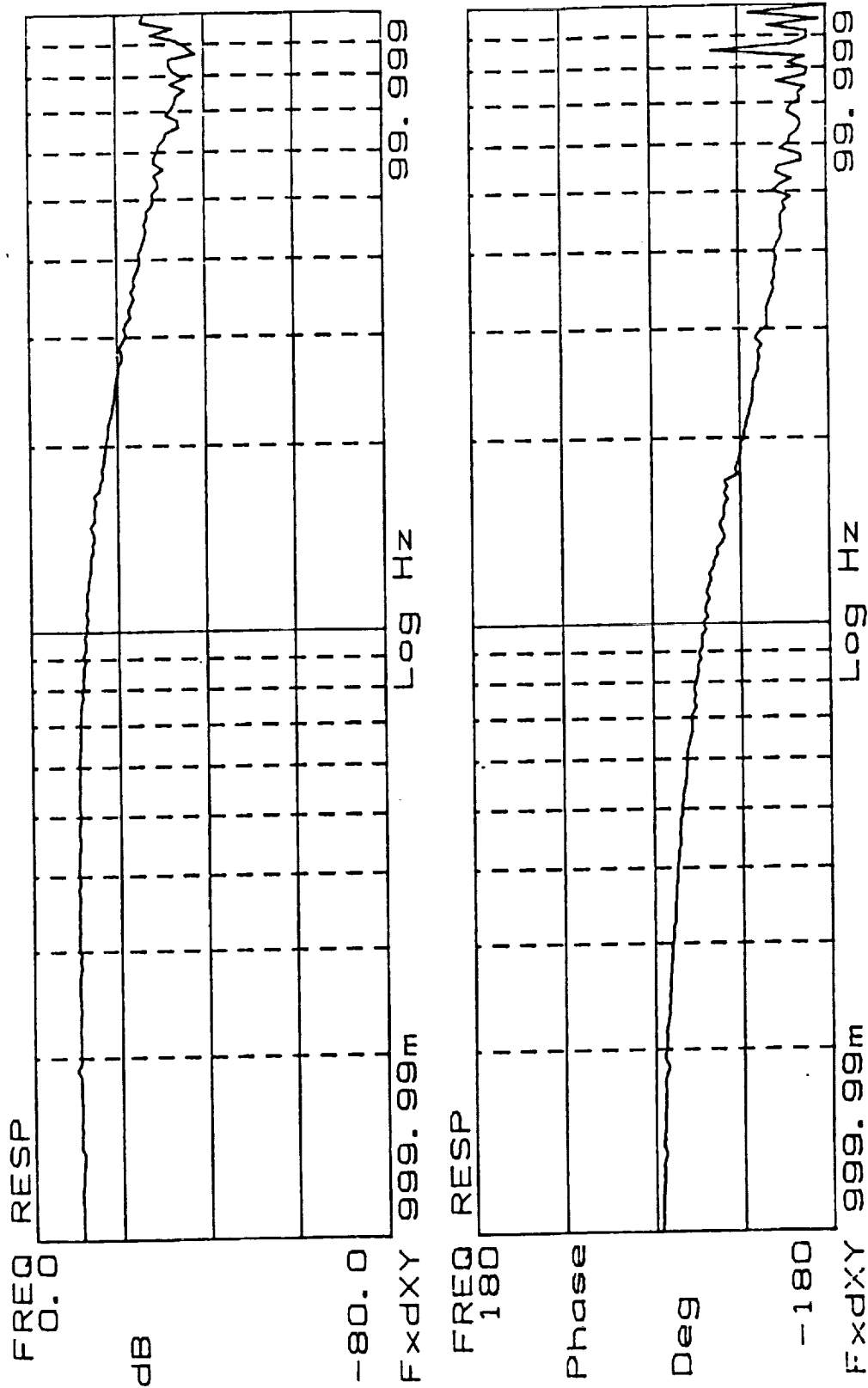


Figure 3.7 System Gain and Phase Shift
(HP Dynamic Analyzer)

stable since all the system poles are within the left hand plane. This is the optimum location for any plant. Since there are no Laplace transforms in the numerator, this system has no zeros. The root locus also demonstrated there is no need for an intricate control system. Therefore a simple proportional controller is used as the controller gain.

3.3.2 Lead - Lag Compensation

Before the motor plant transfer function was determined, it was thought that the system may require a lead-lag compensator. The purpose of such a device is to stabilize the system for varying gains. Since this system is originally stable, there is no necessity for such compensation.

3.3.3 Joystick

The joystick is a bi-directional analog device. This instrument has two axes, X and Y. The Y direction of the stick is representative of translational velocity; the X axis dictates the degree of rotational motion. Program subroutines, discussed further in the **Software Development** section of this report, decipher the desired vehicular response of the LCUV for any combination of the X and Y axes of the joystick.

3.3.4 D/A & A/D Converter

The control of the two driving motors required a fast and reliable processor. This requirement posed the need for a swift computer. This problem was solved easily by the availability of 80286 processor personal computers.

The data acquired is analog in nature. It is a voltage, an electric potential. Therefore, it was necessary for our group to determine a means by which this data could be transformed into a digital signal. The solution was the use of a Keithley conversion board. This device is an analog to digital (A/D) and a digital to analog (D/A) conversion device. It transforms an analog signal into a digital representation which is then conveyed onto the process control procedures for controlling the plant. Once the controller has analyzed the error within the plant, it generates a digital representation of the effort necessary to control the plant. This digital version of the effort is then relayed onto the Keithley board which in turn translates it into a voltage.

3.3.5 Programmable Amplifiers

The signal generated by the Keithley board varies from -10 to +10 Volts. The power requirements of the motor being controlled was between -36 and +36 Volts. Therefore, some method of signal amplification was necessary. This need for an amplifier with a gain of 3.6 presented the programmable amplifier as an ideal method

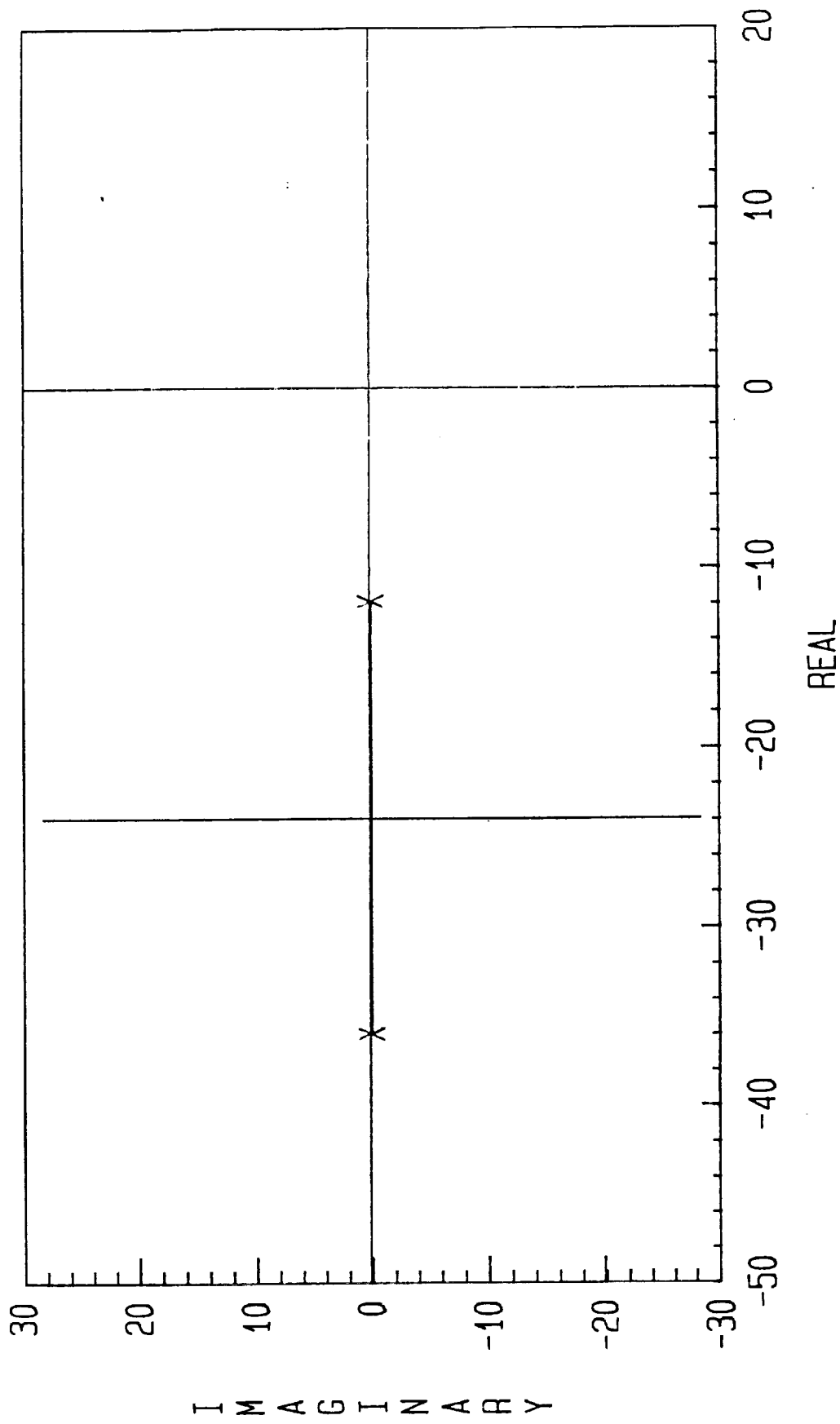


Figure 3.8 Root Locus of System Transfer Function

of signal amplification.

3.4 SOFTWARE DEVELOPMENT

The software development began with the input device of choice, the joystick. The joystick was chosen because its use is instinctive and permits all possible combinations of NCS input. The second phase of software development was the development of a digital control program to drive the motor in accordance to the joystick command input.

3.4.1 Joystick Program Code

As a bi-axial linear analog input device, the joystick is constructed using two potentiometers, one is affected when the stick is moved horizontally, along the x-axis, while the other is affected when the stick is moved vertically, along the y-axis. Also on the joystick are two buttons, A and B.

To access the position of the joystick, a game port is the required interface for the PC. The game port is assigned address 0x201. The position of the stick is proportional to the length of time it takes for certain bits in this one byte location of memory to change from 1 to 0 after a null is output to this address. The joystick driver source code, written in "C", is listed in Appendix A. The computer on which the code was tested returned values of 2 or 3 to approximately 65 from the procedure "joystick".

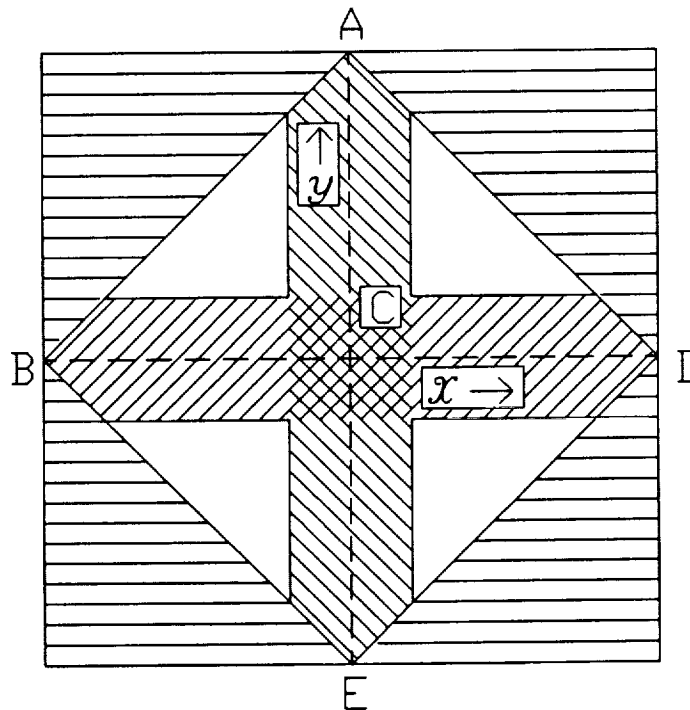


Figure 3.9 Joystick Command Mapping

There was no guarantee that the physical center of the joystick, the location to which the joystick assumes when not otherwise actuated, would be the median logical value. Values ranging from -100 to 100 were desired, with 0 located at the physical center of the joystick. Procedure "calibrate" was written to obtain values *aymh*, *ayml*, *axmh* and *axml*. For example, *aymh* is the linear relation between the values returned by the joystick routine between the physical center and physical "top" of the y-axis and 0 and 100. The actual calculations for each of these values are shown below:

$$\begin{aligned}
 aymh &= \frac{ymax - ymid}{100} ; \\
 ayml &= \frac{ymid - ymin}{100} ; \\
 axmh &= \frac{xmax - xmid}{100} ; \\
 axml &= \frac{xmid - xmin}{100} ;
 \end{aligned}
 \tag{3.4}$$

These values are used in the procedure "main" through an if-else statement, shown here in a simplified form:

```

if (ay < xmid)
    y = -(y - ymid) / ayml;
else
    y = -(y - ymid) / aymh;

```

Here the minus sign is needed to invert the y-axis. Once the x-axis counterpart of this routine is completed the position of the joystick is in the desired form.

It was desired that the joystick control be as simple as possible. Referring to Figure 3.9 point A refers to full throttle forward in both left and right motors. Point E, conversely, corresponds to full throttle reverse in both motors. Point B refers to full throttle reverse in the left motor and full throttle forward in the right, having the net effect of turning on a dime counter clock-wise. Point D is the reverse of point B. When the joystick is not otherwise affected, i.e., when it is released, it returns to the center, C, of the joystick plane, corresponding to a full stop.

Further enhancements were added. As seen in Figure 3.9, the joystick is capable of moving within the square area. However the area useful to the control algorithm is within the diamond shape ABEDA. Outside this diamond corresponds to motor velocities that exceed their maximum. To prevent the controller from requesting

impossible desired responses, the software logically "moves" the joystick horizontally until it is within the diamond. This is portrayed in Figure 3.9 using horizontal hash marks.

Also, since the software must convert the axes from a range of about 60 to about 200, (-100 to 100) There is no guarantee that the joystick will center on precisely zero. Therefore, there was programmed into the software a "dead zone", of +20 or -20 where the values are set to zero. In Figure 3.9 right hand hash marks represent the y-axis dead zone while left hand hash marks represent the x-axis dead zone.

All that remains at this point is to convert these values to forward and angular velocities as a percentage of maximum velocities of left and right motors. This is done through two simple relations:

$$l\text{motr_rat} = y + x \qquad r\text{motr_rat} = y - x \qquad (3.5)$$

Where $r\text{motr_rat}$ and $l\text{motr_rat}$ are the percent of maximum velocity of the right and left motors, respectively.

3.4.2 Controller Programming

The command input from the joystick is in the form of two variables: $l\text{motr_rat}$ and $r\text{motr_rat}$. These ratios represent the percent of maximum angular velocity and direction that each of the motors must travel. It is the task of the controller to ensure that these command values are maintained by the motors. Therefore, a proportional controller (P) and a proportional and integral controller (PI) were digitally constructed.

Proportional control is the type of control which is merely the introduction of a gain to the error between the desired output and the actual system response. This gain is multiplied by the error and reintroduced into the system as an effort. This task was determined to be best if done through some form of digital control. The program code for P type control is available in Appendix B.

Feedback from the tachometer was digitized by the Keithley 570 data acquisition board. This information is in the form of voltage. Some form of translation of voltage to angular velocity is necessary since the original control signal is in the form of angular velocity. The ratio between the angular velocity and output voltage of the tachometers is described by Equation 3.1. Since the actual angular velocity and the desired angular velocity of the motor are known, the computer may determine the process error. This error is in radians per second. A control effort is then applied to the error of each of the motors. The control effort is described by Equation 3.2. Although the control effort has been determined, it is not ready to be fed into the plant. The effort is in terms of radians per second. The plant will only

respond properly if the effort is translated into the voltage proportional to that angular velocity. This conversion is described by Equation 3.6.

$$V_{out} = K_m \cdot \omega \quad ; \quad K_m = .0185 \frac{\text{Volts} \cdot \text{S}}{\text{Radians}} \quad (3.6)$$

The task of converting the error effort from terms of angular velocity to output voltage was executed by the computer at the end of every control cycle. The digital value of control effort is then channeled from the computer controller onto the D/A converter within the Keithley board. The task of controlling and minimizing the plant error is maintained as long as the navigation simulator supplies navigation information. A process interrupt flag is present in the control software in the form of the statement:

```
while (j.a1!=1)
```

This is a flag detector which terminates the program when the user depresses the 'A' button on the joystick. It was implemented into the system in the event that an emergency stop of the LCUV is necessary.

An integrator was employed and integrated with the P controller to reduce the steady-state error. The introduction of an integrator altered the system definition from a type zero system to a type one system. The trapezoidal rule was employed to compute numerically the integration necessary for the PI controller. Theoretically, this process results in the elimination of all steady state error with nearly instantaneous response for large proportional gains. Program code implementing the PI controller is available in Appendix C.

The control system was provided with gains determined through theoretical research only to find that the system did not behave as expected: the motor chattered, with rapid oscillations in velocity. This was due primarily to the high proportional gain which saturated the Keithley output boards. The reduction of proportional gain and the increase of integral gain produced a system behavior where the motor response had significant overshoot and very long settling time. Initially, the large overshoot saturated the Keithley output ports producing motor "chatter". Integrator wind up and the presence of gear stiction accounted for this behavior. Once a suitable combination gain was determined, the control process occurred very slowly and with large time intervals between steps of input.

3.4.3 D/A and A/D Conversion Drivers

The process of acquiring the digital representations of analog signal such as voltage from the tachometer was done by the Keithley Data Acquisition board. The board is not sufficient for the

correspondence of the information from the board to the program code. Software drivers are necessary to ensure that the information get to the required memory locations. Lonnie Love provided the LCS group with software drivers which undertook this task.

3.5 DESIGN PROBLEMS AND SOLUTIONS

3.5.1 Four Motor Design

The original LCUV proposal presented to the control group included a four motor/two track design. The locomotion control of such a design required the continuous monitoring of belt tension. To attain this form of feedback, it would have been necessary to install a tension idler. The rigidity of the present track design rendered this design proposal completely unfeasible. The solution was obtained through a meeting with the LCUV track testing group. A two motor/two track design was agreed upon by both design teams. The prompt recognition of this problem insured the compatibility of the control system with the actual LCUV track design.

3.5.2 Motor/Tachometer Characteristics

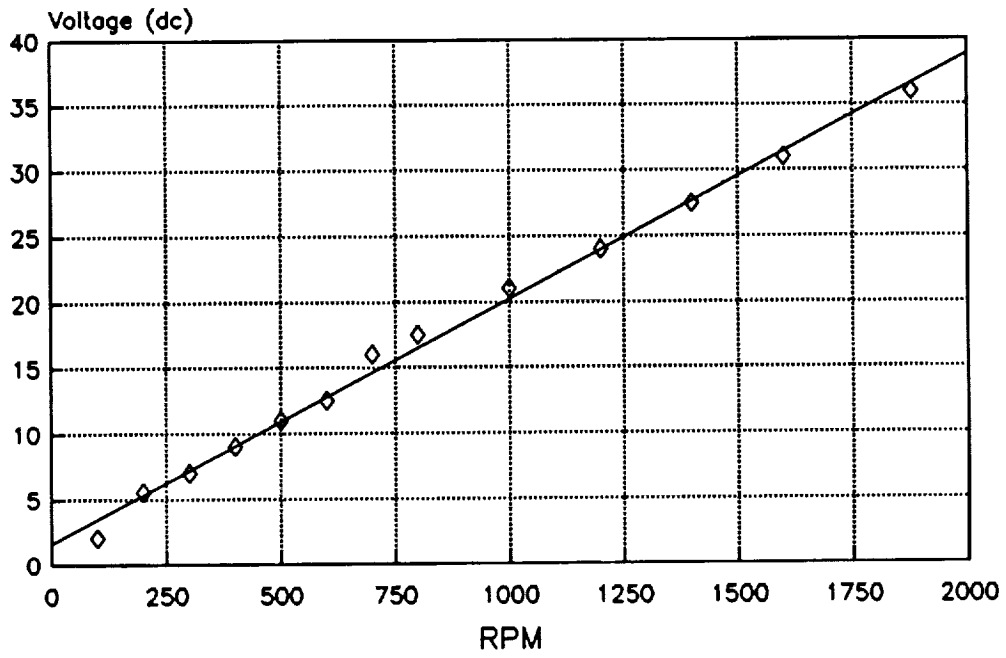
The motors and tachometers were obtained without any manufacturer specifications. To map the control system, the operating characteristics of the motors and tachometers were determined through the use of the Hewlett-Packard dynamic analyzer.

Preliminary testing of the LCUV locomotion system motors demonstrated some non-linearity. The probable causes of this situation are Coulomb frictional damping and gear stiction. The preliminary tests showed that a sufficiently high degree of linearity existed in operating these motors at voltages higher than 2.0 Volts. Therefore, the control system was modeled with linear motors for voltages higher than 2.0 volts (see Figure 3.10).

3.5.3 Assumptions about the LCUV

The inertial values of the LCUV are vital operating characteristics of the locomotion control system. This information is necessary in modelling the locomotion control system to insure that the LCUV will not undergo rapid acceleration and deceleration during simple locomotion maneuvers. The maximum turning rate must also be considered to guarantee that the LCUV will not flip over during sharp turns. Unfortunately, this information is not presently available. Some components of the LCUV are still under design and construction. Units such as the Heat Rejection System, Power Supply and the Excavating Arm facility are not yet fully developed. The effects of such values are to be considered and monitored via use of accelerometers mounted on the body of the LCUV.

Right Motor



Left Motor

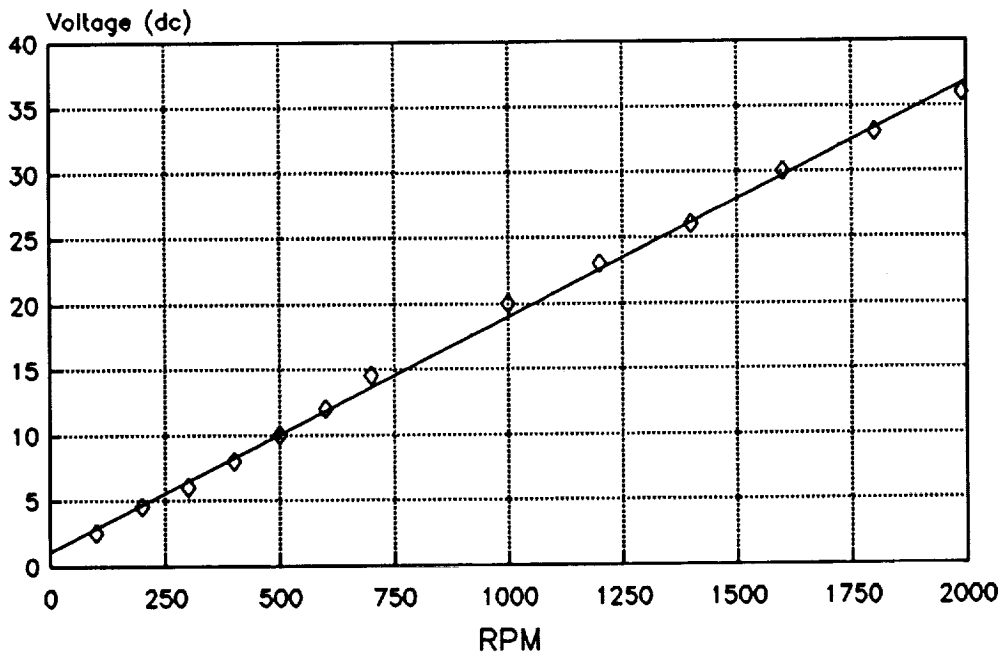


Figure 3.10 Motor Response Characteristics

4.0 POWER SUPPLY

The proposed Lunar Construction Utility Vehicle requires a sustainable source of power for its operation. Analysis must be performed on the LCUV's requirements to determine the kind of power supply available with the present day technology. When a power system for the LCUV is determined, the limitations and resources of the environment within which it operates must be taken into account. Energy from solar radiation and fuel cells were considered here. Most research in this section has been focused on Hydrogen-Oxygen fuel cells.

The lack of an atmosphere on the moon allows the radiation from the sun to reach the surface without any attenuation. The abundance of solar energy opens the path for solar cells to transform the sun's energy directly to electrical power. The LCUV can be equipped with a solar array panel that can supply energy to power the LCUV. During the daytime the solar energy can be used to power the LCUV and to charge a bank of rechargeable batteries for night usage. However, by performing some simple calculations, it was found that, with the efficiencies of the present day technology, the solar panels would be very large compared to the LCUV. For a 25 percent efficient gallium arsenide (GaAs) cell and a maximum power of 35 kW, the panel size has to be about 117 m² (Reference 13).

An alternative to the direct mounting of the solar panels on the LCUV would be to have the solar panels on a stationary base either on the moon or in orbit around the moon. The energy would be transferred through a microwave link to the LCUV. At first sight, this may seem like an ideal situation since with this set up the LCUV would not be burdened with a heavy and bulky power supply and it would not require refueling. Since if the LCUV was not attached to the power supply via a physical link, the LCUV would have greater mobility. However, there are many problems involved that require further consideration. Problems such as efficiency, antenna direction alignment, hazards, and power conversion.

A form of direct energy conversion that does not depend directly on the sun was considered. A direct solar independent source of power is the battery. Batteries directly convert chemical energy to electrical energy. The problem then arises with the life expectancy. Almost all of the batteries available today have a short operation life. One form of battery is the fuel cell. The fuel cell unlike other forms of batteries produces electrical energy by a continuous supply of fuel and oxidizer from an outside source. With this, the fuel cell can operate as long as fuel and oxidizer is available. There are many types of fuel cells available that can be considered. However, the hydrogen-oxygen fuel cell was selected for this study for reasons that will be discussed subsequently.

Hydrogen-oxygen fuel cells seem to satisfy most of the power requirements. The goal of this project is to research and develop a power system based on the hydrogen-oxygen fuel cell which will meet the needs of the LCUV's power requirements. This fuel cell was chosen for several reasons.

- 1) Solar independence
- 2) Use as a direct energy conversion device
- 3) It's by-product, water, can be regenerated back into its reactants, H_2 and O_2
- 4) It is a proven power supply for space application

In this section the basic design considerations of the power system of the LCUV, using a hydrogen-oxygen fuel cell as the energy source, are presented.

The next step was to determine how much hydrogen and oxygen are needed for a given period of operation without refueling. This should be determined by examining the operation of the fuel cell.

Storage of the reactants is another important issue. The location, size, and method of insulation of the storage tanks are determined.

As it will be demonstrated in the following sections, the fuel cell requires certain conditions for proper operation. To achieve the variables such as pressures, temperatures, and flow rates the current should be closely monitored and adjusted. Thus, since the LCUV is an unmanned machine, then a power supply with a highly reliable-automated control system is required.

4.1 FUEL CELL OPERATION

The fuel cell is a fairly simple electro-chemical device. Its primary parts consist of an anode, a cathode, and an electrolyte (Reference 14). The energy conversion occurs at the anode where the fuel, hydrogen, enters and is ionized. As this occurs, electrons are removed and travel across a load which generates a current. This process is shown in Figure 4.1. The hydrogen ions then diffuse across the electrolyte. At the cathode, oxygen enters and combines with the hydrogen ions and the electrons which traverse the load. This recombination forms water which is removed from the system (see Figure 4.2). Each fuel cell can then be placed in series to form a fuel cell stack which delivers a combined power output (Figure 4.3).

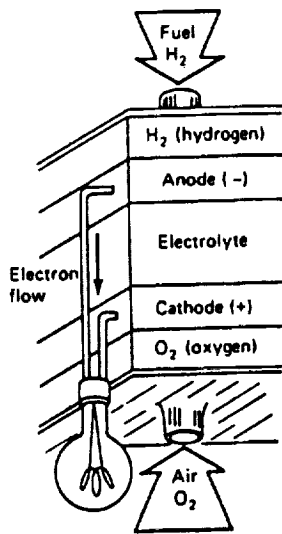


Figure 4.1 Fuel Cell Reaction Sequence

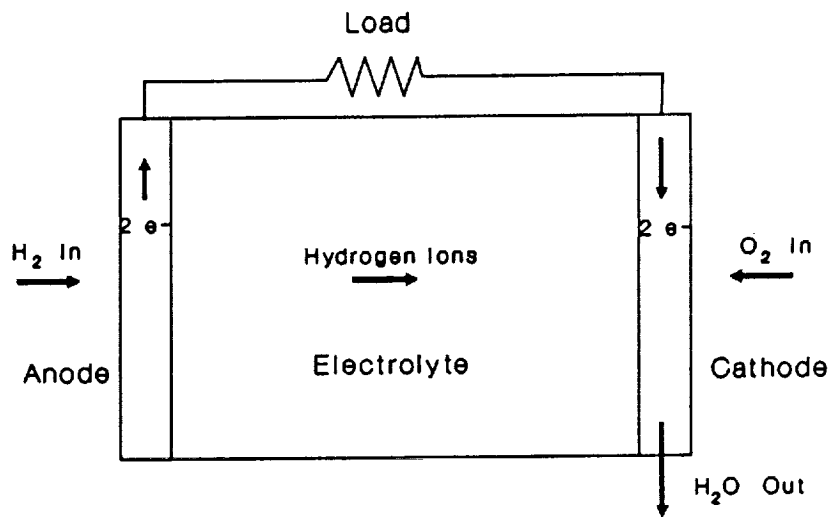


Figure 4.2 Schematic of Electro-Chemical Process

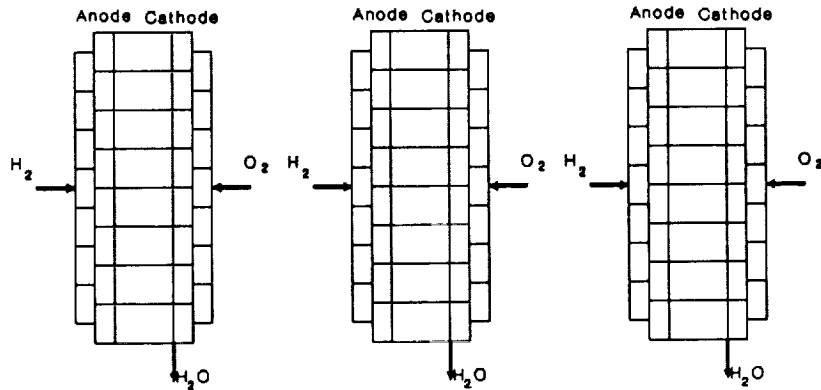
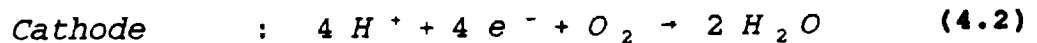


Figure 4.3 Schematic Showing Three Stacks of Eight Fuel Cells

The primary equations (half cell reactions) for the combustion at the anode and cathode are (Reference 13):



4.1.1 Power Output

The dimensions of the fuel cell stack are based on the plant currently in use by the NASA space shuttle. Each cell stack can deliver an average power output of 5 kW (Reference 15). The dimensions per cell stack are:

L=101 cm
W=38 cm
H=35 cm
Mass=91 Kg

Each stack is actually a series of individual fuel cells put together to produce a combined output of 5 kW. Typically, one fuel cell can produce about one volt of potential difference. As these cells are combined to produce a stack, the voltage is also increased. The average power output for three stacks has been specified to be 15 kW. This is the power output that has been used to size this system and to assume the maximum average power.

For the purposes of estimating fuel and oxidizer requirements, the assumed time length between LCUV refueling is 30 days; this is the operation time of the fuel cell. For purposes of mass flow calculations, the total voltage difference has been assumed to be 24 volts. Since one fuel cell can only have a potential difference of one volt, eight fuel cells per stack will need to be placed in series (Figure 4.3). For an average power output of 15 kW and a combined voltage of 24 V, the required current will be 625 amps per cell. Since each cell has a potential difference of approximately one volt, the power output per cell would be 625 W.

4.1.2 Mass Flowrate Determination

In order to size the reactant and product storage tanks, the mass flowrate through the cells must be determined. With a specified current of 625 amps per cell, the electron flux can be determined from the definition of a Faraday:

$$\begin{aligned} 1 \text{ Faraday} &= 96493 \text{ coulombs/mole of electrons} \\ 1 \text{ amp} &= 1 \text{ coulomb per second} \\ \text{molal electron flux} &= \text{amps(coulombs/s)}/\text{Faraday} \\ &= 6.477 \cdot 10^{-3} \text{ moles } e^{-}/\text{s} \end{aligned}$$

This is the theoretical flux of electrons. Due to current efficiency, reaction efficiency, and voltage efficiency, a good overall efficiency (n_{oa}) of a fuel cell has been found to be 70% (Reference 16). With this efficiency, the actual flux would be e^{-} flux/ n_{oa} :

$$e^{-}_{\text{act}} \text{ flux} = 9.253 \cdot 10^{-3}$$

From the half cell reaction at the anode, Equation 4.1, the H_2 flux can be determined:

$$\begin{aligned} H_2(\text{moles/s}) &= 1/2e^{-}(\text{moles/s}) \\ &= 4.626 \cdot 10^{-3} \text{ mol } H_2/\text{s} \end{aligned}$$

This is for an average power output of 625 W/cell. The mass flowrate can be determined by:

$$\begin{aligned} m(\text{kg/s}) &= \text{kmol/s} \cdot M(\text{kg/kmol}) \\ &= 9.326 \cdot 10^{-6} \text{ kg } H_2/\text{s} \end{aligned}$$

where M is the molecular weight of hydrogen.

The mass flowrate of O_2 can be determined similarly from the cathode reaction as 7.4×10^{-5} kg/s. Combined with the anode reaction, these mass flowrates are required to produce an average power of 625 Watts/cell, or 15 KW total power for all three cell stacks. For thirty days the required mass of reactants per cell would be:

$$m_{total} = \left\{ \begin{array}{l} 24 \text{ Kg } H_2 / \text{cell} \\ 192 \text{ Kg } O_2 / \text{cell} \end{array} \right. \quad (4.3)$$

With 24 cells, the total mass of reactants required would be 580 kg H_2 and 4605 kg O_2 . Figure 4.4 shows the mass flowrate of the reactants and the product vs power output.

To minimize volume, the reactants would have to be stored in their liquid state. To achieve this, the hydrogen would have to be stored at 20°K and the oxygen at 83°K. The nominal operating temperature of the fuel cell has been found to be 373°K (Reference 13).

4.1.3 Heat Generation

With a specified power output of 15 kW and with given inlet and exit temperatures of the fuel cell, the heat generation can be determined. By taking a control volume around the fuel cell stacks, as shown in Figure 4.5, a 1st law analysis yields:

$$Q_{cv} = W_{cv} + nH_2O (h_f + dh) T_e - (nO_2 + nH_2) (h_f + dh) T_i \quad (4.4)$$

where:

- Q_{cv} = Heat generation rate
- n = molal flux of substance
- h_f = enthalpy of formation at 25 C and 0.1 MPa
- dh = enthalpy change with respect to the reference
- W_{cv} = rate of work output

The enthalpy of formation for hydrogen and oxygen is zero at 21°C. If the inlet temperature for the reactants is 80°C, then the change in enthalpy (dh) for hydrogen is 1593.12 kJ/kmol, and the change in enthalpy for oxygen is 1630.75 kJ/kmol. The product, water, has an enthalpy of formation of -241827 kJ/kmol and the change in enthalpy, corresponding to the exit temperature of 100°C, is 2536.97 kJ/kmol. From the half cell reaction at the cathode, it can be seen that molal flux of H_2 and H_2O are the same.

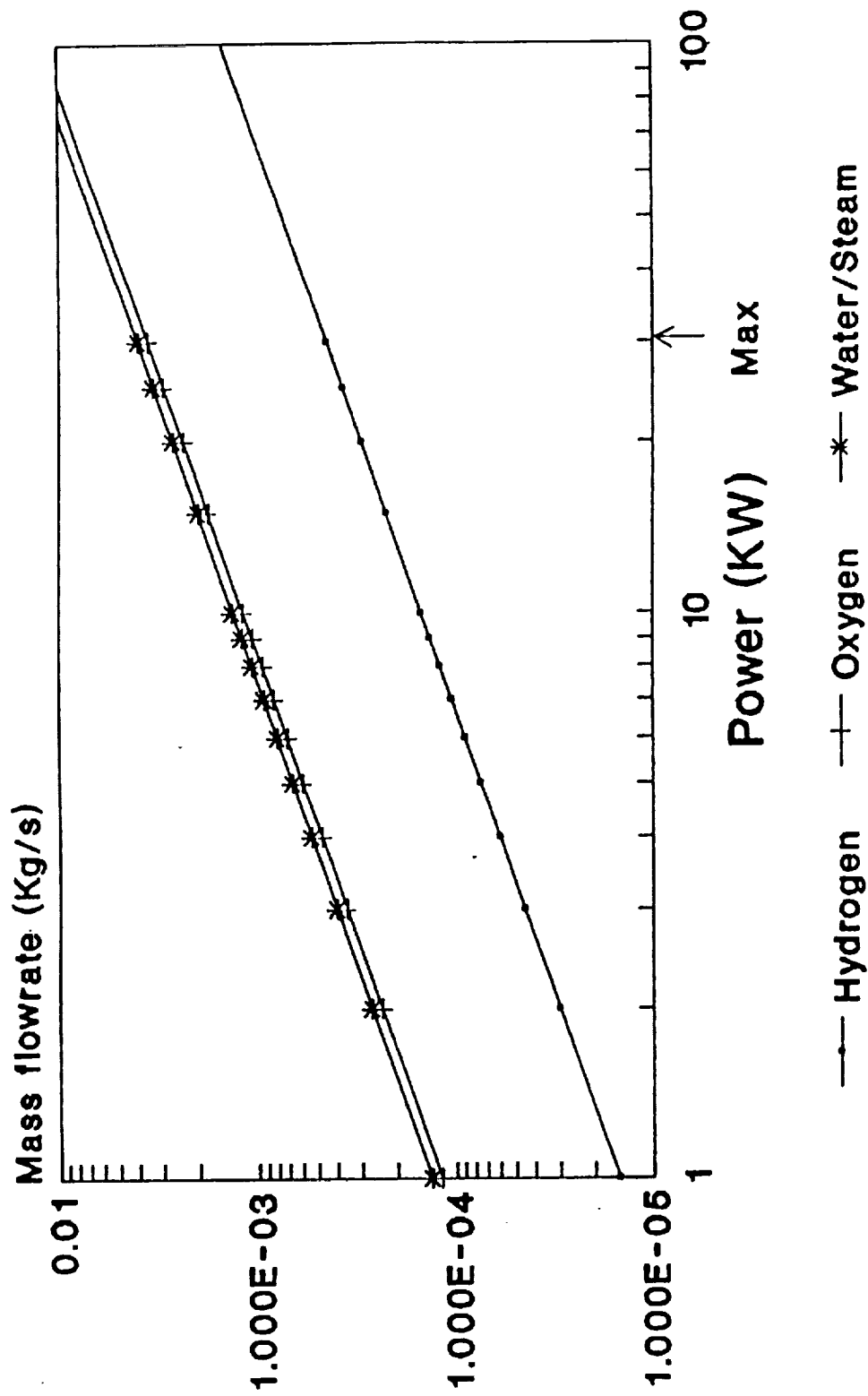


Figure 4.4 Flowrate to power relationship

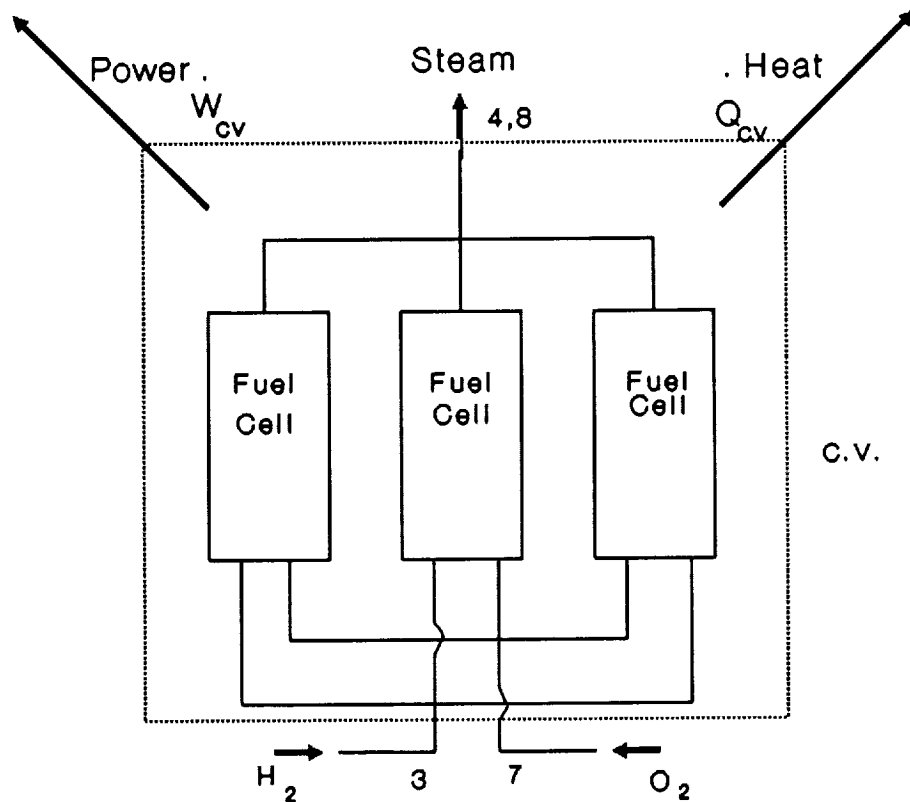


Figure 4.5 Control Volume of Fuel Cell

From the first law equation above (Equation 4.4) it can be seen that the heat generation per cell is -0.4931 kJ/s per cell. For 24 cells, this corresponds to $Q_{cv, total} = -11.83$ kW. This $Q_{cv, total}$ is the heat generated for all 24 cells. Figure 4.6 shows the power output and heat generation vs. fuel (H_2) flowrate. The number of cells chosen was 24; however, this is arbitrary for purposes of total mass flowrate calculations. The overall efficiency may be affected as the number of individual fuel cell units are increased. An overall efficiency of 70% is somewhat optimistic at an average power of 15 kW.

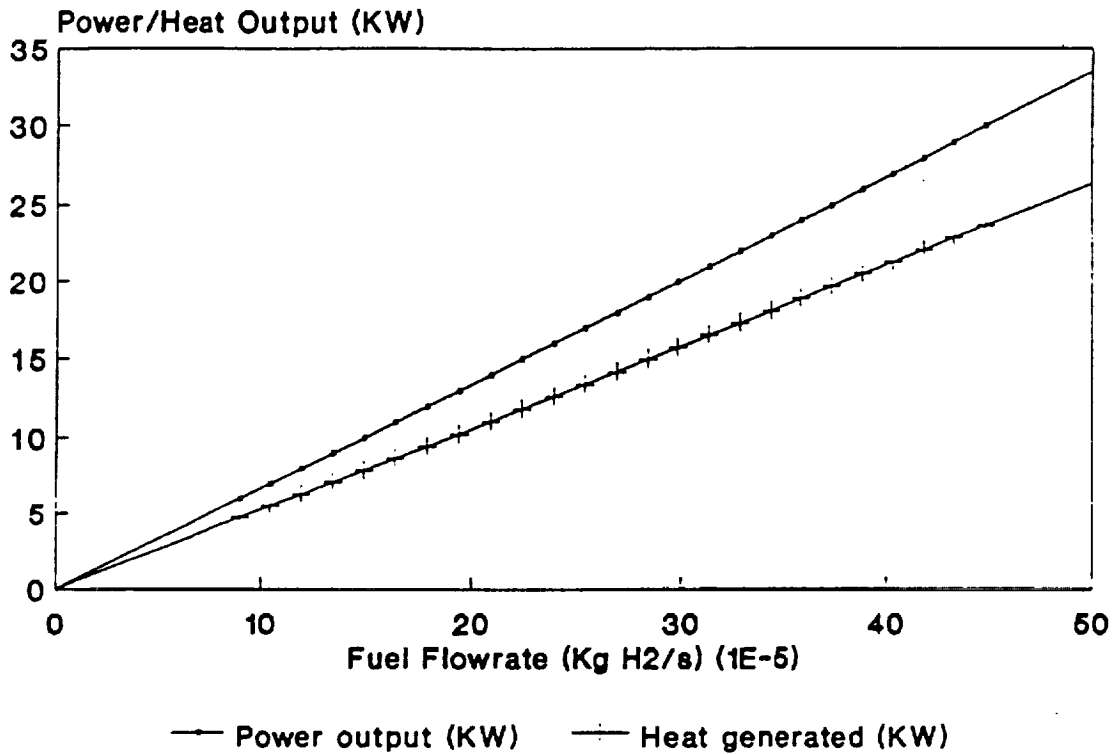


Figure 4.6 Power and Heat Output vs Fuel Flowrate

Shown in Figure 4.7 is a schematic of the overall system detailing the piping of the working fluids throughout the system. States 1 and 5 are the exit states of the reactants from the storage tanks where they are stored at low temperature. The fluids are then expanded at states 2 and 6 where they enter a heat exchanger. In the heat exchanger, the reactants exchange heat with the product of combustion, water, and are superheated to 80°C at states 3 and 7. At this point, the reactants, hydrogen and oxygen, enter the fuel cells, produce power, and combine to form steam, which exits at states 4 and 8. The steam then enters the heat exchanger, cools to a saturated mixture, and then exits at state 9. The remaining steam is then condensed by the heat rejection device and then entered into the water storage tank at state 10. Here, the product is stored for regeneration at a later time.

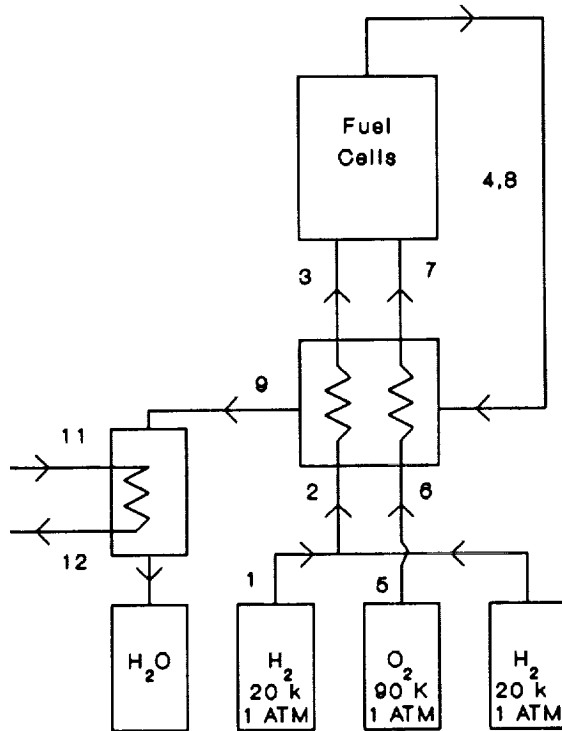


Figure 4.7 Fluid Flow and Thermodynamic States

4.2 HYDROGEN, OXYGEN, AND WATER TANKS

Tanks used to store the reactants and by product of a fuel cell under lunar conditions must be made with several constraints in mind. A gaseous reactant would occupy too much space as compared to the mass of the same reactant under liquid conditions. The problem then arises in the area of maintaining hydrogen and oxygen in their liquid form. This is due to the fact that both hydrogen and oxygen have a very low boiling point. Hydrogen's boiling point is -252.8°C and oxygen's boiling point is -183°C (Reference 17). Since the moon's lowest temperature is never below -180°C , heat would constantly flow into the reactants container. A critical requirement is to insulate around the containers to keep heat gain to a minimum.

In order to design appropriate insulation for the tanks, a worst case environmental condition was considered in the energy balance for the tanks. The inner tank temperature was kept at

below the boiling point temperature of the reactants and the outer surface temperature at a maximum. Since hydrogen has the lowest boiling temperature, an insulation technique which would reduce the heat transfer to a reasonable level for the liquid hydrogen tank would also satisfy the oxygen and water tanks.

Since there is no atmosphere on the moon, the best type of insulation (a vacuum) has been provided. The only forms of heat transfer that need to be considered are radiation and conduction. Since radiation is the more dominant form, a radiation shielding technique needs to be employed. For this project a multi-layer insulator has been chosen.

4.2.1 Multi-Layer Radiation Insulation

Energy from the sun is released as electromagnetic waves that travel in all directions. These waves have a broad spectrum in terms of wavelength. The wavelengths that affect insulation are from the infrared region to the ultra-violet region, including the visible spectrum (Reference 18). Therefore, the insulation materials used should be studied over that wavelength range.

The design chosen for the tanks consists of having a tank with several layers of radiation insulation mounted on its surface, as shown in Figure 4.8. With this set up, the outermost layer will absorb the radiation from the sun and will increase in temperature. The outer layer will radiate energy to the layer beneath it. In this process, every layer will transfer heat to the layer directly below it. This process continues until the heat reaches the surface of the tank. Therefore, by selecting the number of layers and the emissivity of the shielding material, heat transfer can be controlled. By allowing the liquid inside the tanks to boil, the heat gain can be expelled.

The insulation shield would be composed of highly polished aluminum film having low emissivity values. Low emissivity is required because resistances associated with the radiation shield become very large when emissivities are small. This would mean that lower heat is gained by the cryogenic fluid (Reference 18). Also, polished aluminum is currently available with high solar reflectance, good durability, and high flexibility.

A computer program was written to estimate the heat transfer into the tank. In this program, see Appendix D, the number of layers of insulation, the spacing between the layers, and the emissivities were varied. The computer analysis showed that increasing the number of shieldings per unit volume, using a constant emissivity, would decrease the heat gained by hydrogen. Also, increasing the spacing between each shield brought about a larger amount of heat gained by the hydrogen. It would be impossible to reduce the heat transfer to zero having such a large temperature gradient. At least, that would be impractical because

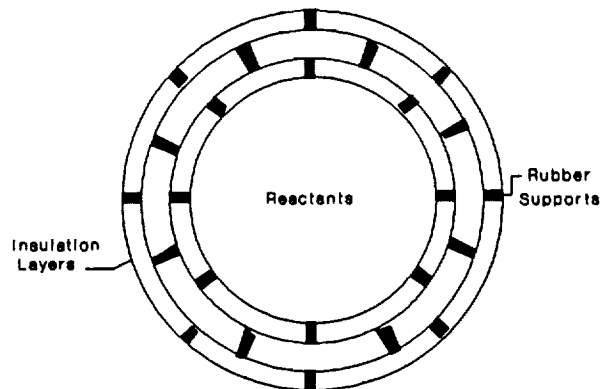


Figure 4.8 Multi-Layer Insulation

such a system would require infinite insulation layers and infinitesimal distance between each shielding.

The principal described above is closely related to the basics of Dewar flasks. An example would be the thermos bottle used to keep beverages hot or cold. Boil off is inevitable and it is directly related to the heat flux which enters the insulation. Heat flux equals the amount of gas vaporized times latent heat of vaporization (Reference 19). Heat gain can be reduced to a minimal amount by selecting the optimal amount of spacing and insulation. Also, not included in the calculation, is the thermal conduction that would take place between the shielding supports. These supports are necessary to prevent the shielding from coming in contact with one another. In order to reduce conductive heat transfer, the supports must have low thermal conductivity, a minimum support area, and long heat path length (Reference 20). A good example of a shield to shield spacer would be a radial bumper. They are insulated bumpers which are mounted between the shielding so as to support the inner and outer vessels (Reference 20).

The assumptions used to calculate the radiation heat flux and boil-off rate are:

- 1) Internal pressure of tanks are at 1 atmosphere.
- 2) Surface temperature of outermost shield is 110°C.
- 3) Temperature of tank is the boiling point of reactant.
- 4) Conduction heat flux is small through the shielding

supports.

- 5) Diffuse heat flux from the moon's surface is negligible compared to heat flux from the sun.

The program calculated the heat flux in W/m^2 for a variable number of shielding layers. This was done for both the hydrogen and oxygen. Using the radiation heat flux formula (Reference 13):

$$Q_{in} = \frac{B (T_2^4 - T_1^4)}{(R)} \quad (4.5)$$

where:

B = Boltzmann's constant,
 T_1 = temperature of the outer shielding
 T_2 = internal tank temperature
R = resistances of the shielding

The radiation gap resistances Q_{in} were calculated. The temperature of the internal tank was set at slightly below the boiling point of each reactant, the hydrogen tank was set at $21^\circ K$ and the oxygen at $90^\circ K$. This criteria served as the determining factor for the radiation heat flux into the tank. The difficulty arose in the determination of the shielding resistance which varied with the number of layers. The shielding was made of highly polished aluminum having low emissivity. The temperature dependance of the emissivity was taken into account in the program. A spacing gap between shielding layers of 0.005 meters was used. The purpose of boiling off fluid is to remove heat added to the tank so that the reactants remain in a liquid state. If boil-off did not occur, then H_2 and O_2 would turn into a gaseous state. Although the total heat flux is caused by radiation and conduction through the shielding supports, this program did not include the conduction term. This was due to the assumption that the heat flux through the rubber bumpers is small compared to the radiation term. However, the conduction error needs further investigation. A graph of the results is illustrated in Figure 4.9 and Figure 4.10.

4.2.2 Tank Sizing

The sizing of the tanks was done using the calculated masses of each reactant needed to provide on-line service for 30 days. The mass of hydrogen was calculated to be 580 kg. Using this data and the density of hydrogen, at its boiling point of $20^\circ K$, a volume for the hydrogen tank was calculated to be $8.055 m^3$. This makes each tank a volume of $4.027 m^3$. Since this volume compared to the oxygen requirement is almost double, the hydrogen was separated into two tanks. Using an oxygen mass of 4605 kg and density of $1190.3 kg/m^3$, at $90^\circ K$, the tank volume was calculated to be $3.86 m^3$. The volume was adjusted to be slightly higher in order to leave a vapor space at the top for boil off to take place. For the Hydrogen

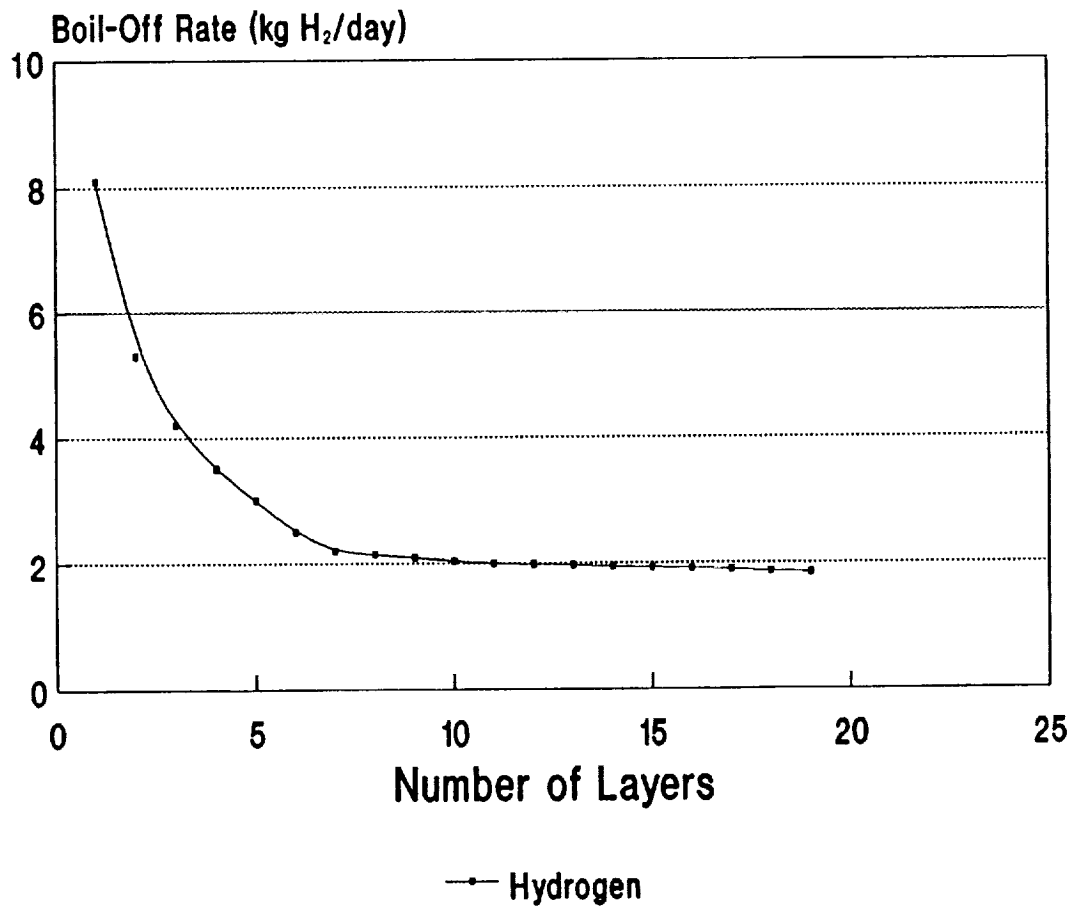


Figure 4.9 Hydrogen Boil-Off Rate

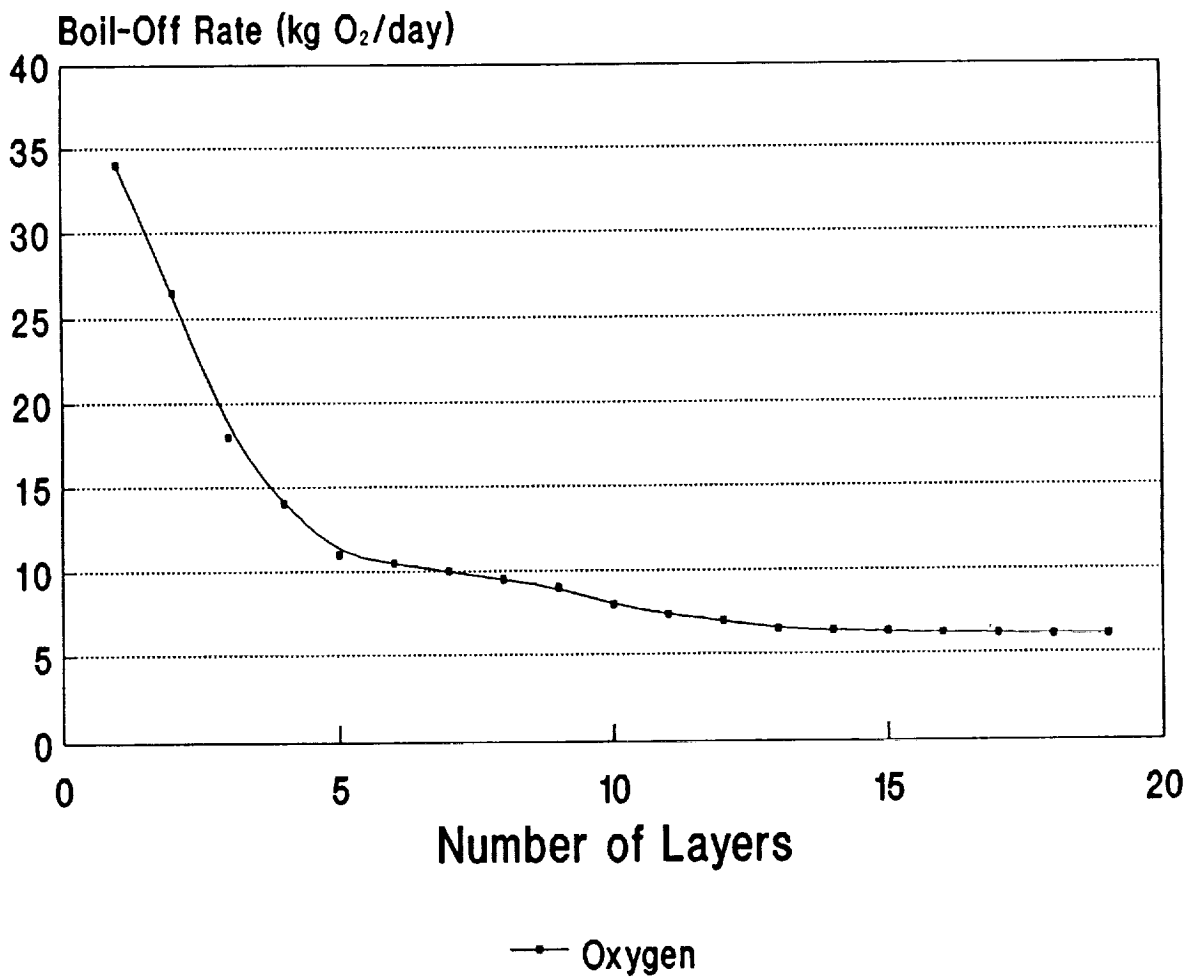


Figure 4.10 Oxygen Boil-Off Rate

tank, volume was increased to 4.5 m³. This yielded a diameter of 1.07 m. This diameter does not include tank shielding. Since the shielding width and the spacing gap was decided to be .005 m this would mean that at 22 shields, the diameter of the hydrogen tank would be 1.5 m. For the oxygen tank the same dimensions were used in the heat flux calculation. Using conservation of mass the volume of the water tank was computed. That is, the combined mass of hydrogen and oxygen gave a total of 5180 kg. The volume was increased slightly to 5.5 m³.

4.3 HEAT EXCHANGE SYSTEM

The primary purpose of heat exchangers is to transfer heat from one fluid to another. The transfer may involve latent heat which is the case for evaporators and condensers, or it may involve sensible heat which is the case for heaters and coolers. Considering water as the primary stream, the other, or secondary fluid stream, has two imposed requirements:

- 1) The heat transfer rate must be the same magnitude (but opposite in sign) to that of the primary fluid stream.
- 2) The temperature differences between the primary and secondary fluid streams must provide the required heat transfer rate.

In the design and analysis of heat exchangers, the aspects of the hot fluid, the coolant, and the heat exchanger structure must be considered individually. The hot fluid gives up heat:

$$\dot{Q}_h = \dot{M} \cdot c_p \cdot (T_{h,i} - T_{h,o}) \quad [W] \quad (4.6)$$

The coolant picks up heat:

$$\dot{Q}_c = \dot{M} \cdot c_p \cdot (T_{c,o} - T_{c,i}) \quad [W] \quad (4.7)$$

The heat exchanger structure transfers heat from the hot fluid to the coolant:

$$\dot{Q} = U \cdot A \cdot \delta T \quad [W]$$

U = overall heat transfer coefficient [W/m² °C]

A = effective heat transfer surface area [m²]

δT = effective mean temperature difference [°C]

Thus, $\dot{Q}_h = \dot{Q}_c = \dot{Q}$

Heat exchangers can be grouped according to the characteristic geometric arrangement between the direction of the flow paths of the two fluids passing through the heat exchanger. They are:

- 1) parallel flow
- 2) counterflow
- 3) cross flow
- 4) multipass

The log mean temperature difference for heat exchangers transferring latent heat as sensible heat to the other stream is:

$$\delta T_{lm} = [(T_{h,i} - t_{c,o}) - (T_{h,o} - t_{c,i})] / \ln[(T_{h,i} - t_{c,o}) / (T_{h,o} - t_{c,i})]$$

T refers to the shell side flow

t refers to the tube side flow

In order to understand the need for a heat exchange system, the condition of the reactants and by-product of the fuel cell process must first be analyzed. The reactants (H_2 and O_2) leave their respective tanks at near their saturated vapor condition. It is desirable to increase the temperatures of these reactants to near the operating temperature of the fuel cells ($100^\circ C$). This is to avoid introducing cryogenic gases into the fuel cells. Also, the water exiting the fuel cells is at a saturated vapor condition. It is desirable to condense this steam to a fully liquid form to conserve space for storage. Therefore, the objective is to develop a heat exchanger which allows energy transfer between the reactants and steam.

4.3.1 Assumptions

- 1) The reactants entering the heat exchanger are at a saturated vapor condition for analysis purposes.
- 2) The by-product of the fuel cell process (H_2O) is at a saturated vapor condition upon entering the heat exchanger.
- 3) The outlet temperature of the reactants is $350^\circ K$.
- 4) Constant specific heats (c_p) are assumed for H_2 and O_2 .
- 5) Heat exchanger efficiency is approximately 95%.

4.3.2 Design Advantages

The heat exchanger will be of a coiled tubular type (Reference 21). The advantages of this design (Figure 4.11) are:

- 1) More than two fluids can be used.

- 2) High pressure and large temperature ranges can occur.
- 3) There is a large heat transfer area.
- 4) The geometry can be modified to suit the requirements (compact design).
- 5) Thermal expansion and contraction can occur without inducing undue stresses
- 6) No vibration problem is encountered.

4.3.3 Heat Transfer Analysis

The required energy transfer to condense the steam is determined by the following (Reference 22):

$$\dot{Q}_h = \dot{m}_h \cdot h_{fg} \quad , \quad h_{fg} = 2257 \text{ kJ/kg}$$

$$(\dot{Q}_h)_{\max} = 11.3 \text{ kW} \quad , \quad (\dot{Q}_h)_{\text{avg}} = 4.514 \text{ kW}$$

The energy removal available in elevating the temperatures of the reactants to 350°K is determined by the following:

$$\dot{Q}_c = \dot{m}_c \cdot c_p \cdot dT$$

$$(c_p)_{O_2} = 0.915 \text{ kJ/kg}^\circ\text{K} \quad , \quad (c_p)_{H_2} = 13.3 \text{ kJ/kg}^\circ\text{K}$$

$$(\dot{Q}_{O_2})_{\max} = 1.055 \text{ kW} \quad , \quad (\dot{Q}_{O_2})_{\text{avg}} = 0.422 \text{ kW}$$

$$(\dot{Q}_{H_2})_{\max} = 2.453 \text{ kW} \quad , \quad (\dot{Q}_{H_2})_{\text{avg}} = 0.981 \text{ kW}$$

Figure 4.12 and 4.13 show heat transfer rates vs. mass flowrates for oxygen and hydrogen respectively. The overall heat transfer coefficient is determined by (Reference 23):

$$U = [(1/a_h) + (1/a_c) + r_h + r_c]^{-1} \quad (4.8)$$

$$a_c = 110 \text{ W/m}^2 \cdot ^\circ\text{K} \quad (\text{film coefficients})$$

$$a_h = 8175 \text{ W/m}^2 \cdot ^\circ\text{K}$$

$$r_c = 2 \cdot 10^{-4} [\text{W/m}^2 \cdot ^\circ\text{K}]^{-1} \quad (\text{fouling factors})$$

$$r_h = 1 \cdot 10^{-4} [\text{W/m}^2 \cdot ^\circ\text{K}]^{-1}$$

$$U = 105.12 \text{ W/m}^2 \cdot ^\circ\text{K}$$

The log mean temperature differences are as follows:

$$(\delta T_{lm})_{H_2} = 121.11 \text{ }^\circ\text{K} \quad , \quad (\delta T_{lm})_{O_2} = 103.79 \text{ }^\circ\text{K}$$

$$\dot{Q} = U \cdot A \cdot \delta T_{lm} \quad \rightarrow \quad A = \dot{Q} / (U \cdot \delta T_{lm})$$

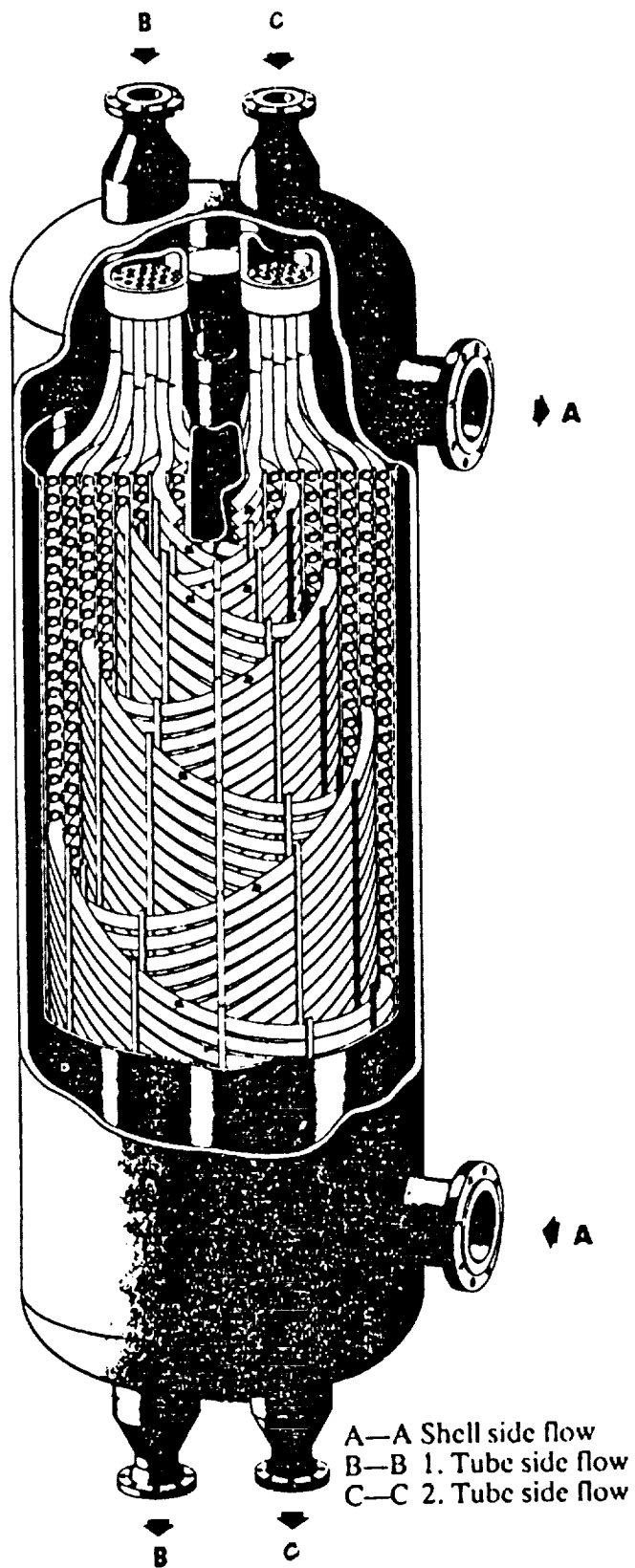


Figure 4.11 Heat Exchanger

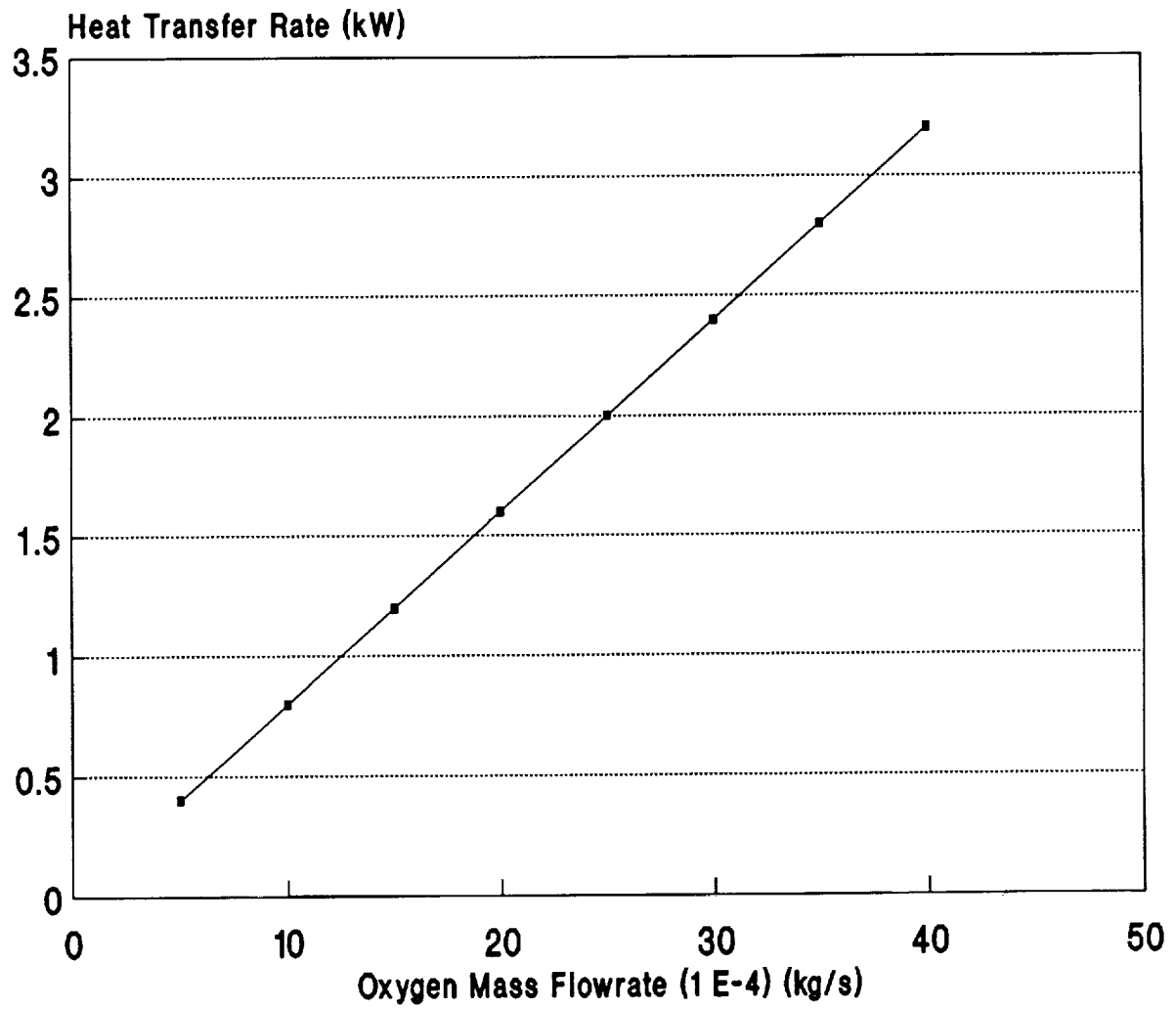


Figure 4.12 Oxygen Heat Transfer to Mass Flowrate Comparison

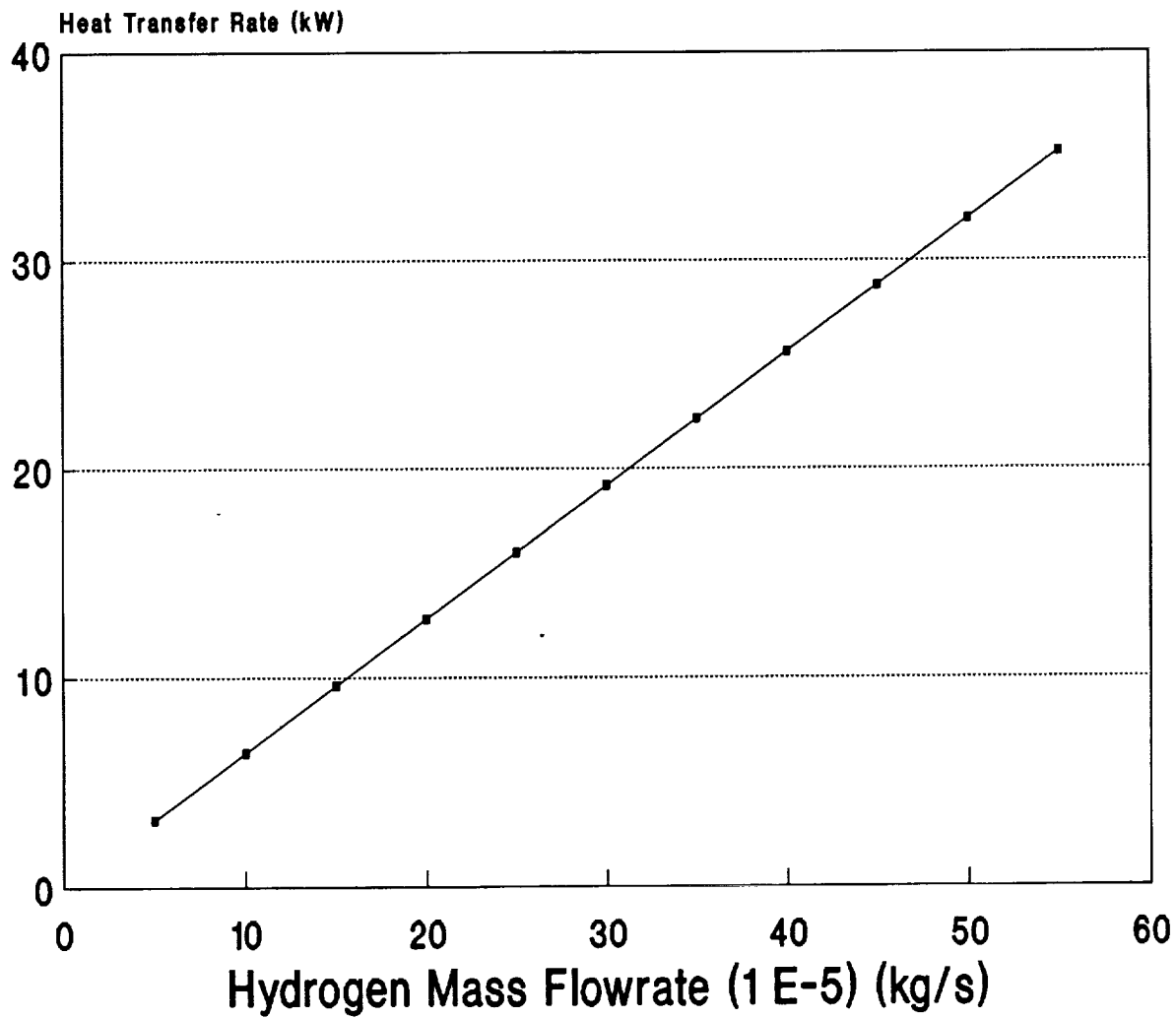


Figure 4.13 Hydrogen Heat Transfer to Mass Flowrate Comparison

The required areas are as follows:

$$\begin{aligned} A_{H_2} &= 812 \text{ cm}^2 && \text{(under max. conditions and 95\% efficiency)} \\ A_{O_2} &= 408 \text{ cm}^2 \end{aligned}$$

It is determined that if the hydrogen temperature is to be increased to the desired temperature, an enthalpy change of 490.54 kJ/kg will occur in the steam. Also, if the oxygen temperature is to be increased to the desired temperature, an enthalpy change of 211.11 kJ/kg will occur in the steam. This total of 701.65 kJ/kg of enthalpy change is not sufficient to fully condense the steam. The steam exits the heat exchanger at a quality of 68.9%. Final condensing of the steam is left to the heat rejection system. The energy rejected is 7.8 kW (average).

4.3.4 Materials

The tube material is to be of a 36% nickel steel, also known as Invar. It was chosen due to its low thermal expansion characteristics (Reference 24). The casings will be made of stainless steel. It was chosen due to its strength and resistance to the harsh conditions of the lunar environment.

4.3.5 Problems and Solutions

A major problem which may occur in the heat exchangers is a "hydrogen attack" on the tube steel. Hydrogen atoms may permeate the steel and combine with the carbon atoms to form methane pockets which can accumulate in voids. This can cause the tube surface to lose strength and hardness and promote ductility (Reference 23). Carbon dioxide may also form due to this process. A system which removes undesired gases may be needed to eliminate this problem.

Contaminants can pose a problem at the point where the outer pipes connect to the heat exchanger. A method of keeping lunar dust out of these areas is needed.

Precise analysis of the coiled tubes must be done. Stress analysis and calculation of exact heat exchanger efficiency is needed to assure that the required effects are achieved.

Possible shielding of the heat exchanger must be addressed since it may be exposed directly to the sun's rays. Multi-layered shielding such as those used for the tanks are very effective when subjected to a high vacuum, in reducing the heat input (Reference 13). This additional heat to the steam due to the incoming heat load places additional requirements on the heat rejection system.

The decarburisation of the steel can cause problems. It must be determined if this process is fast enough to cause system failure before the mission of the LCUV is completed. Other materials may be required.

4.4 ELECTRICAL AND CONTROL SYSTEMS

The fuel cell along with its associated parts require a highly reliable control system. Because of its configuration, the fuel cell should be as maintenance free as possible. The control system under study for the LCUV monitors temperature, pressure, flow rate, voltage, and current. Using the signals from all sensors, the controller insures proper operation at all times. The controller will also be equipped with a digitized communication capability to receive and send data to and from the earth. This will allow earth based operators to override the automatic systems if necessary.

A simplified block diagram of the power supply system is illustrated in Figure 4.14. In this figure some important variables for each component are indicated.

4.4.1 Temperature Control

Temperature is a critical variable that needs to be controlled in the tanks as well as the fuel cells. Since the heat flow penetrating into the reactant tanks is dependent on the outer surface temperature, these temperatures should be monitored closely to track the boil-off rate. By attaching an array of thermocouples to the surface of the tanks and insulators, the task of monitoring the boil-off rate can be accomplished. An analog to digital convertor would convert the continuous signals from the sensors to digital data. These data can be used by the main microcontroller to send commands to the flow actuators for proper operation. The pressures inside the tanks are functions of the temperatures, and the temperatures are functions of the incoming heat flux. If the pressure is kept constant, the liquids will boil at a constant temperature. Therefore, by keeping the inside pressures of the tanks at constant elevated pressures minimum boil-off rate can be achieved.

The temperature of the fuel cell is an important parameter in terms of efficiency. The fuel cell walls are equipped with coolant pipes for heat removal. The coolant fluid is linked to the heat rejection bus pipe. By controlling the mass flow rate of the coolant, the temperature of the fuel cell can be kept within a tolerable range. Again, thermocouples can be employed to monitor the fuel cell temperature and the bus coolant temperature. For the case where the coolant temperature is below the required fuel cell temperature, coolant valves can be opened as needed. However, in the case where the coolant bus temperature is above or close to the fuel cell temperature, the microcontroller will limit the reactant flow to reduce heat generation within the cell. This can be viewed in Figure 4.15.

Storage of the water produced by the fuel cell requires close attention. The water leaving the fuel cell is in a vapor state. To minimize space, water should be kept in liquid phase. As

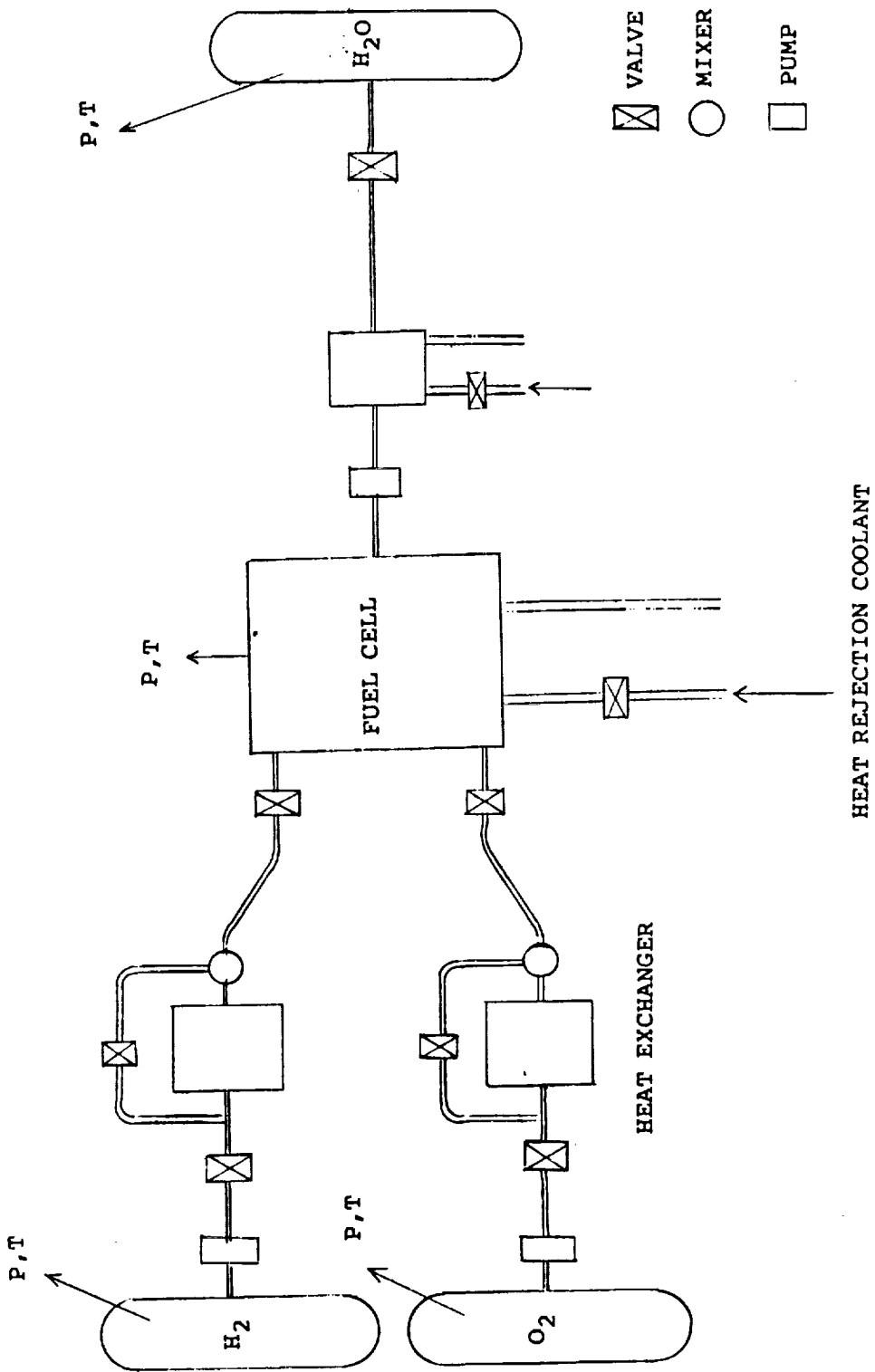


Figure 4.14 System Control Requirements

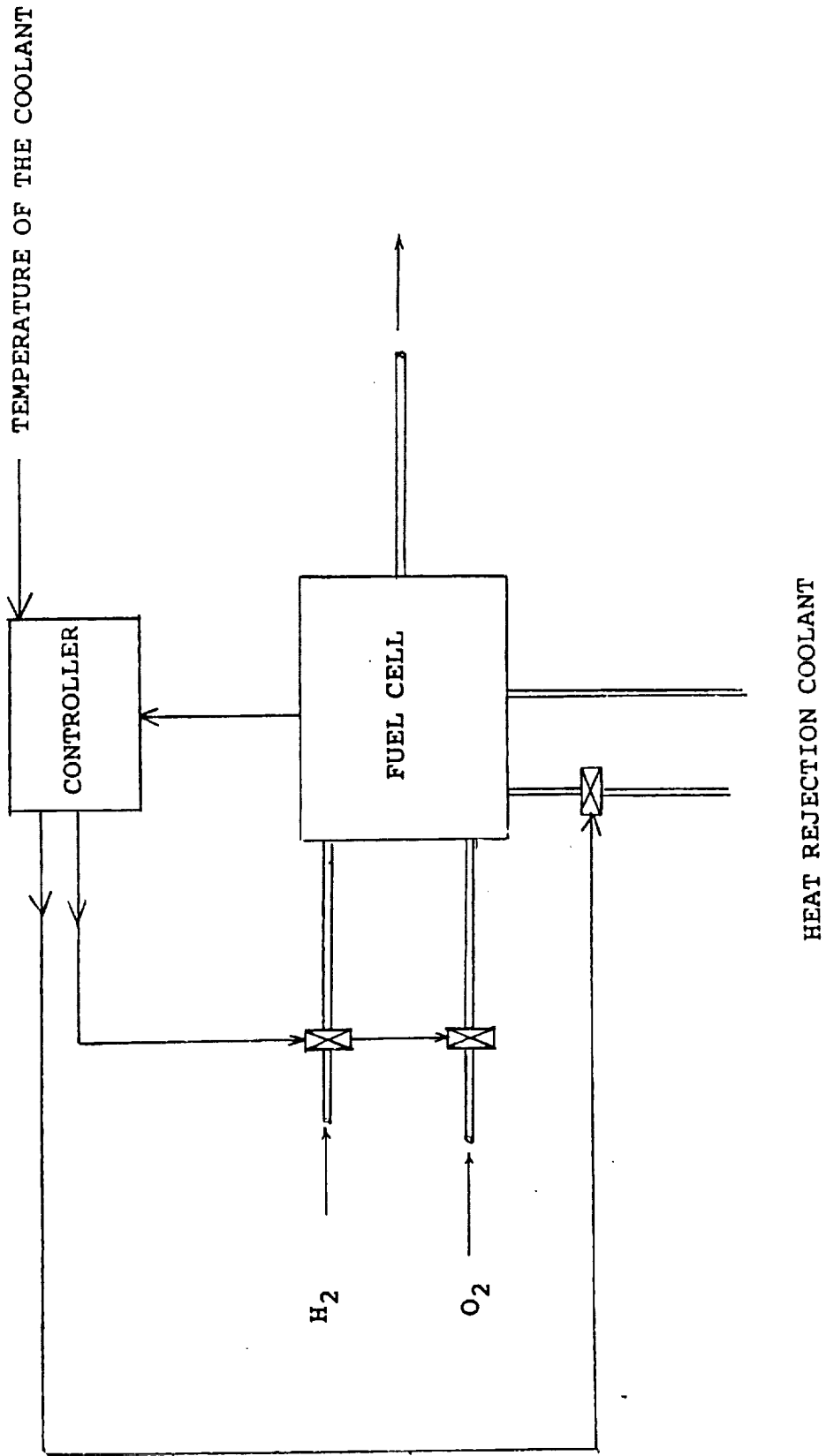


Figure 4.15 Fuel Cell Control

mentioned in the previous sections, the heat would be transferred from the steam to the cold gases. In this process the steam is partially condensed and the gases are heated to the operating temperatures. The water is further condensed using the heat rejection fluid. Again, the controller has to monitor the temperature to assure proper condensation. When the temperature of the gases rise above the required level the flow of the gases is bypassed from the heat exchanger as shown in Figure 4.14. This will maintain the efficiency of the fuel cell within limits and reduces the chances of overheating.

4.4.2 Pressure Control

Pressure is another important parameter in proper operation of the fuel cell. A high pressure in the fuel cell can force reactants through the membrane without combusting. A low pressure level, on the other hand, would not supply enough reactants for a given power requirement. Proper water-vapor pressure needs to be maintained to transport the reactants (Reference 13). One of the tasks of the controller unit is to regulate pressures within the fuel cells by actuating proper pumps and valves.

In the reactant tanks a pressure sensing device should be installed to keep the pressure below a critical level. The high pressure limit depends primarily on the construction of the tanks. A relief valve would release excess pressure into space in an emergency situation. The same principle applies to the water tank. Diaphragm type pressure sensors can be utilized for most applications. Strain gages can be attached to the tanks surfaces as a mean of pressure measurement.

The internal sensor set-up of the tanks is illustrated in Figure 4.16. The temperature and pressure sensors are in the gaseous volume. The amount of reactant used can be monitored by using a flow meter. However, a level indicator has been provided for safety. In case of power interruptions the electronic system may lose its memory. A direct level indicator does not depend on the memory.

In situations where power consumption is at minimum, the reactant used is only dependent on the boil off rate. In the case where more power is needed, a scheme should be employed to deliver more reactants to the fuel cells. One method would be to covert the liquid to a gas as needed. This is accomplished by installing a heating element in the tanks. As more reactant is needed, the controller allows current to flow through the element, thus adding heat to the tanks.

In the above mentioned technique, the system tends to respond slowly. If a current surge is needed, such as when the LCUV lifts up a load, it would take a relatively long period of time for the controller to sense the need for more current and to increase the

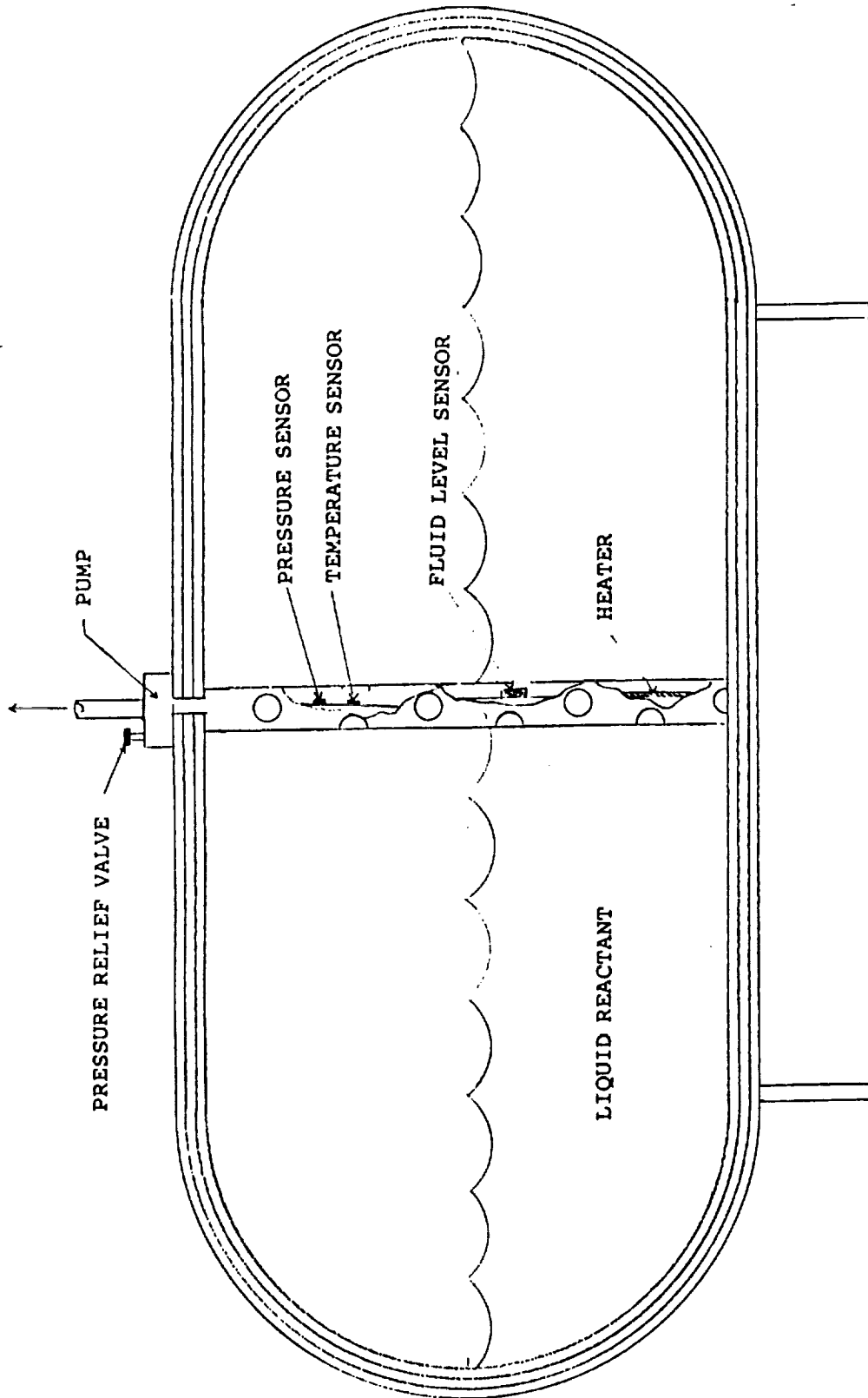


Figure 4.16 Reactant Tank Monitoring System

current through the heating coils. The gas would still need to travel through the tanks to get to the fuel cell. One method of solving this problem would be to install a charging battery bank to supplement the fuel cell supply.

4.4.3 Current and Voltage Considerations

When calculating the volume of the reactants, it was found that the reactant tanks would be fairly large in comparison to the LCUV. This requires the tanks to be mounted on a separate carriage that would be attached to the LCUV. Since the heat rejection system is already contained on a separate carriage, it was decided to combine the two into one independently mobile unit. This posed further problems to be addressed. Two options were considered.

The first option is to put the tanks on the carriage and the fuel cell on the LCUV with the reactants, water, and control lines extending from the carriage to the LCUV. The other option is to put the tanks and the fuel cell both on the carriage with only the power cable extending from the carriage to the LCUV.

In studying the options, it was decided that the second one has more advantages. If the tanks are separated from the fuel cell the three hoses carrying sub-cooled hydrogen, sub-cooled oxygen, and saturated water vapor will have to be extended from the carriage to the LCUV. In addition to adding heat to the system by exposing the hoses to the radiation from the sun, the LCUV has to waste energy to move the hoses while moving. In the second option only the power cables will link the power system to the LCUV.

If the fuel cell voltage is taken to be 24 V, for a maximum power of 35 kW, the maximum current in the cables is 1458 A. If copper is used as transmission line, the resistance of the wire at 150°C is $S = 26.44$ nano ohms/m. For a length of wire of 10 m and assuming a 200 W loss in one wire, the total resistance of the wire is:

$$R = W/I^2$$
$$R = 9.4 \times 10^{-5} \text{ ohms}$$

Therefore, the cross sectional area of the wire can be calculated from:

$$a = S L / R$$
$$a = 28.11 \text{ cm}^2$$

This will give a radius of 3 cm. A wire with such diameter would be very difficult to manage. However to overcome this problem a voltage boosting technique can be used. With this method, if the voltage is boosted to 5000 V, using the same calculations, only 7 A is carried by the wires. This reduces the wire diameter to about 0.3 mm. It can be seen that this method reduces the link between

the carriage and the LCUV to two wires of 0.3 mm in diameter.

The voltage boosting technique is a well known practice. Almost all power companies use this scheme to transfer power to their consumer homes. In fact it would be impractical to do otherwise. The problem would be to transform the low voltage of the fuel cell to a high voltage. This can be accomplished by the use of transformers. A transformer can either step up or step down an incoming alternating current. Since the fuel cell supplies a DC voltage, a device can be used to convert the DC signal to an AC signal using SCR technology. Other advantages of the AC signal on the LCUV would be voltage flexibility. Without AC only the 24V supply is available on the LCUV. With AC, different transformers can be used to generate different voltages. A general block diagram of such system is illustrated in Figure 4.17.

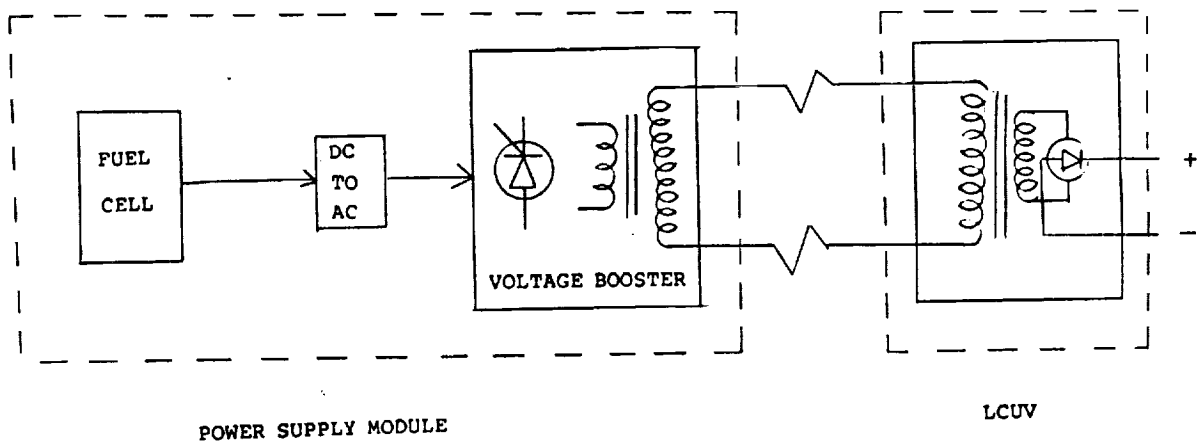


Figure 4.17 Power Transfer System Elements

In the above mentioned method, the LCUV is totally dependent on the fuel cell supply. A back-up system should be available on the LCUV in case of emergencies. This can be accomplished by installing an array of rechargeable batteries on the LCUV. Several types of rechargeable cells were studied. Among those are the Nickel-Hydrogen and Nickel-Cadmium sealed batteries. The Nickel-Hydrogen cell has a relatively high power density, but its efficiency reduces at higher temperatures. Nickel-Cadmium has a lower power density but it can operate at higher temperatures (Reference 15).

5.0 HEAT REJECTION SYSTEM CARRIAGE & STRUCTURE

The only way to release heat in a lunar environment is through the use of a radiator. This method of heat rejection is discussed in this and the following section. To optimize the operation of the LCUV, a logistics trailer is designed to be used for housing the power supply and the heat rejection system. In order to supply coolant fluid and power to the LCUV from the carriage, a telescoping truss structure is incorporated to support the lines. This carriage and structure is conceptualized in this section.

5.1 ASSUMPTIONS AND CONSTRAINTS

The Daytime Heat Rejection carriage is designed to be twice the size of the construction vehicle. This assumption of a six meter by six meter and three meter deep vehicle is to allow for added stability and utility.

Another major assumption is that when the radiator is fully deployed it will remain stationary in a predetermined location during a particular operation. This stationary configuration however, requires a collapsible truss type system to couple the radiator to the LCUV. This collapsible truss system will allow the LCUV to operate in a predetermined radius around the radiator and also provide protection for the lines which will carry the fluid and power to the radiator and its carriage.

There is also a weight limitation which must be placed on the heat rejection unit. An assumption that must be made is that the weight of the radiator carriage unit can be reduced through improved design and materials in the near future. This will become an important factor if the system is to be deployable.

5.2 CARRIAGE CONFIGURATION

An important consideration in the configuration of the carriage is stability. The effect of a rotating radiator on the ability of the carriage to resist an overturning moment must be taken into account. If the center of gravity of the radiator extends out over the wheels of the carriage, the resulting moment will overturn the carriage and could destroy the system. For this reason, the center of gravity of the radiator and carriage should be kept as low as possible to help prevent overturning.

Another way that overturning can be prevented is by the use of retractable supports very similar to those used on fire trucks and construction equipment. These retractable supports will lower themselves when the radiator is in the process of being deployed to insure stability. The supports should lift the wheels off of the lunar surface to provide a wider base of support.

The internal arrangement of the radiator carriage requires

further analysis by future design groups, currently, the top 1.5 meters of the six meter high vehicle will contain the subsystems for the heat rejection unit. The lower 1.5 meters will contain the fuel tanks and fuel cells required to power the entire LCUV system. This arrangement has been discussed with the group designing the fuel cells and was accepted.

The top portion of the LCUV carriage will house the pump, two concentric ringed turntables, coolant reservoir, turntable drive motors, and the collapsible truss. The exact placement of these specific devices will require further study. The tentative design is shown in Figure 5.1.

The concentric ring turntables allow the collapsible truss and radiator to turn freely and independently, thus allowing the LCUV to work in a full circle around the stationary radiator and carriage system. These turntables will be motor driven and sealed to prevent penetration by dust particles. Future design work is required in these areas. The use of a torque box, a centralized C-channel frame, is suggested in order to transmit the loads on the structure to the frame.

5.3 LOCOMOTION SYSTEM

The size and complexity of the heat rejection unit necessitates the use of a passive locomotion system during operation of the LCUV. The unique lunar conditions demand the following requirements from the locomotion system.

- Reliability
- Mechanical Simplicity
- Efficiency
- Traction
- Stability

A single design that has all of these characteristics is not available. Therefore, a design which satisfies a majority of the requirements will have to be chosen. At the beginning of the semester two possible locomotion systems were being examined for use on the heat rejection unit. One choice was to use a wheeled system while the other choice was to use a track system similar to the propulsion system used on the LCUV. Therefore, an investigation into the advantages and disadvantages of each system is presented below. Prior to investigating each system, it is necessary to explore the lunar soil conditions in which the locomotion system will be required to operate.

Soil samples obtained from the Apollo Missions indicate that there is a mixture of "weak" and "firm" soil properties on the moon. The differentiation between weak and firm soils is made on the basis of the cohesive forces and internal friction which binds the soil together. Cohesion is simply a measure of the sticking

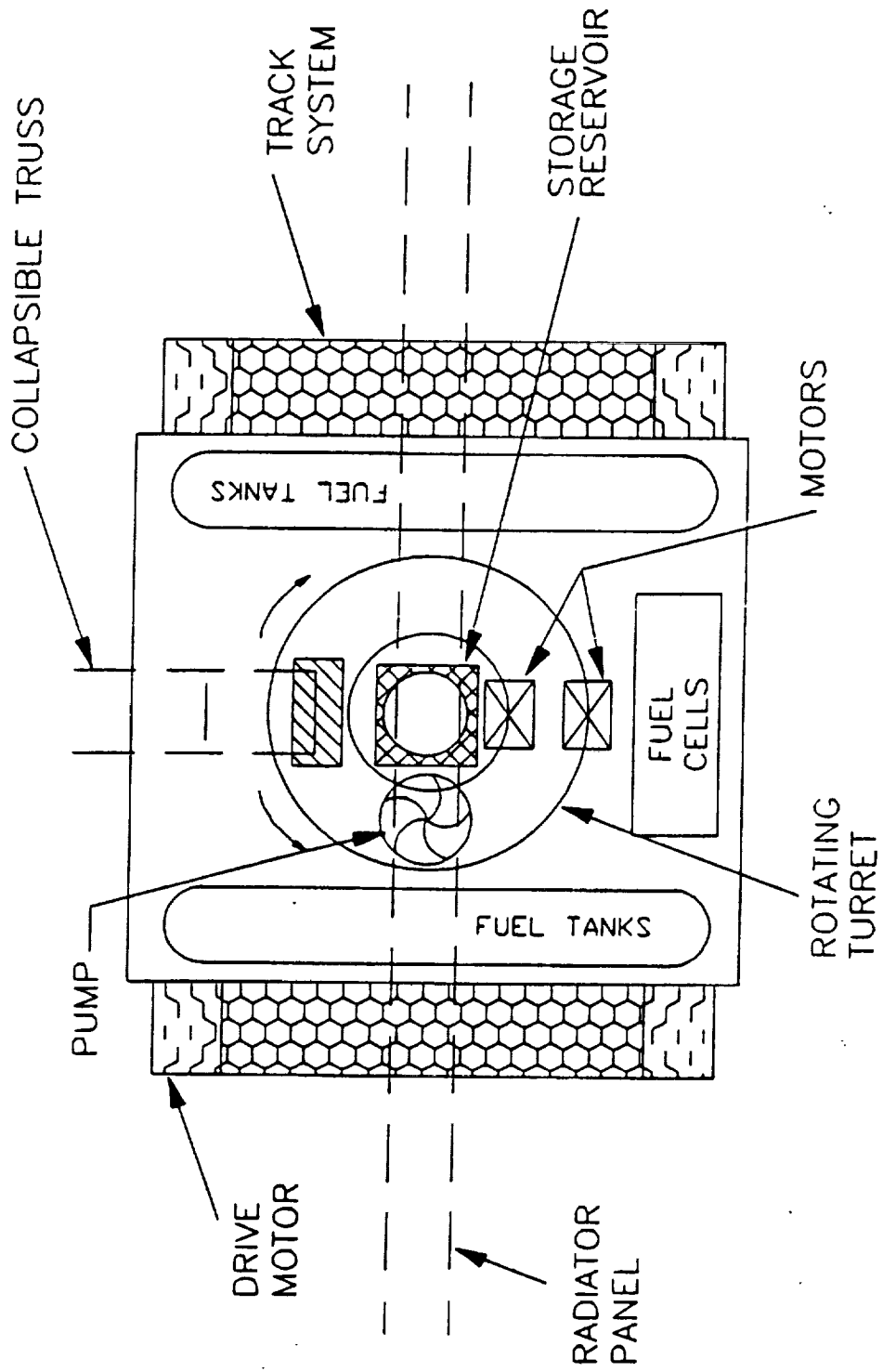


Figure 5.1 Top-Sectional View of the Heat Rejection System

power of the soil, while the angle of internal friction is a measure of the frictional force the soil offers. Table 5.1, from McAdams, Reese and Lewandowski (Reference 25) contains the lunar soil data.

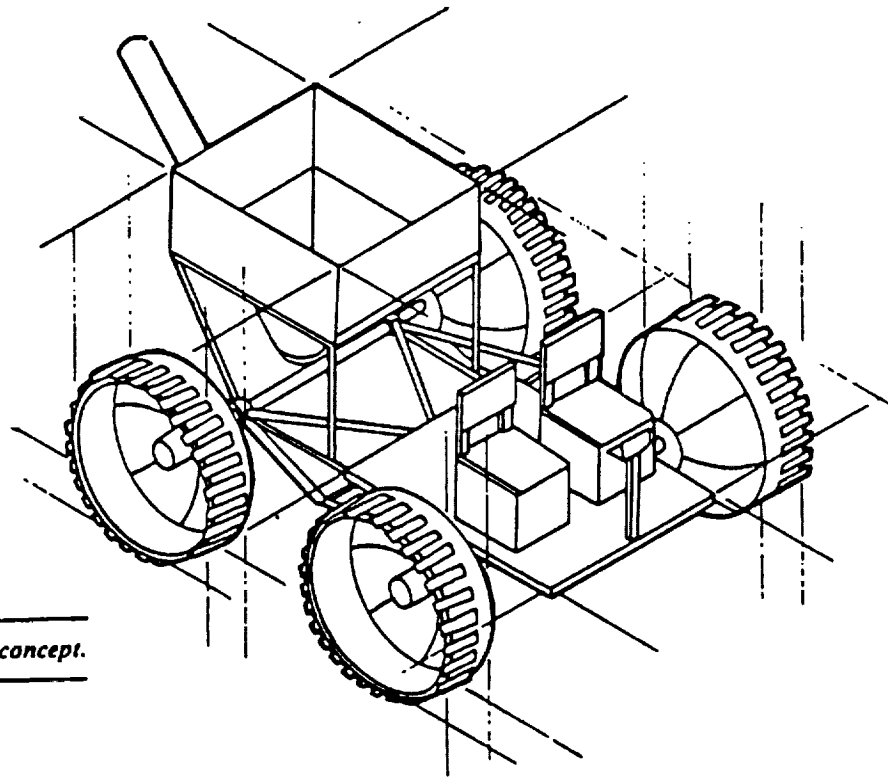
Table 5.1 Lunar Soil Data

	Cohesion kN/m ²	Internal Friction Angle Degrees
Weak Soil	0.36	35
Firm Soil	1.42	45

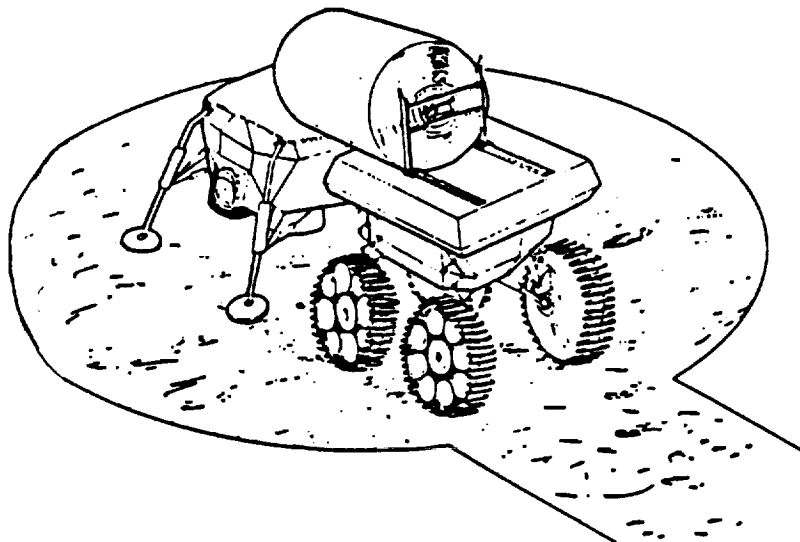
The dimensions of either a wheeled system or a track system must be based on the mechanics of weak soil in order to produce a design that is appropriate for the worst case.

The first candidate under consideration, shown in Figure 5.2, was a wheeled system constructed of either a metal rim/rubber tire configuration or an entirely metal wheel design (Reference 26). For clarity, a metal wheel is simply a rim/tire design that is constructed entirely of metal. The outer surface of the wheel has ridges which protrude from the rim in order to provide traction. Metal wheeled vehicles are frequently used in landfills where traction is difficult to attain for obvious reasons. The term "rubber tire" is somewhat deceiving since the tire used in lunar applications are not the same as ordinary street tires. The tires are either constructed of solid rubber or they are filled with a rubber gel since a punctured tire in a vacuum would result in a complete failure. A wheeled system also has the advantage of being light weight in comparison to a track system. However, the system does have the disadvantage of limited surface area contact, which is vitally important to the stability of the heat-rejection carriage. Also, fine particles of dust would impregnate the bearings that are a necessary part of a wheeled system. Finally, with bearings it is necessary to provide lubrication so the bearings will not seize inside the retaining cup. Lubricants are susceptible to breakdown in the harsh lunar environment, which would result in failure.

The second candidate under consideration was a track system similar to the design chosen for the LCUV; refer to the **Track Construction Section**. The two main disadvantages of a track system are the increased mechanical complexity and power drain that the system will place on the LCUV. The track system produces problems during turning maneuvers and a separate motor/control system may be necessary to turn the heat-rejection unit at the same rate as the LCUV. However, there are a host of advantages that make a track system feasible. First, the system has been chosen for the LCUV. and the design can be adapted directly to the heat rejection unit.



Lunar truck concept.



A logistics module is unloaded from a landing craft.

Figure 5.2 Wheel Based Locomotion Systems

Additionally, the parts will be interchangeable with the track system for the LCUV. Therefore, when astronauts are finally stationed at the lunar base, repairs to both the LCUV and heat rejection propulsion systems can be accomplished with the same parts. Another advantage is the large "footprint" or surface contact area that the tracks provide, this allows the large weight of the heat-rejection unit to be spread out evenly over a large area. The distribution of the weight over a large area has two major implications. First, this provides much needed stability for a structure that is in excess of fifty feet tall. Second, the distributive action of the tracks keeps the heat-rejection unit from sinking into the soft lunar soil. Finally, tracks have proven to be a strong, all terrain means of locomotion on tanks and other military vehicles that are subjected to harsh conditions. Therefore, based on the consideration of the advantages and disadvantages of each system, tracks seem to be the logical choice.

5.4 TELESCOPING STRUCTURE

At the beginning of this project, two different radiator/carriage configurations were under consideration. The first system consisted of a "piggy back" radiator which was permanently mounted on the back of the LCUV. The second design called for a detachable carriage to be towed behind the LCUV during daytime operation. With this design the radiator could be detached from the LCUV during nighttime operation when the radiator was not needed, resulting in increased mobility and decreased power drain from towing unnecessary weight. At this stage of development it was believed that the radiator would have to dissipate 12-18 kW of heat. Preliminary calculations showed that the radiator surface area was too large for a permanently mounted system. Therefore, the "piggy back" system was discarded and the conceptual design continued on the basis of a detachable radiator.

Further investigation by the radiator design group revealed that the power dissipation requirements could increase from 12-18 kW to 100 kW. These new requirements drastically increased the radiator size and it was decided that the heat rejection system should remain stationary while the LCUV works. It was decided that in order to satisfy this requirement, a telescoping arm would have to be developed to connect the LCUV and heat rejection unit. The focus of the carriage group's work then shifted from a locomotion system to designing a telescoping arm. The conceptual designs that have been considered are discussed below.

The first telescoping arm design considered was a deployable and retractable truss structure shown in Figure 5.3 (Reference 27). This truss was designed for use in deploying large space antennas from the space shuttle and retracting the antenna when operation is complete. The structure consists of a deployable mechanism which unfolds into a triangulated truss. The structural members are double tapered graphite-epoxy tubes which exhibit a high

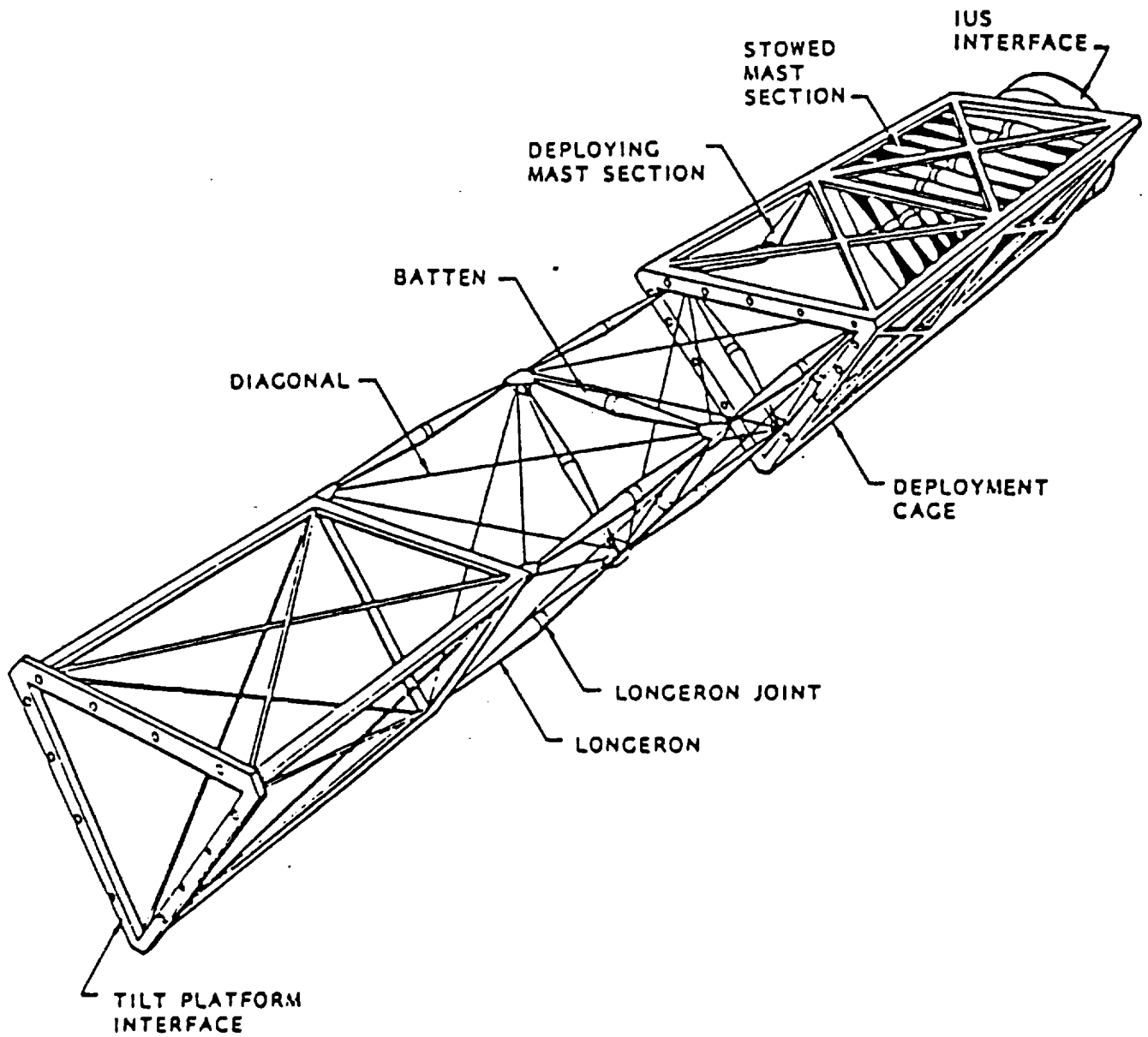


Figure 5.3 Deployable/Retractable Truss

strength/weight ratio. The truss design has the capability to extend to a length of 122 meters, when it is composed of 40 bays and has a mass of 172 kilograms. The device stows to a height of 3.32 meters (Reference 27). The truss is driven from a cage by means of a motor/pulley system which deploys/retracts one bay every two minutes. Consultation with Dr. Mason Chew revealed that the motion of the truss could not be sufficiently regulated by a control system, and the structure was not strong enough for its intended use. The retractable truss also has the disadvantage of limiting the motion of the LCUV. Also, the rate of deployment/retraction was too slow to be of benefit. Therefore, this conceptual design was discarded and the search for a new design began.

The second arm design under consideration involved the use of sleeved cylinders that extend outward as the LCUV moves away from the stationary radiator (Figure 5.4). The arm itself would provide the protection for the fluid and power lines which would lie inside of the hollow interior. A spool inside of the heat-rejection unit, consisting of runners and torsional springs, was intended to store the additional lengths of fluid and power lines necessary for operation when the arm was extended. A canopy or shielding for the arm is also being considered since heat could be transferred to the fluid lines from the surroundings.

Preliminary calculations for a beam geometry have been based on a simplified model of a beam fixed on both ends with a distributed load over the length of the structure. The loading is based on the structure's own weight and the weight of the cooling fluid inside the beams. The loading has been adjusted for the decreased gravity on the moon. Rough calculations have shown that cylinders may not be the best geometric shape to choose. For example, a square beam provides a greater moment of inertia thereby reducing the amount of deflection and increasing the working length of the beam. Similarly, another telescoping arm design under consideration involves the use of sleeved hollow square beams. However, the square beams require more storage area.

In either case, sleeved cylinders or square beams, the end points of the arm are based on a pivoting and rotating base which allows for maximum maneuverability of the LCUV. The arm needs to be as long as possible while still being able to provide structural stability. The structure must be capable of withstanding the distributed load of the fluid lines and an axial force applied by the LCUV.

A computer program, contained in Appendix E, has been written to assist in the calculation of deflection and stresses in both a round and square beam geometry. The graphs generated from the computer program data are a representation of the deflection and stresses in the beams. The sleeved beam design was eventually

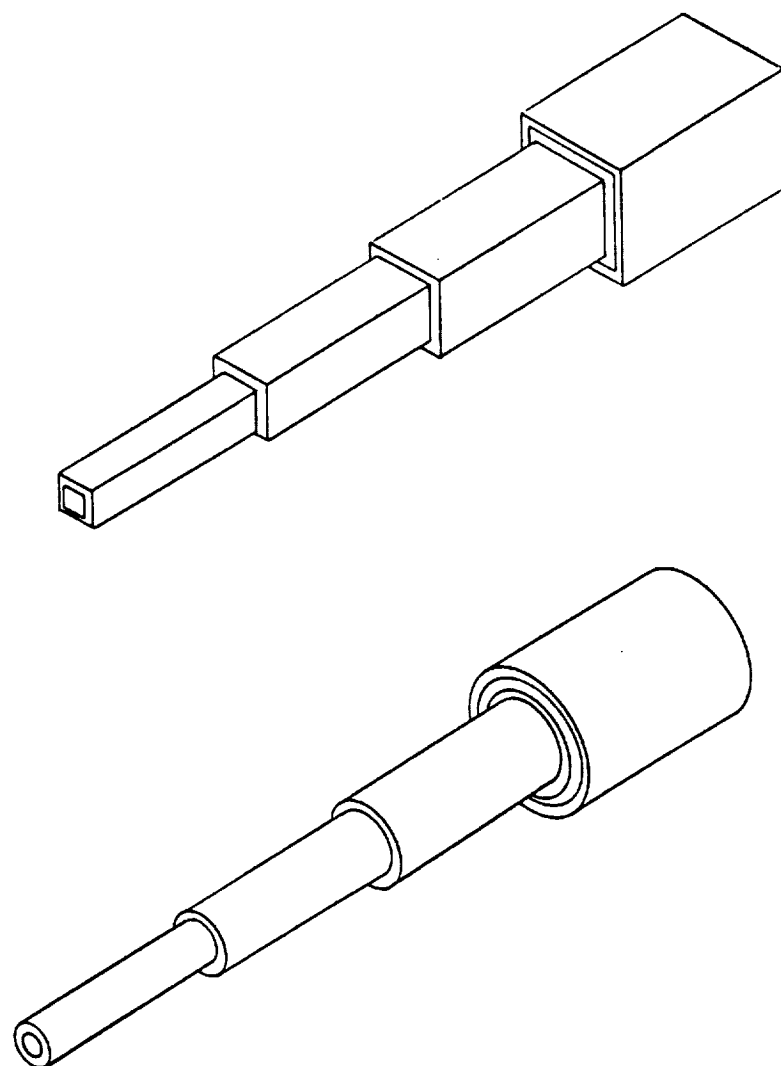


Figure 5.4 Sleeved Beam Structure Design

abandoned because of the possibility of jamming the telescoping arm when the LCUV was at an odd angle with respect to the heat-rejection unit. Jamming the telescoping arm would render the LCUV inoperable and this was a possibility that could not be accepted.

The final design under consideration was a variation on a fire truck extension ladder. The system was observed at Fire Station One in Norfolk Virginia, so that the feasibility of such a design could be assessed. The ladder itself possessed many of the qualities that were necessary to satisfy the design requirements for application to the LCUV and heat-rejection unit. Additionally, a telescoping aluminum cylinder device for transporting water to the top of the ladder was discovered. The feasibility and utility of this device are also discussed in this report. The extension ladder, also referred to as an aerial, was produced by Emergency-One, a safety vehicle manufacturer located in Ocala, Florida.

Members of the carriage and telescoping structure group visited the Emergency-One facility to gain information about the extension ladder. The following is a series of topics concerning the ladder performance and their relevance to the design of a collapsible structure for the heat rejection unit.

5.4.1 Maximum Elongation and Loading

For a 110 foot long Emergency-One ladder at full extension and zero degrees inclination (horizontal) under an 800 pound point load at the free end, the maximum deflection is 18 inches (Reference 28). For application to the heat-rejection unit, distributed loads are more of a concern than point loads. The distributive loading consists of the structure's own weight, along with the weight of the fluid and power lines. Also, for the LCUV the extension ladder will be supported at each end, thus deflection will occur in the center and not at the end. Due to this fact, greater extension lengths may be achieved. Finally, the entire structure is designed on the basis of a factor of safety of three (Reference 28).

5.4.2 Structure

Engineer Jeff Aiken of Emergency-One stated that the structural content of the ladder was based on minimizing deflection. The hand railing and base bars mainly resist horizontal and vertical deflections, while the K-bars on the bottom of the ladder resist torsional deflections. The overall structure, hand rails, base rails, and K-bars are all shown in Figure 5.5. The Emergency-One design is not based on an efficient strength to weight ratio. The majority of the design is based on a compromise between utility and ease of manufacturing. As production is not a concern for the LCUV project, certain parameters may be redefined to achieve a desired strength to weight ratio. Possible modifications to increase the strength to weight ratio for application to the heat-rejection unit include: use of a box truss design and alteration of the truss members, for example, changing the square members to round members. The Emergency-One design uses square extrusions for ease of manufacturing and welding. A box truss design provides more torsional stiffness than the Emergency-One ladder design, and therefore reduces the possibility of jamming the structure. The weight breakdown of the ladder, on Earth, is as follows (Reference 28):

Base Section	2300 pounds
Section One	890 pounds
Section Two	550 pounds
Tip Section	300 pounds
<hr/>	
Total	4040 pounds

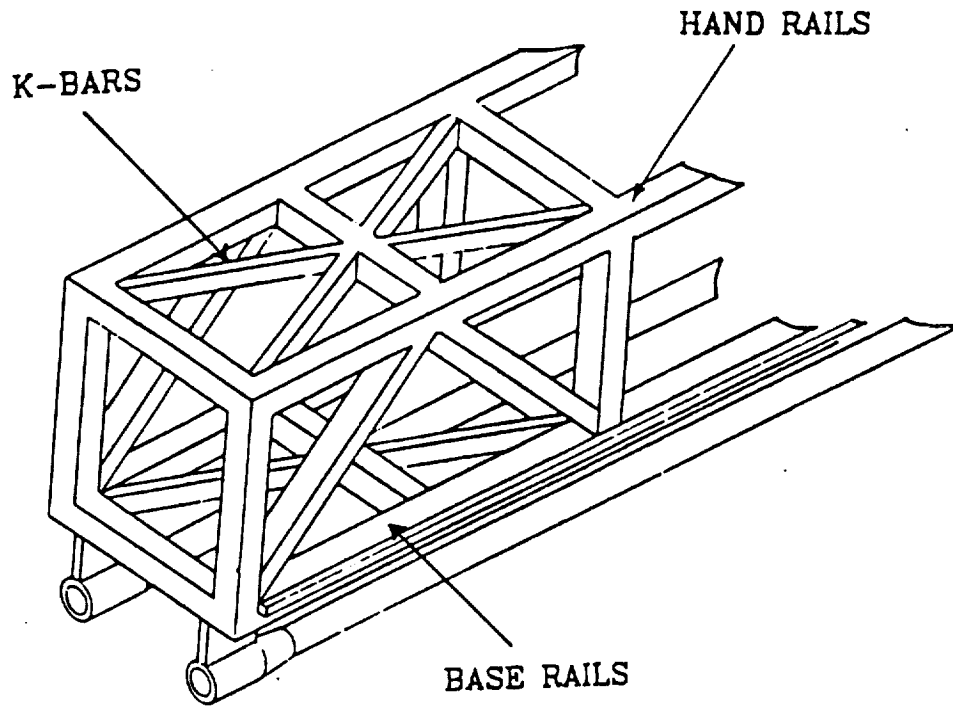


Figure 5.5 Box Truss Bay of Ladder

5.4.3 Materials

The Emergency-One ladder is constructed mainly of 6061-T6 aluminum. The material was chosen based on its high strength, low weight, versatility, and ability to be welded. Under the extreme temperatures of the lunar environment the strength of the material may be reduced to the characteristics of 6061-T4 aluminum. Table 5.2 shows the properties of each grade of aluminum (Reference 29).

Table 5.2 Properties of 6061 Aluminum

	Yield Strength (kpsi)	Tensile Strength (kpsi)	Fatigue Strength (kpsi)
Al 6061-T6	40	45	13.5
Al 6061-T4	21	35	13.5

Since welding is not a necessity, a 20 series aluminum could be used and the structure riveted together. The 20 series aluminum provides a better strength to weight ratio, but it can not be welded. The properties of 2014 aluminum are shown in Table 5.3 (Reference 29).

Table 5.3 Properties of 2014 Aluminum

	Yield Strength (kpsi)	Tensile Strength (kpsi)	Fatigue Strength (kpsi)
Al 2014-T6	60	70	18
Al 2014-T4	40	62	20

5.4.4 Sliding Mechanism

The Emergency-One assembly uses hydraulics to drive a pulley system which proportionally extends and retracts the ladder sections. Each bay extension is controlled by the bay beneath it. Two sets of slots, A and B, shown in Figure 5.6, guide the ladder bays as they slide inside of each other. Set A, also referred to as slide pads, are fixed to bay 1 and slide pad set B is mounted to bay 2. The pulley system acts to ensure that jamming of the system does not occur. Thus a pulley system will be necessary for dependable operation. Either a passive pulley system operated by the movement of the LCUV, or an active system operated by motor driven pulleys can be used. Advantages exist for each option. A passive system minimizes weight, power drain, and heat loads. An active system allows for the extension device to pull the LCUV in the event of an emergency. Emergency-One employee Bill Alm stated that the aerial devices were capable of pulling the fire engine in the event of an emergency.

The slide pads (Figure 5.7) are coated with a synthetic material named Nylotron to prevent wear and are lubricated with white lithium grease (Reference 28). However, neither the grease or the Nylotron material will be applicable to a lunar environment. Another lubricant and slide pad material will need to be found for proper operation. The pads act as point loads on the truss and are positioned to attain the desired loading conditions. Correct positioning of the slide pads also allows for retraction of the ladder while it is deflected. By increasing the amount of overlap of the truss bays the load on the slide pads is reduced (Reference 28).

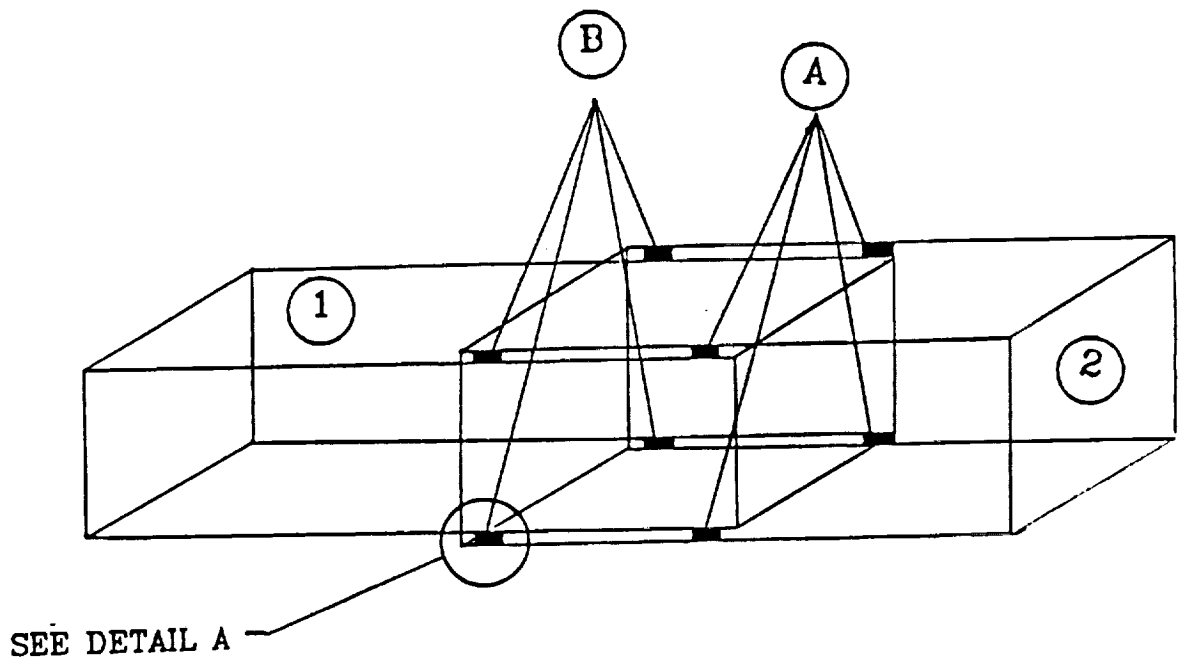


Figure 5.6 Slide Pad Locations

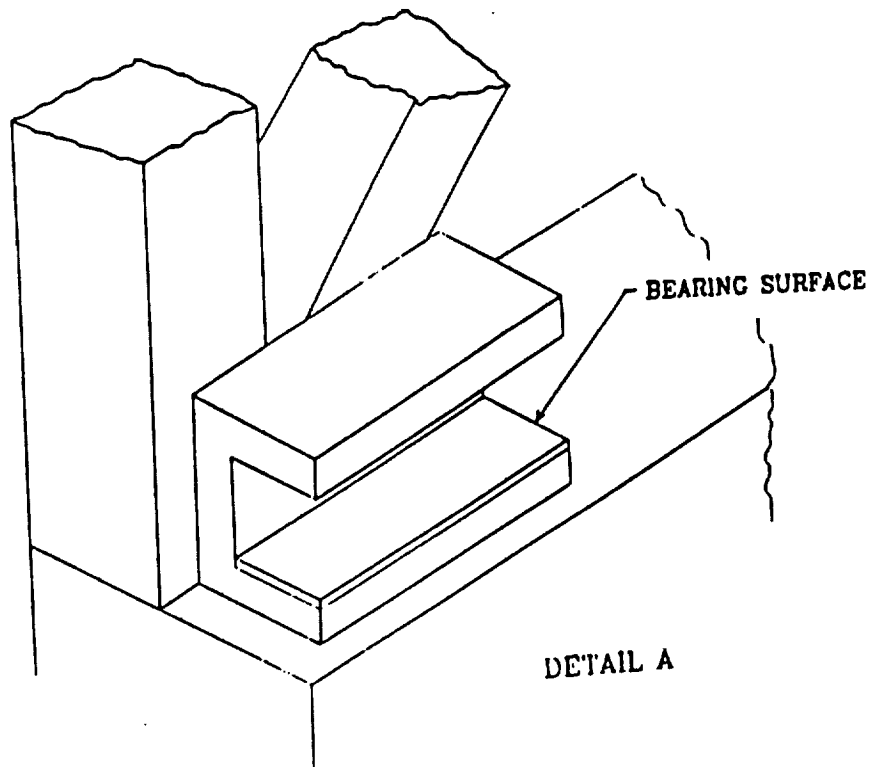


Figure 5.7 Detail of Slide Pad

5.4.5 Thermal Problems

Expansion and contraction of the tolerance fits will create a problem since this could result in jamming the mechanism. Also, thermal stresses will occur in all of the welds and joints. As stated earlier, the material properties of the 6061-T6 aluminum may assume the properties of 6061-T4 aluminum due to high thermal gradients on the moon.

A variation of the fire truck extension ladder appears to be the best option for the extension arm between the LCUV and the heat rejection unit. This design is recommended for its structural rigidity, simplicity, and the fact that the current design proves the ability of such a structure to meet the performance needs of the heat rejection unit. As of this writing, no calculations or analyses had been performed concerning the length of the truss bays, maximum feasible extension lengths, or possible alterations to the geometry of the truss. A box truss is recommended as an alteration to the geometry for an increased strength to weight ratio. Increased strength to weight ratio will increase the extension length of the truss structure. Structural soundness of the truss is an important factor as it would be desirable to use the base bay of the truss as an overhead crane to transport habitation modules.

5.5 FLUID LINES

The initial purpose of the collapsible truss structure was to provide rigid support and protection for the lines carrying coolant from the LCUV to the Heat Rejection Unit (HRU). There have been two proposed methods of transporting the fluid to and from the LCUV. The first system requires the use of flexible hosing, and the second employs a collapsible tubing structure to provide a path for fluid flow. Currently it is believed that the collapsible tubing structure is the most desirable system.

There are several criteria to which the fluid transportation system must adhere. The most important is that the system must be able to provide leak-free service. Because the Lunar atmosphere is essentially a vacuum, any leak would be disastrous. The system must provide reliable service under the harsh lunar temperature conditions, for which temperatures range from +266° to -274°F, and the system must transport fluid for which temperatures range from +350° to -207°F. The system must be as simple and maintenance free as possible. This requirement is due to the fact that there would be no personnel present to provide service, and that any failure would result in a shutdown of the LCUV. One of the more demanding parameters is that the system must be capable of extension and retraction as the LCUV moves relative to the HRU. This parameter is demanding because it requires that the system be capable of great extension lengths and still be compact in storage when not deployed. This cycle of extension and retraction also places a

condition of wear on the fluid transportation system, such that the system must be both durable.

5.5.1 Design Concepts

The flexible hosing system is a more traditional approach to the method of transporting the fluid and would consist of two fluid lines composed of an as yet unspecified material. One hose would transport hot fluid to the radiator from the LCUV and the other would return the coolant to the LCUV. The lines would run within rings on the bottom of the collapsible truss, as shown in Figure 5.8. The hot and cold fluid return hosing would be stored on two large spools, as shown in Figure 5.9. Originally it was assumed that a constant tension would be kept on the lines by use of a torsional spring in the reeling spool. The constant tension would keep the lines from getting slack and possibly being tangled or caught in the truss as it extended and retracted. This would also provide a passive means of automatically retracting the hose as the LCUV moved toward the HRU. The idea of the torsional spring was dismissed as impractical in regards to reeling approximately 200 feet of hosing filled with fluid. In the absence of the spring design, it was decided that motors would be most practical for use in controlling the extension and retraction of the fluid lines.

Were the flexible hosing system to be employed, it would also be necessary to create some sort of shielding to prevent the hosing from being heated by the sun and to protect it from damage. In the event that this system were chosen at a later time, the telescoping tube design may be useful in providing the necessary protection for the hosing.

The flexible hosing scheme presents several foreseeable problems. The foremost problem is that there is no material currently available which can withstand the extreme temperature gradients on the moon and still retain its flexible properties. Most materials are designed to behave well at high or low temperatures, not at both extremes. While this is a current concern which must be addressed in detail later, there are other concerns about this design which make it a less than attractive option. A major problem is the room within the HRU that the respective reeling systems would occupy. Due to increased amounts of support equipment to be placed within the HRU, a system that requires a minimum of space is beneficial. There is also the concern of the extra weight such a system might add. Having the hot fluid lines coiled up inside the HRU also creates an unwelcome heat source. The reeling system represents a complexity and added chance of failure. In the event that the reeling system was to become inoperable due to a failure of any of its components, the heat rejection unit would be disabled.

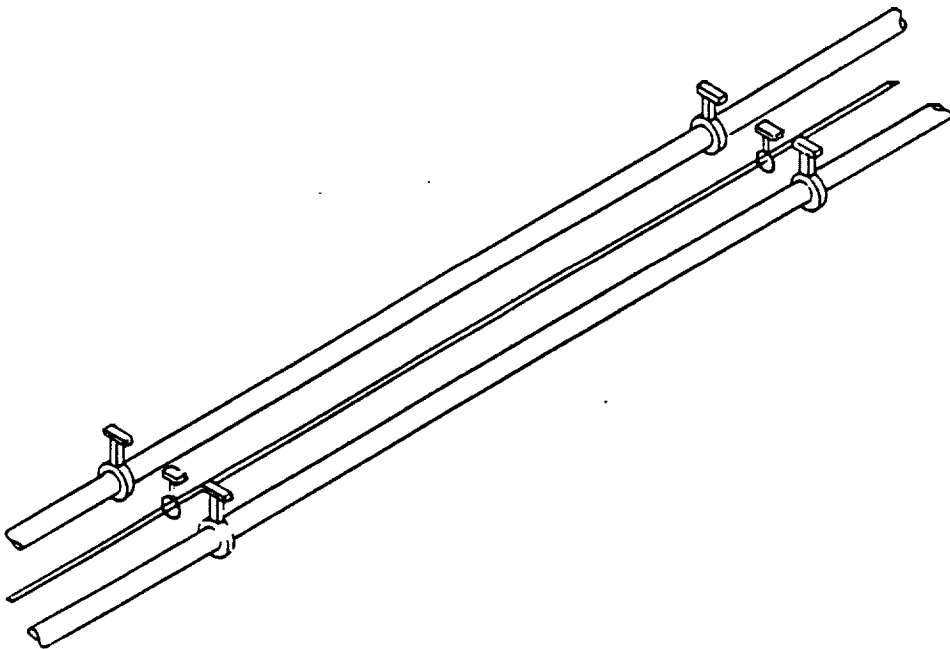
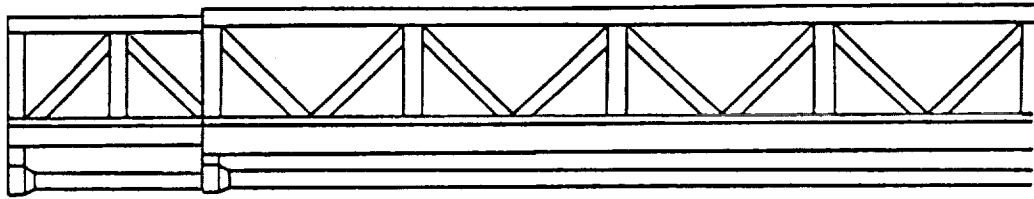


Figure 5.8 Flexible Fluid Lines Beneath Truss

WENCH SYSTEM

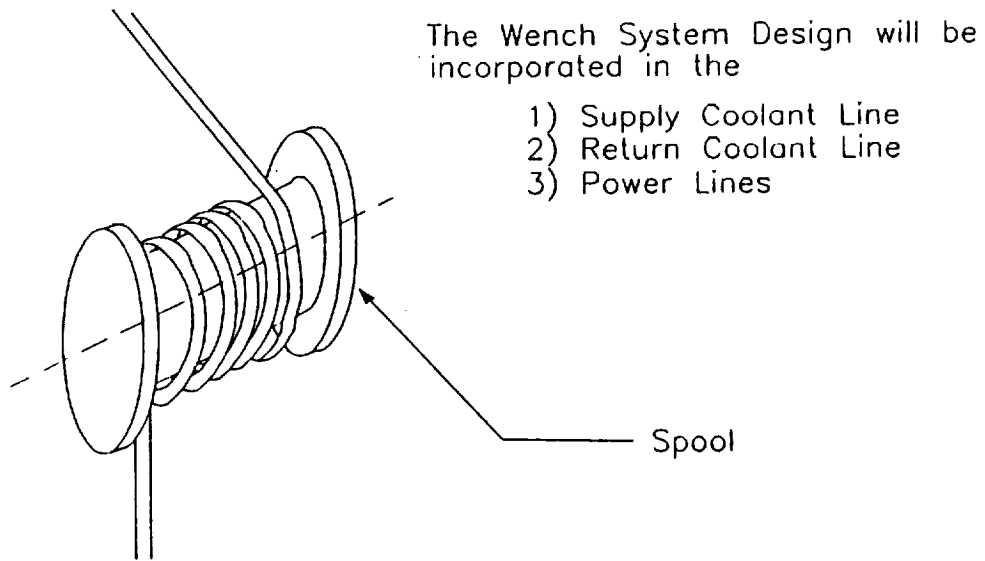
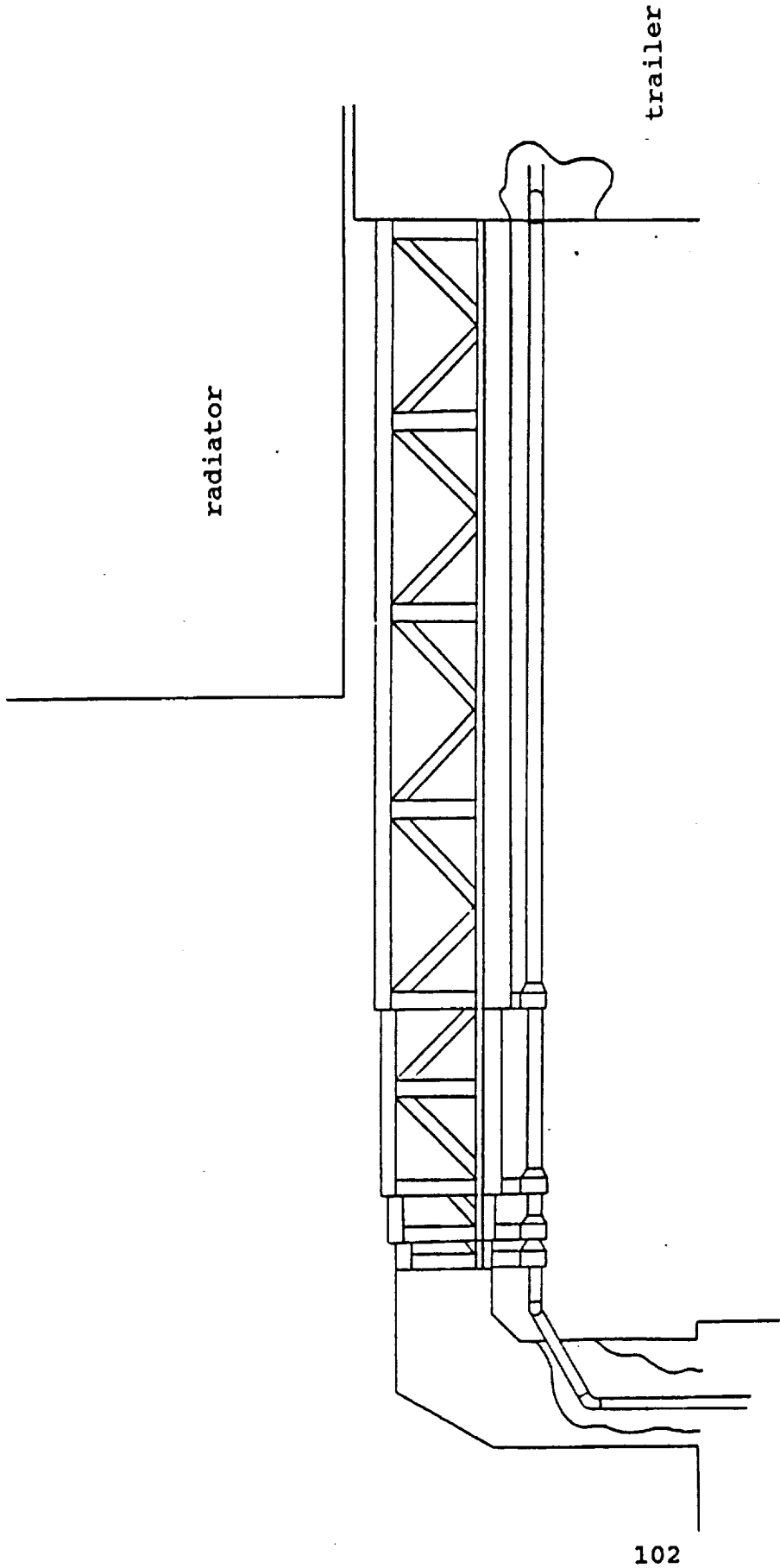


Figure 5.9 Reeling System for Flexible Hose and Power Lines

The telescoping pipe system was derived from a design by Emergency One, Inc. used for their aerial fire truck ladders. The system shown in Figure 5.10, consist of two telescoping structures mounted rigidly on the underside of the extension truss which connects the LCUV and the HRU. As with the flexible hosing there are two fluid lines, one for the return fluid and another for the working fluid from the radiator. At the base of the truss system the telescoping structures are connected to lines which lead to and from the pump. This pump is responsible for moving the fluid throughout the system. As with the Emergency One system the pipes are made of 1/8 inch T-6 Aluminum. As shown in Figure 5.10, the end of each section of pipe is fixed rigidly to the end of each bay of the extension truss. Thus, as the extension truss deploys the tubing extends. At the end of each tube section is a housing, detailed in Figure 5.11, which is welded to the pipe. This housing contains the seal for the pipe and the bearing surface for the internal sliding pipe. The seals for this structure are just one of the concerns for this design (Reference 28).

The preliminary seal design is shown in Figure 5.11. This design is based on a one piece seal design which was inspected at Emergency One in Ocala, Fla. The seal is mounted inside the housing at the end of each tube and consists of a seal material, a bearing surface for the inner sliding pipe, and a scraper to remove debris from the surface of the pipe before it enters the seal. A suitable seal material is still being sought at this time.

Jeff Aiken of Emergency One directed our attention to Fluorocarbon Mechanical Seal Division for the location of a seal



radiator

trailer

LCUV

Figure 5.10 Truss and Telescoping Tube Location

COLLAPSIBLE PIPING
Coolant Lines Through The Collapsible Truss

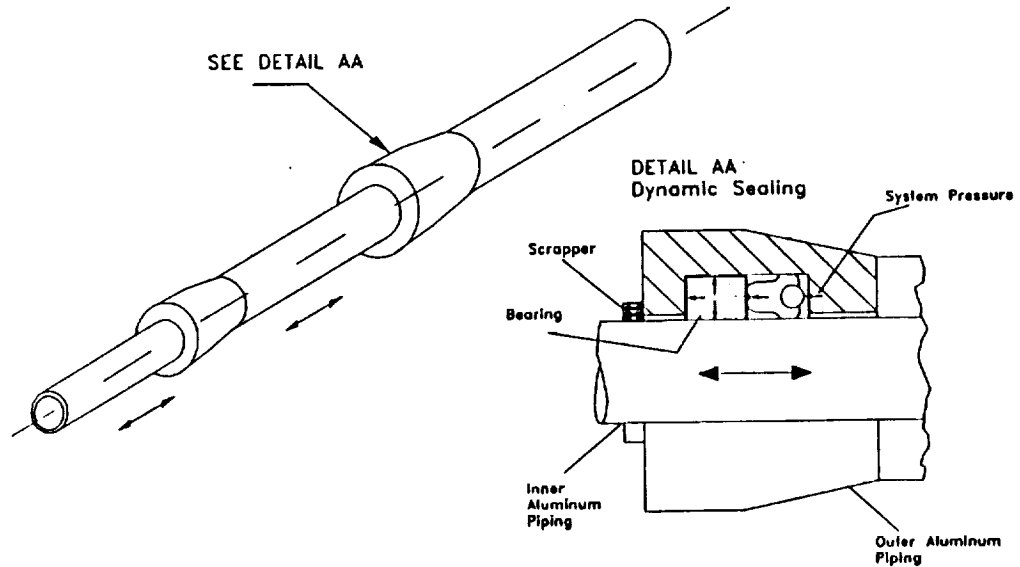


Figure 5.11 Telescoping Fluid Tube Housing

material which could withstand the harsh lunar environment. Fluorocarbon Mechanical Seal Division has been contacted and a sketch of the seal design and its parameters conveyed to Mr. Mark Malone. The information concerning the seal material had not arrived as of the writing of this paper. However, an initial inspection of the Fluorocarbon Mechanical Seal Division sales catalog revealed a listing for dynamic seals in a vacuum. Under this listing, Virgin Teflon was listed for a temperature range from -200 to 500 F. This initial information gives us confidence as to the ability to find a satisfactory seal material (Reference 30).

There are several problems which are unique to the seals involved in this structure. Because the Lunar environment is essentially a vacuum, leaks can be disastrous. The design of the Emergency One tube structure has an allowable amount of leakage for earth design, but is unacceptable for lunar application. Jeff Aiken, project engineer for Emergency One, stated that no seal is perfect in eliminating leakage but the leakage could be limited to drops per hour (Reference 28). Fire fighters who operated the Emergency One equipment at Norfolk's Fire Station One stated that there was a minimal amount of leakage from the system. However, close inspection of the device revealed that debris trapped in the seals was most likely the cause of the leaks. Mr. Aiken confirmed

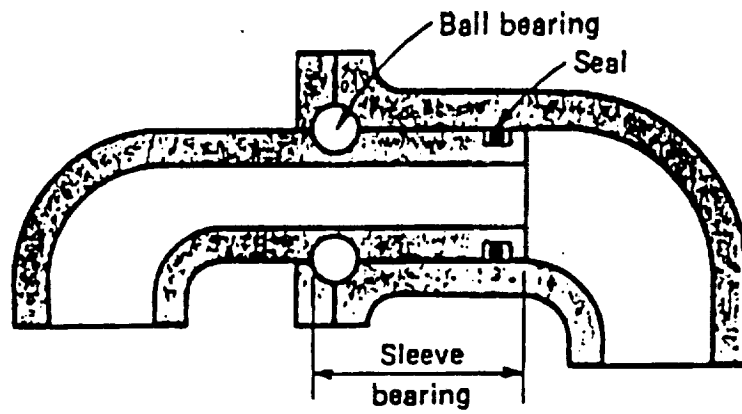
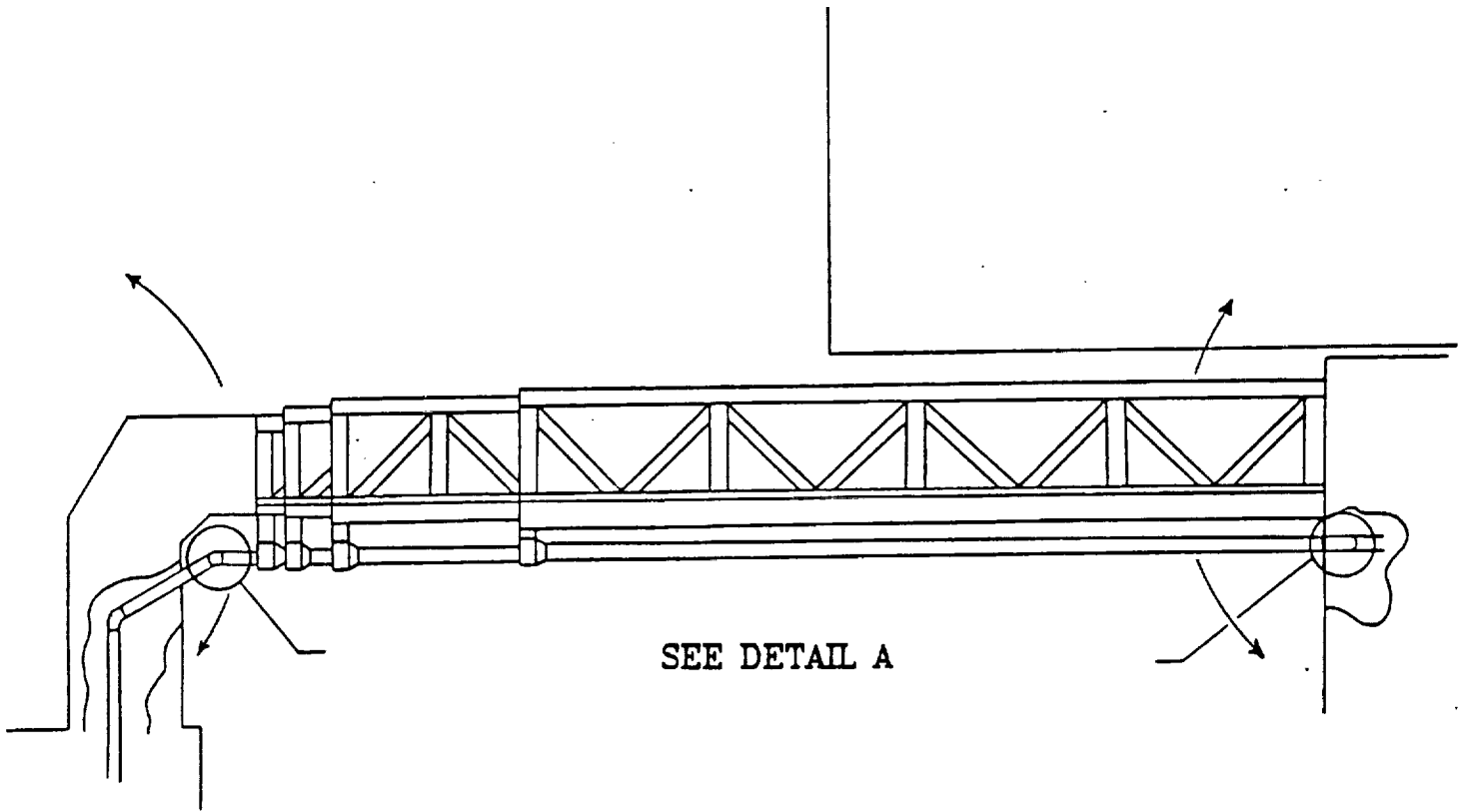
this analysis by stating that seldom are leaks due to worn out or failed seals, but due to abrasions of the tube surface by debris in the seal. These gouges in the tubing then allow for the fluid to seep past the seal (Reference 28).

The scraper on the front of the seal is designed to remove debris that may damage the seal. The Emergency One design does not prevent all debris from entering the seal compartment as evidenced by the passing of sand and grit into the seal area (Reference 28). It must be assumed that lunar dust will collect on the surface of the tubing and that this dust will be able to get past the scraper and possibly into the seal. The effects of lunar dust entering the seal and possibly getting into the coolant system must be addressed. There is also the possibility that the operating parameters of the system will have to be altered in order to accommodate proper sealing. In particular, the system pressure may have to be elevated in order to activate the seal. This would call for arranging valves at the ends of the telescoping structure to elevate the system pressure within the telescoping tubes and then bring the system pressure down to the 30 psi design pressure within the radiator and the LCUV.

Problems with seal wear may also become evident if the LCUV remains attached to the HRU during nighttime operations. During nighttime operations when the heat rejection needs are low, the system is designed to drain the fluid into a reservoir which would be heated to keep the fluid from freezing. In the event of system drainage, there would be large amounts of seal wear as a result of friction on the dry seal as the truss system telescoped in and out. To prevent excessive wear a self lubricating seal should be sought if at all possible. Many types of Teflon seals possess this self lubrication attribute (Reference 29).

There are other major areas in which leakage may become an important factor. Either end of the truss system is designed to accommodate vertical displacement as shown in Figure 5.12 (Reference 30). The dynamic fluid connections represent a problem in that difficulty may be encountered in providing a leak-proof method for those connections. Suggested pipe fittings to allow for leak-proof dynamic connections are described in later sections.

Other problems involved in the telescoping tube structure which remain to be addressed include the selection of a tube material based on researched information. The exact sizing of the tubes and dimensioning of clearances and tolerances also remain to be investigated. The sizing should be based on the smallest tube size necessary to achieve the necessary flow rate. From this basic size each larger tube section should be sized in accordance with the ability of the larger tube to accommodate the smaller tube sliding within it.



DETAIL A

Figure 5.12 Truss and Swivel Joint Connections

Both methods of fluid transportation have their problems mainly in the lack of materials which can accommodate the impending needs of the system. In the case of the flexible hosing it is the hose material. In the case of the telescoping tube structure it is the seal material. In neither case should the designs be ruled out on the basis of inadequate materials available from today's technology. The assumption must be made that those materials will be developed in the presence of the need. The telescoping tube design was chosen based on its utility and reduction in complexity, not on the greater chance of finding a material for seals over a suitable hosing material.

5.5.2 Fluid Line Connections

The purpose of the telescoping fluid line is to transport coolant to the LCUV from the radiator unit and back. The extendible truss will be required to allow vertical displacement as the LCUV travels over inclines and slopes. The fluid lines must also accommodate this movement of the truss arm via pivoting fluid connections.

A possible swivel joint connection for the fluid lines is shown in Figure 5.12 (Reference 30). As with the seal for the telescoping tubes, the proper seal material must be sought. The same concerns addressed towards the seals in the telescoping tube structure must be applied to this connection. Seal wear, debris contamination and leak-proof behavior are as important in this application as they are in any other system within the HRU.

5.6 POWER LINES

The current design is for the HRU to contain the fuel cells that will supply power to the LCUV. Thus, it will be necessary for the collapsible truss to support the power lines as well as the fluid lines running to the LCUV. The power lines will be supported by rings on the bottom of the truss much like the plan for the flexible fluid lines (see Figure 5.9). The power lines would be housed on a spool reeling system within the HRU. This spool reeling system would use a torsional spring to maintain a constant tension in the power lines and to control the retraction and feeding out of the line as the truss is extended and retracted.

It is the assumption of small size and weight of the power lines which makes the use of the reeling system with the torsional spring feasible. It is assumed that the reeling system would be small in size and could easily be housed within the HRU. It is recommended that an alternate power line be run to the LCUV from the HRU as a backup, this will require the use of two separate reeling systems. The actual sizing of the components of this system such as the line size, spool size, and spring size still remain to be investigated.

6.0 HEAT REJECTION SYSTEM RADIATOR

The Lunar Construction Utility Vehicle (LCUV) has a major problem with its ability to reject excess thermal energy. The solution to this problem is not an easy one; however, it is attainable through the use of a radiator. This radiator would need to be of considerable size and complexity in order to meet the heat rejection needs of the LCUV operating in the harsh lunar environment. The goal of this group has been to thoroughly research the problems associated with the development of a daytime heat rejection unit that will meet the needs of an LCUV working under the worst possible conditions on the lunar surface and to make design recommendations where possible.

6.1 ASSUMPTIONS

The research and design for the Daytime Heat Rejection Unit has been carried out with certain assumptions in mind. The first assumption is that the LCUV should have the ability to perform heavy construction in the hottest lunar environment. This means that the heat rejection unit will be designed to operate at noon on the lunar equator and still reject sufficient thermal energy to allow productive LCUV operation.

The amount of thermal energy that realistically needs to be rejected is assumed to be 100 kW. This is a generous assumption and is meant to be intentionally large to prevent design shortfalls.

6.2 RADIATOR SIZING PROGRAM

The program used to determine the radiator's surface area from a series of input variables has been modified and upgraded from David Alcorn's work from the previous year's design group. The equations in this program were developed from "Design Studies on the Effect of Orientation, Lunation, and Location on the Performance of Lunar Radiators" (Reference 31). The completed program named "PRGRAD" is listed in Appendix F.

The program was run for different combinations of parameters which include, surface coating, angle of the sun, return fluid temperature, flow rate, and location on the moon; these parameters affect the external thermal loads on the radiator. This is illustrated in Figure 6.1.

The program has been run for the worst case lunar surface conditions and LCUV operating conditions which are:

- Solar noon at equator, moon's surface temperature 102°C.
- Assuming 100 KW of heat rejection needed to cool the LCUV and the radiator carriage systems.
- Direct sun light on one side to the vertical radiator surface.

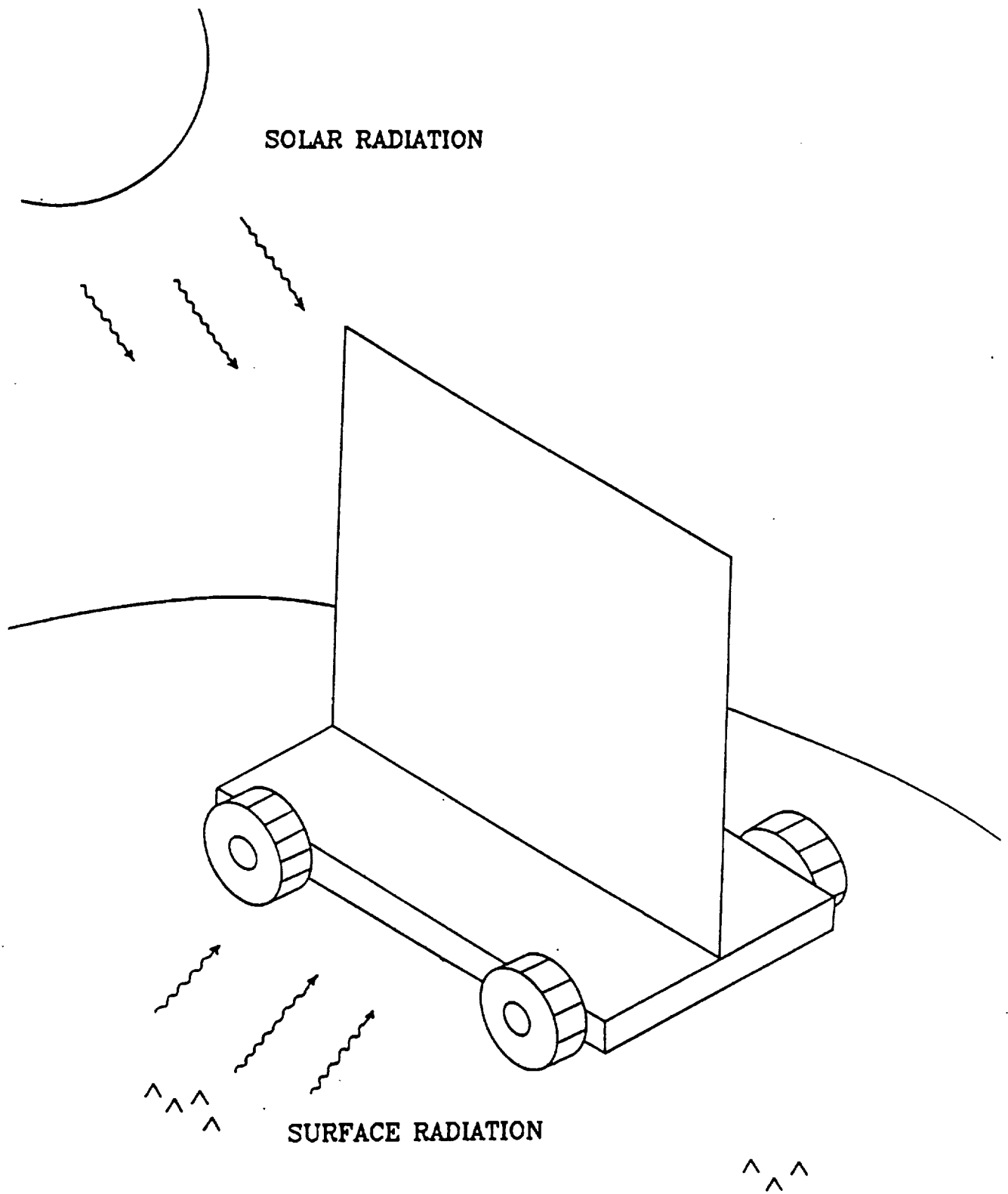


Figure 6.1 External Loads on Radiator

After running the different cases it became evident that one of the main variables was the return temperature of the fluid from the radiator. Operating the radiator at a very high temperature allows for reduction in the overall radiator size, thus increasing utility and efficiency. However, the radiator must supply a return fluid that will maintain an acceptable operating temperature for the LCUV components.

6.3 RADIATOR DESIGN

A double sided vertical radiator has been proposed for use in the heat rejection process. Ideally the radiator would provide the needed heat rejection while not being massive in size. The program has been used to determine how low the return temperature can be and still maintain a reasonable radiator size. Once the return temperature is reduced below that limiting value the radiator becomes ineffective and will reject no heat. In this case, heat will actually be absorbed into the system from the surroundings.

For basic radiation heat transfer (Reference 18):

$$q = A \epsilon \sigma (T_s^4 - T_{sink}^4) \quad (4.9)$$

where:

- q = heat transfer (Watts)
- ϵ = emissivity
- σ = Stefan-Boltzmann Constant (=5.67x10⁻⁸ W/(m²K⁴))
- T_s = Surface Temperature (°K)
- T_{sink} = Surrounding Temperature (°K)
- A = Radiating surface Area (m²)

Examining this equation, it is seen the radiator surface temperature has an extreme impact on the amount of heat rejection for a fixed surface area, since it is raised to the fourth power. If the heat transfer is fixed at 100 kW, any change in the radiator's surface temperature will have a strong affect on the radiator size necessary to reject a sufficient amount heat.

Figures 6.2 and 6.3 show the relationship between radiator size and fluid return temperature for a coolant fluid of ethylene glycol. Figures 6.4 and 6.5 show the relationship between the radiator area and the angle of the sun with a fluid of ethylene glycol and a surface coating of silverized teflon and zinc oxide. Figures 6.6 and 6.7 are similar to the previous figures except that the coolant fluid is propylene glycol.

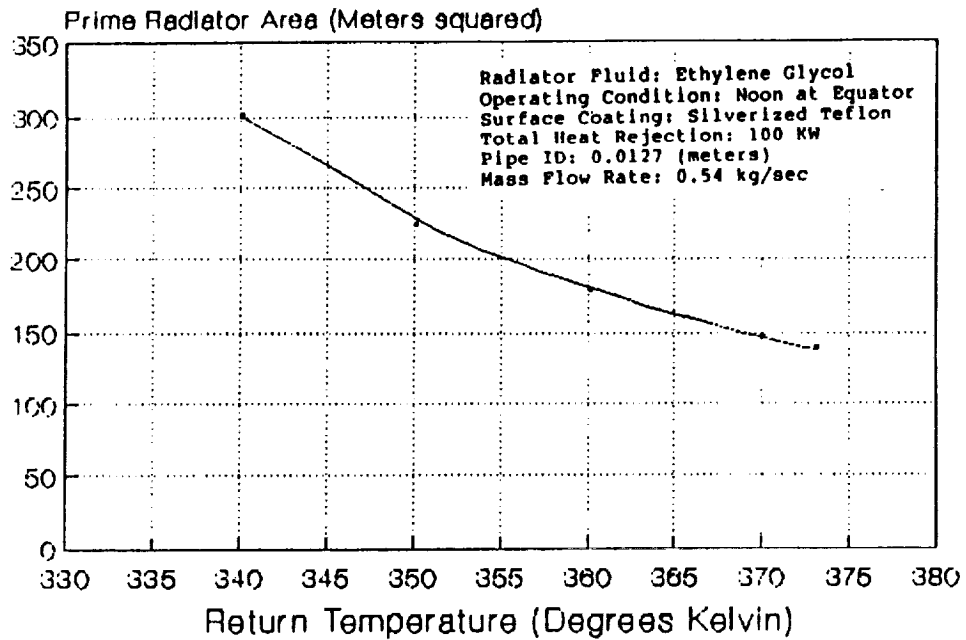


Figure 6.2 Radiator Size vs. Fluid Return Temperature

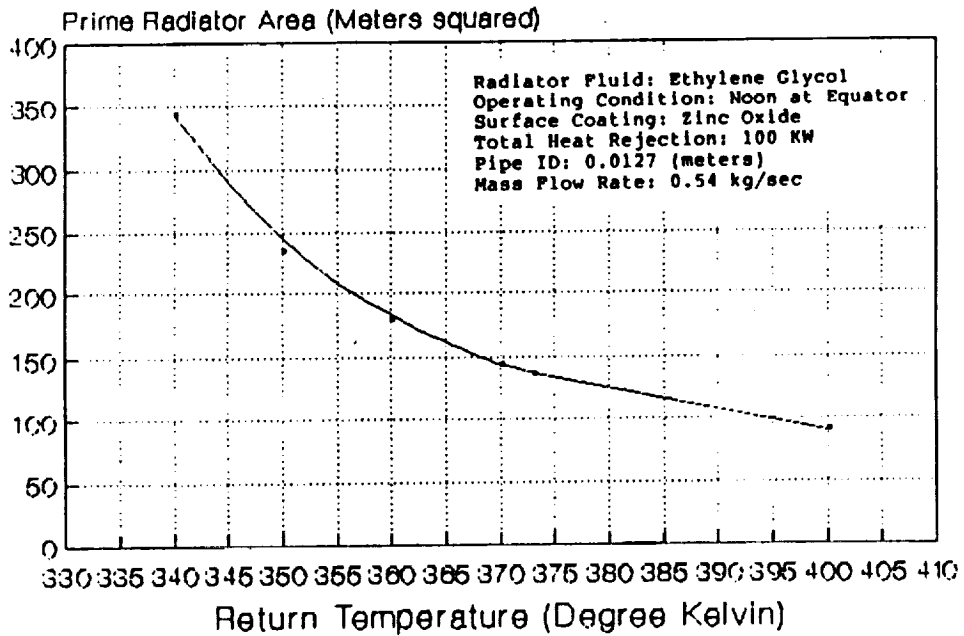


Figure 6.3 Radiator Size vs. Fluid Return Temperature

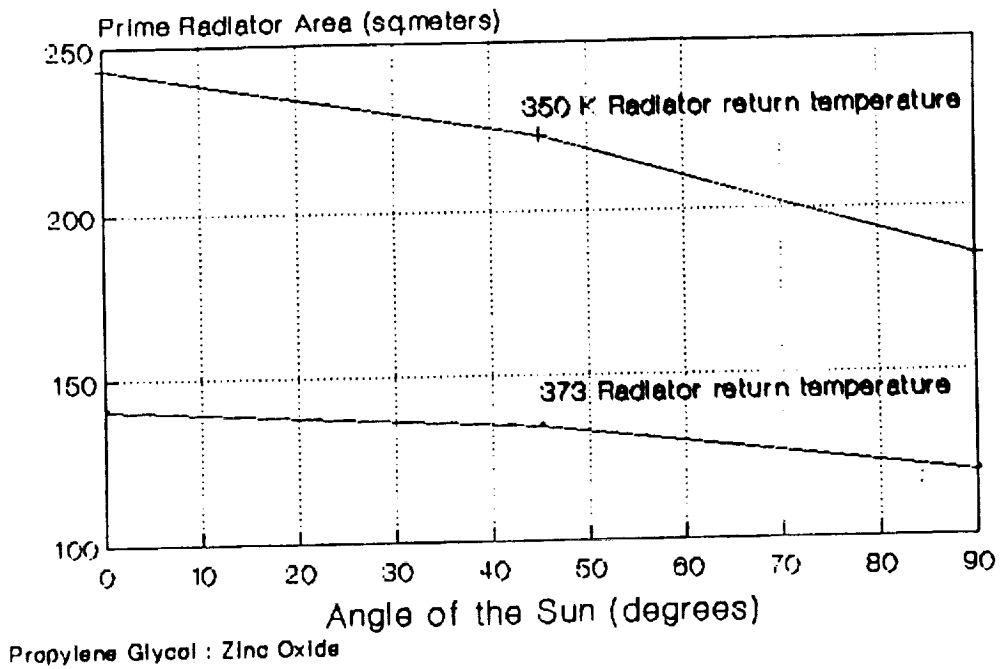


Figure 6.4 Radiator Size vs Angle of the Sun (Zinc Oxide Coating)

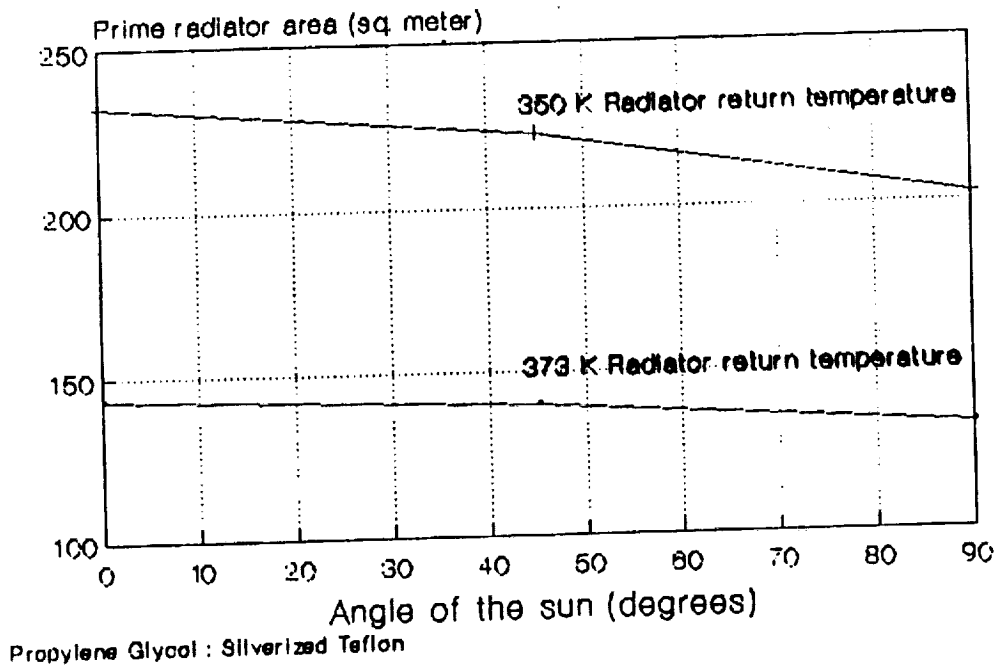


Figure 6.5 Radiator Size Vs Angle of the Sun (Silverized Teflon Coating)

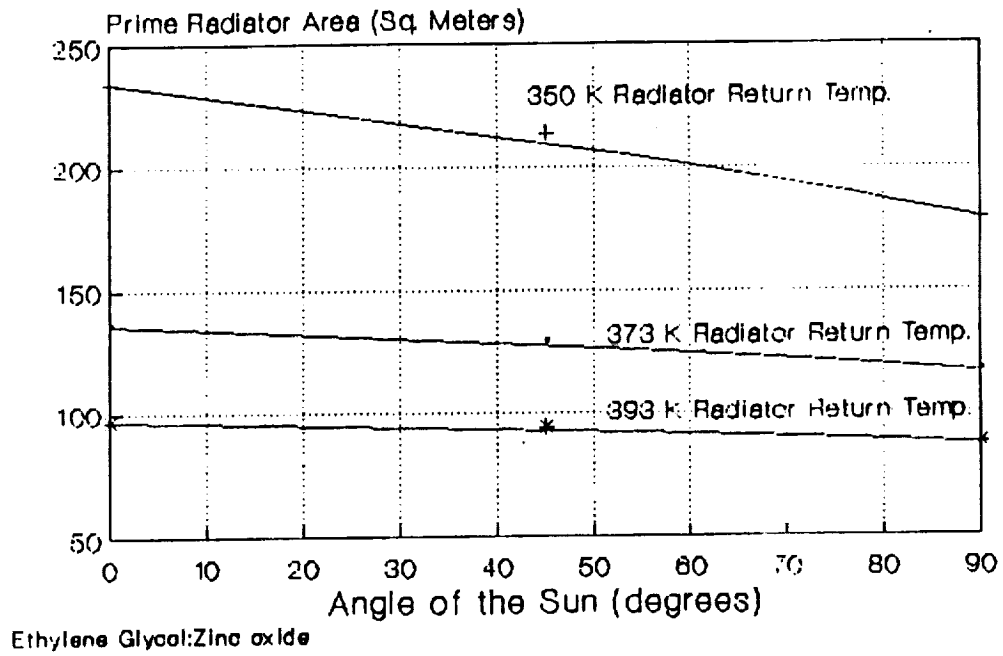


Figure 6.6 Radiator Size vs. Angle of the Sun

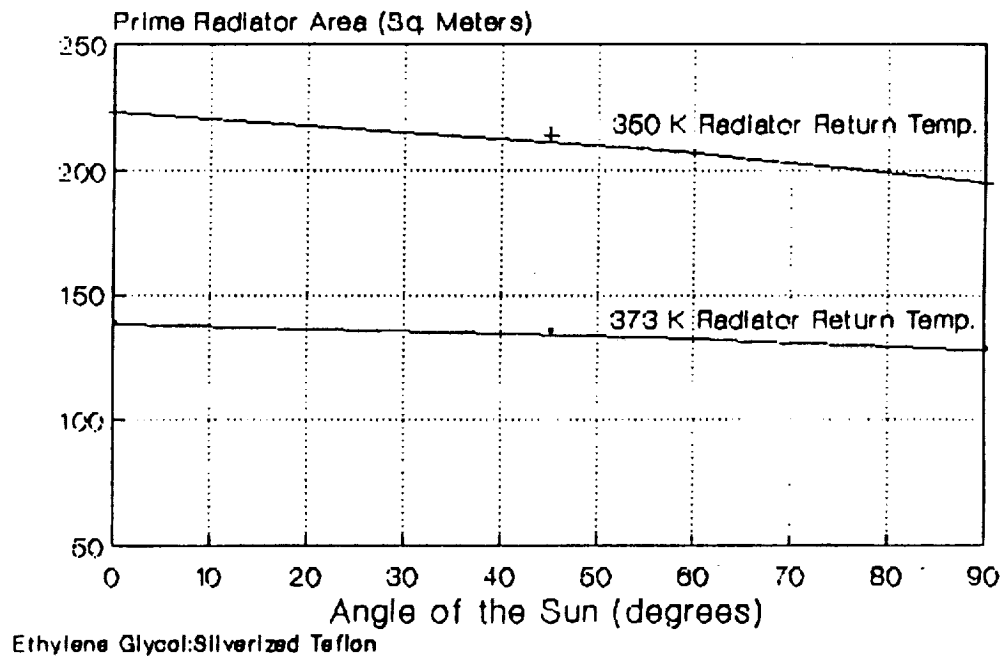


Figure 6.7 Radiator Size vs. Angle of the Sun

It is desired to operate the radiator at the lowest possible return temperature which is approximately 340°K. This requires a radiator that is 50 feet in length and 50 feet high. Operating the radiator below this temperature is not feasible because it will cause the radiator to absorb thermal energy rather than reject it.

The radiator's large size will require it to be collapsible. It will be collapsed when the heat rejection unit is being transported to the lunar surface and during transport on the lunar surface. This will allow for ease of transportation. If the radiator was not collapsible, considerable vibration problems would arise during transportation. The radiator can unfold in five hinged vertical panels, as shown in Figure 6.8. This will require pipe connections between the panels that can pivot to allow for this motion. The panels will be lifted from the top by one solid member that is hoisted by a cable and pulley system.

Two sides of the radiator will have vertical truss sections similar to the collapsible truss discussed for use between the LCUV and the heat rejection unit. When this truss is fully deployed after being unloaded onto the lunar surface, the vertical trusses will extend upward to approximately 55 feet and will remain fixed. These members will carry the radiator panel's load and also act as guides for the radiator as it is raised and lowered.

A pulley system will be placed on top of each truss system that will be used to deploy the radiator. There will be two cables, one on each side, that will connect to the solid member that is hooked to the radiator panels. The cables will run from the panels up through the vertical trusses and into the carriage body where a hoist mechanism will either release or reel in the cable.

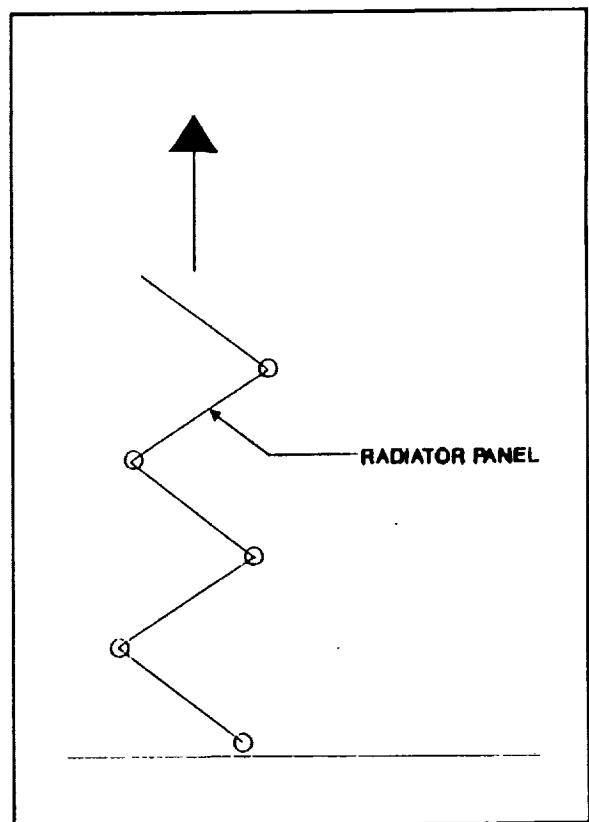


Figure 6.8 Radiator Being Deployed

These systems will keep the weight of the radiator support to a minimum. Other ideas for extending the radiator panels have been introduced, such as using the working fluid to pressurize the radiator to the fully erect position, or using gear boxes between panels. These ideas are not realistic because of the weight involved in their design. Initial weight calculations of the

overall heat-rejection system were determined to be of considerable magnitude; therefore, an effort should be made to minimize the systems weight.

The radiator panels will be constructed in two different sizes. The large panels will be 10 ft by 15 ft and the small panels 10 ft by 10 ft. The purpose is to allow the incoming fluid, which is at a high temperature, to enter into the smaller panels. As the working fluid is cooled it will return through the large panels. This should allow the radiator surface temperature of the larger panels to be kept at a constant high temperature. This is desirable because of their combined surface area. Whereas, the small panels will be returning the fluid that has been cooled to a certain degree while passing through the larger panels. The configuration will include 10 large and 10 small radiating panel, as shown in Figure 6.9.

Taking this into account, the radiator panels should be made of parallel piping connected by very thin aluminum fins to reduce the radiator weight. A considerable amount of work should be focused on the most efficient design of this radiator. Aspects to be considered are the pipe diameters, thickness, and the distance between the parallel piping, as seen in Figure 6.10. The pipe thicknesses should be as thin as possible, but be able to withstand the system pressure and manufacturing methods of attaching the fins to the pipe. This is all in an effort to produce an efficient radiator configuration and minimize its design weight.

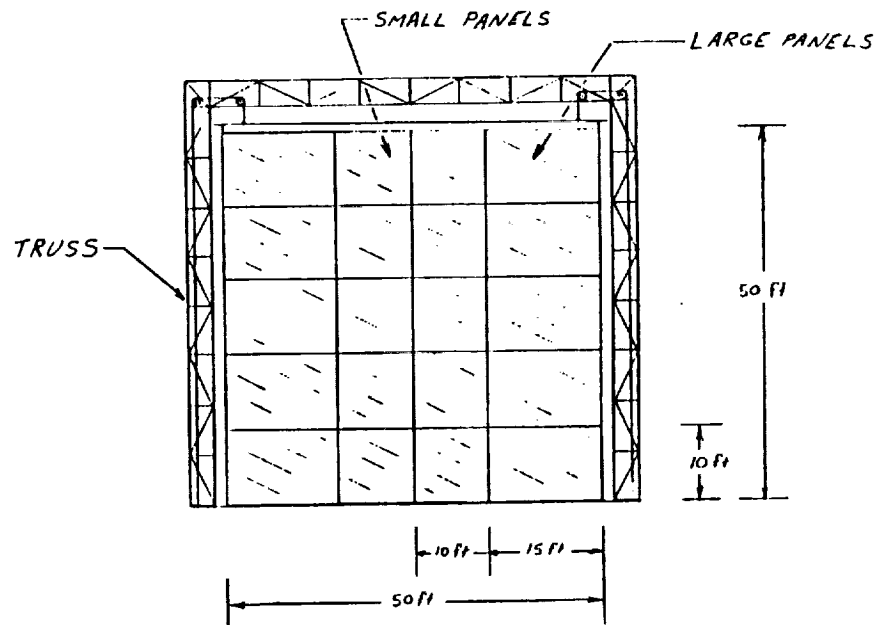
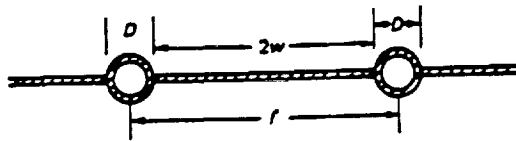


Figure 6.9 Basic Radiator Configuration



D = Pipe Diameter

l = Length of Fin between Center of Piping

2w = Length of Fin between Piping

Figure 6.10 End View of Radiator

6.4 RADIATOR ORIENTATION

The radiator panels will absorb thermal energy from the sun's rays. If one of the panels has direct or partial view of the sun it will reduce the efficiency of the radiator to reject the system's thermal energy. In trying to minimize this effect, the goal is to keep the panels oriented such that they do not have direct view of the sun.

This has been addressed by placing solar sensors on each side of the radiator to give feedback on the sun's position. With this information the radiator will be able to rotate about its vertical axis and position itself in an orientation to minimize the amount of solar energy absorbed (See Figure 6.11). Originally the radiator was also supposed to rotate about its horizontal axis. This was rejected after realizing that if the radiator was rotated in this manner it would have an increased view of the solar surface and thermal energy from the surface would reduce efficiency. Therefore, it was decided to limit the radiator to rotation about its vertical axis only.

6.5 RADIATOR MATERIAL

In choosing a material for the radiator, several aspects needed to be considered: weight, strength, and material evaporation rate. The evaporation rate is important because of the high temperature and low pressure on the lunar surface. Figure 6.12 shows the evaporation losses for several materials (Reference 32). For aluminum, evaporation does not occur at any significant rate until temperatures reach 800°C (Reference 32). Aluminum was chosen

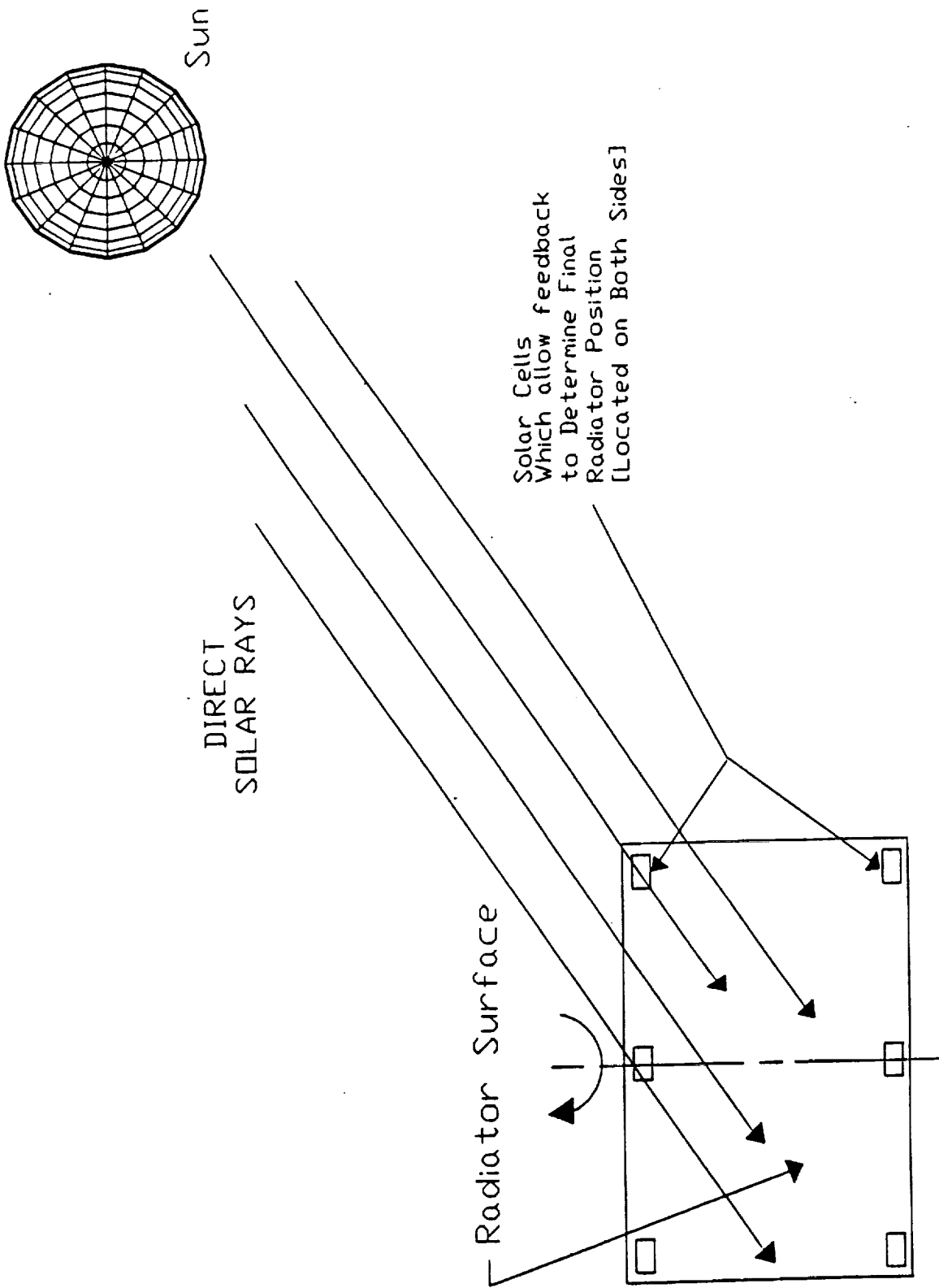


Figure 6.11 Radiator Positioning

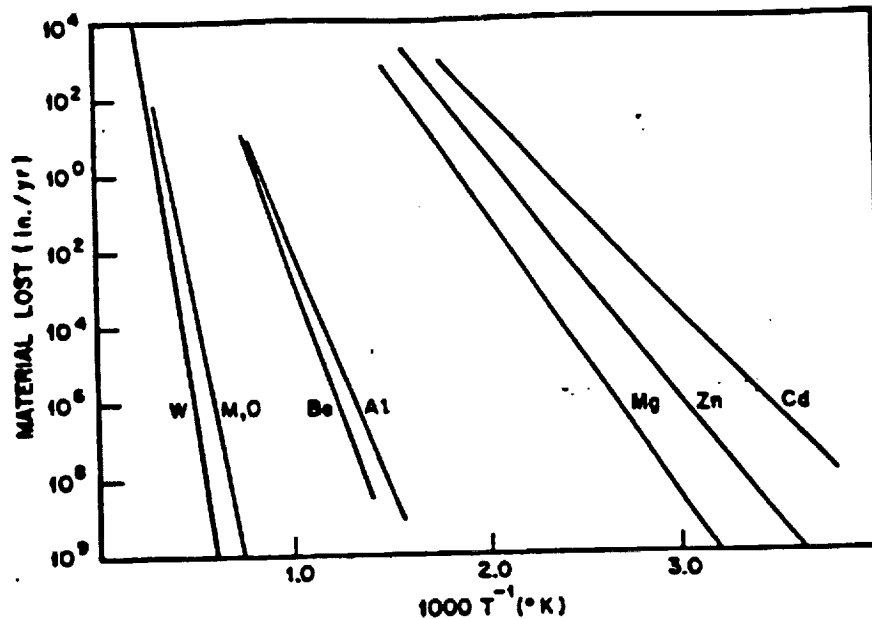


Figure 6.12 Evaporation Rates

for its light weight, suitable strength, compatibility with working fluids, and past performance in space.

6.6 RADIATOR COATING

When designing the radiator, every effort should be made to increase the heat rejection rate from the system. A thermal radiative coating is desirable for this reason as well as to inhibit the absorption of heat from the surroundings. The two most important factors in choosing a coating are the ratio of ultraviolet absorptivity to infrared emissivity and coating stability.

At the start of the project, it was determined that the ratio of absorptivity to emissivity needed to be small. This was to allow the radiator to dissipate heat into space without absorbing a large amount from the surroundings. Listed in Table 6.1 are several coatings that satisfy this criteria (Reference 33).

Table 6.1 Surface Coating Properties

COATING	ABSORPTIVITY	EMISSIVITY	RATIO
Zinc Oxide	0.16	0.93	0.17
Zinc Orthotitanate	0.19	0.84	0.17
Anodized Aluminum	0.14	0.84	0.17
Silverized Teflon	0.08	0.85	0.10

The second factor, stability, is important because the coatings and their properties degrade for numerous reasons. The natural effects of primary importance are (Reference 33):

- 1) electromagnetic solar radiation
- 2) particle radiation due to protons, solar wind, and electrons
- 3) to a lesser extent, physical impacts due to atmospheric particles and micrometeorites

Much research, experimentation, and development has been conducted into the area of coating stability. Zinc oxide was the most stable "white paint" coating for a while, but it was found that although it offered a good ultraviolet radiation resistance, the solar absorptance was degraded by electron and proton radiation. Zinc orthotitanate, a more recently developed coating, has proven to be more stable than its predecessor (Reference 34). It is said to have "excellent optical properties and the potential for a long space life when correctly applied to a surface" (Reference 35). The application of zinc orthotitanate is its major hindrance because it is an inorganic substance and therefore, extensive surface pretreatment and primers are required. This is necessary to ensure good adhesion between paint and surface (Reference 35).

Silverized teflon has a very low absorptivity to emissivity ratio which makes it very attractive. But the long term effects of ultraviolet radiation on the absorptivity are still uncertain, as shown in Figure 6.13. Cost and weight are also a problem with metallic coatings, such as silverized teflon and anodized aluminum.

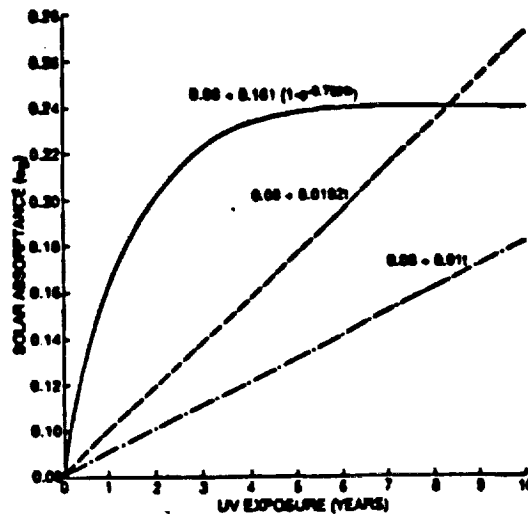


Figure 6.13 Silverized Teflon Absorptance

Extensive research has been located on the effects that radiation has on absorptance. Some of the results have been compiled and are presented in Table 6.2 for zinc oxide (Reference 30), zinc orthotitanate (Reference 34), and silverized teflon (Reference 36).

Table 6.2 Surface Coating Exposure Effects

COATING	INITIAL ABSORPTANCE	FINAL ABSORPTANCE	ELAPSED TIME
Zinc Oxide	0.16	0.18	1050 hrs
Zinc Orthotitanate	0.19	0.28	900 days
Silverized Teflon	0.08	0.20	720 days

Two coatings were chosen for comparison, based on their absorptivity to emissivity ratio: zinc oxide and silverized teflon. After making many runs of the computer program, discussed earlier, with different fluids and coatings, it was determined that the radiator area was a little larger using zinc oxide than using silverized teflon. Since the difference is so small, choosing zinc oxide for a coating is a more logical choice since it is much more stable and reliable.

6.7 RADIATOR MOUNTING

The large size of the current radiator configuration will require that considerable attention be given to its design, including its mounting on the HRU carriage. Proper consideration could not be given to the mounting of the radiator at this time due to a lack of specifics on radiator weight and configuration. There are, however, several parameters which are important in investigating the radiator mounting scheme. First of all the radiator will be required to pivot at least 180 degrees. This means that the radiator must be mounted on a turntable and driven by a motor. The turntable must support the load of the radiator and transmit the load to the carriage frame. The load which must be supported, when considering the radiator mounting, includes the collapsible truss systems on either side of the radiator, which provide support for the radiator, as well as the radiator when it is full of fluid.

The motor and transmission used to turn the radiator will need considerable torque to overcome the inertia of a mass as large as the radiator. Another consideration involved with the motor and the inertia of the radiator is stopping the radiator once it has been rotated into position. Since the radiator will move very slowly, it may not be necessary to brake its movement. Further evaluation is required.

6.8 RADIATOR SHADING

The radiator system performance depends upon its ability to radiate thermal energy to the surrounding environment. This performance is enhanced by reducing the view factor between the radiator and the ground. Also if the radiator coating begins to become susceptible to absorbing solar energy, performance drops off greatly.

The solution to both of these problems is a shading system. This shading system would consist of a ground shading unit as shown in Figure 6.14, and a radiator shading device as shown in Figure 6.15. Both of these devices are collapsible type fan structures that can be deployed and retracted to increase mobility of the carriage.

The main purpose of this ground shading is to keep the hot lunar surface from affecting the radiator's performance. The ground shading unit will be attached to the side of the Daytime Heat Rejection Unit. It will deploy from back to front, extending a reflective cloth.

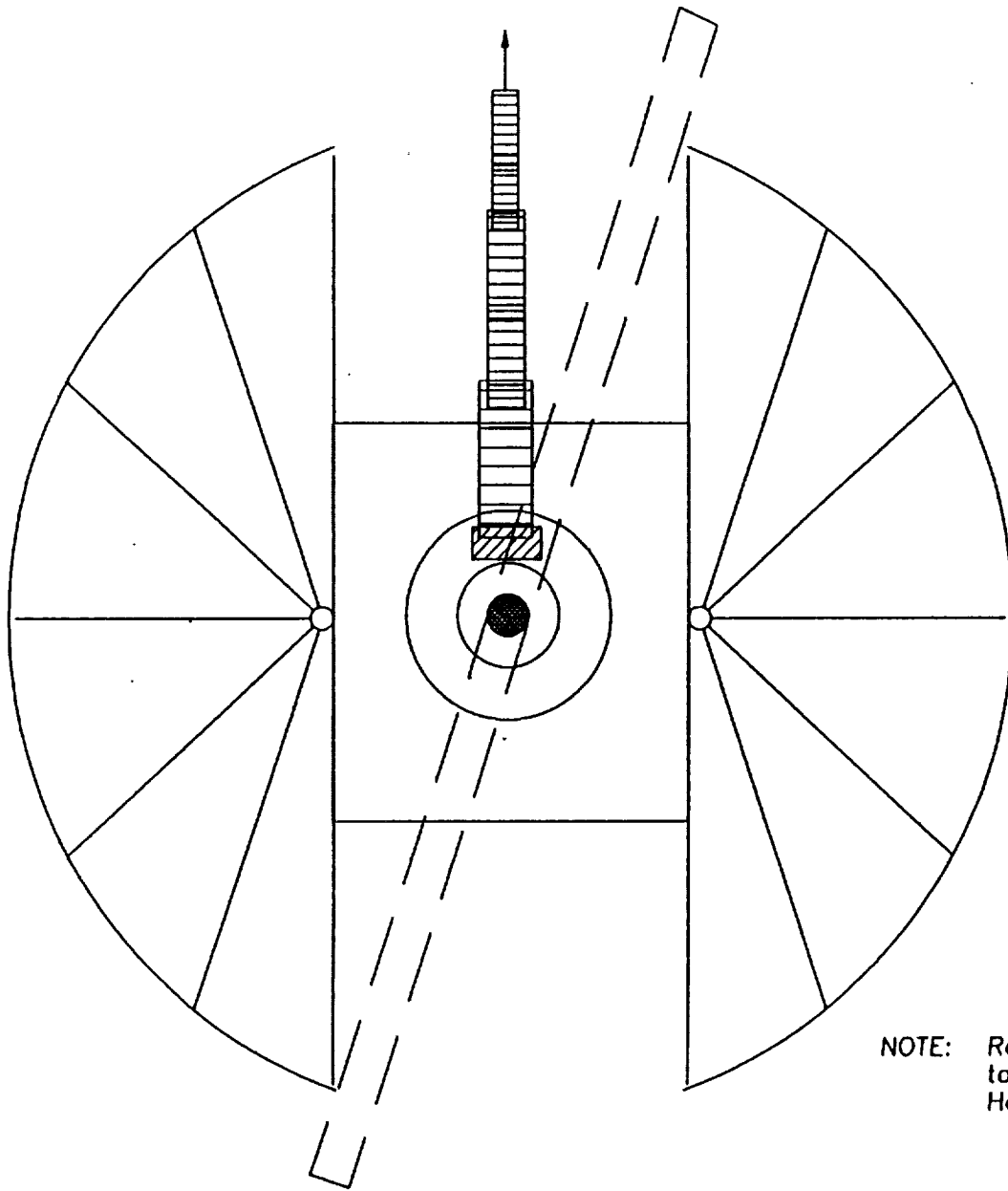
The top radiator shading device will be used to keep the sun from shining directly on the surface of the radiator. It is also a fan type shade with a reflective material shield. It will have the capability of generating electricity through the use of photoelectric cells. The radiator shading will deploy back to front for the left half and front to back for the right half. This will insure a full 360 degrees of coverage.

These shading systems will need further research, and a full analysis of photoelectric capability. It may even be feasible to use these shades to generate enough energy to power the carriage and reduce the LCUV's dependence on bulky fuel cells.

6.9 RADIATOR CLEANING

Another source of damage to the coating is lunar dust. If dust collects on the surface of the radiator, it will degrade the optical properties of the coating. This will cause the efficiency of the entire system to decrease. There are two possible solutions to this problem. First, some type of method could be designed to actually clean the surface of the radiator. Secondly, the dust could be allowed to build up on the surface.

The first solution to this problem involves designing a reliable and economical system to clean the surface of the radiator. At the beginning of the semester, several ideas were suggested for further investigation. They included:



NOTE: Radiator not to scale with Heat Rejection System.

Figure 6.14 Conceptual Design of Ground Shading

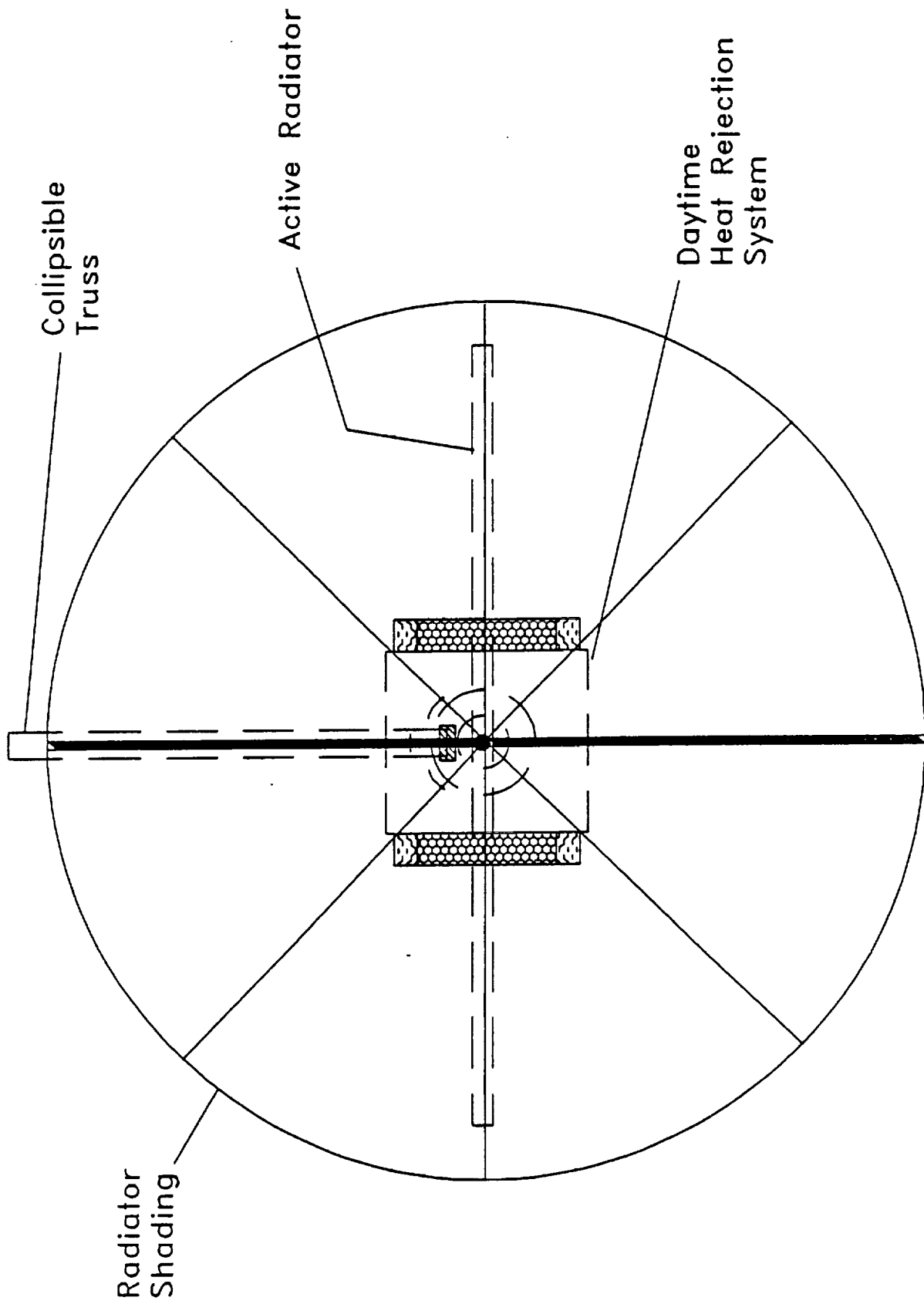


Figure 6.15 Conceptual Design of Radiator Shading

- 1) relying on the vibrations caused by motors and travel over the rough terrain to shake the dust free
- 2) using some sort of wiping or brushing mechanism
- 3) placing gas jets throughout the radiator panels to actually blow the dust from the surface

The first idea, to rely on vibrations caused by motion over terrain, was discounted as being unreliable. An extension of this idea, to actively induce vibration and shake dust free was also abandoned upon realization of the massive size of the radiator and the possibility that an induced vibration would take a long time to damp itself out. Also, since it has been decided to collapse the radiator while moving it, this idea would no longer apply.

The second idea was to brush the dust away from the radiator surface. But such action could produce damage to the radiator coating. Also, the lunar dust is considered to be a fine powder and it might not easily brush away. Therefore, it was decided that this would not be an appropriate means of radiator cleaning.

Finally, a last idea was to use gas jets to "blow" the lunar dust off of the radiator surface. After a meeting with Dr. Arthur Taylor, it was decided that it would be possible to approximate the flow pattern leaving the jets as plumes leaving rocket engines (Reference 37). Any calculations made in this area will have to be completed using experimental approximations. This is necessary due to the fact that the flow will be turbulent and in order to solve turbulent problems exactly, it is necessary to solve the Navier-Stokes equations. At this time, no solution to these equations has been calculated. Using these plume approximations, the cross sectional area as a function of distance from the jet nozzle could be calculated, and the number of jets and their placement could be calculated.

The major drawback to this idea is that the gas used would be lost in space with no means of recovery. When weighed against the cost involved in transportation of the gas to the moon, this waste might prove to be economically prohibitive.

The second solution to the surface coating problem is to allow the dust to collect on the radiator and design a shading system. By allowing the dust to collect on the surface and act as a coating itself, the system approaches a black body. This means that it absorbs all radiation incident on its surface, and it emits more energy than any other surface at that temperature. This situation would make the ratio of absorptivity to emissivity too high. It is advantageous for the emittance to be high, but it is extremely detrimental for the absorptivity to be high. A solution to this problem is to design and create a shading system for the radiator to reduce the amount of radiation impinging on its surface. The

radiator would then be able to operate in a much more efficient manner. One conceptual design for this shading system is shown in Figure 6.16. This mechanism would open and close in a fan-like manner to allow it to collapse along with the rest of the radiator panels.

The idea of placing solar cells on the top of the shading system has been addressed earlier. These cells could be used to store energy that could be used during the frigid days of darkness to heat the radiator fluid. The stored energy could also be used to power the heat rejection unit in the event of an emergency.

6.10 REFRIGERANTS

One of the most important areas of radiator design is the choice of a working fluid. The working fluid, or refrigerant, for the LCUV radiator was chosen on the basis of it's ability to withstand the temperature extremes on the lunar surface and remain in a liquid state. The fluid should remain in a liquid form since a vapor would be more easily lost through any leak in the piping system due to the vacuum conditions on the moon. The lunar temperature ranges are listed in Table 6.3 (Reference 38).

Table 6.3 Lunar Temperature Variations

LATITUDE	MINIMUM TEMPERATURE	MAXIMUM TEMPERATURE
Equator	-148°C	102°C
45°	-148°C	72°C
75°	-148°C	-3°C

There were no refrigerants found that could withstand the large temperature range on the equator or at 45° latitude on the moon. However, there were several found that could possibly withstand the temperature range at 75° latitude. Some results for commonly used refrigerants are listed in Table 6.4 (Reference 38).

Table 6.4 Freezing and Boiling Points for Various Fluids

REFRIGERANT	FREEZING POINT (°C)	BOILING POINT (°C)
717-Ammonia	- 77.7	-33.3
Ethylene Glycol	- 12.7	198.0
Propylene Glycol	(Sets to glass)	187.0
600-Butane	-138.5	- 0.5
160 Ethyl Chloride	-138.3	12.4

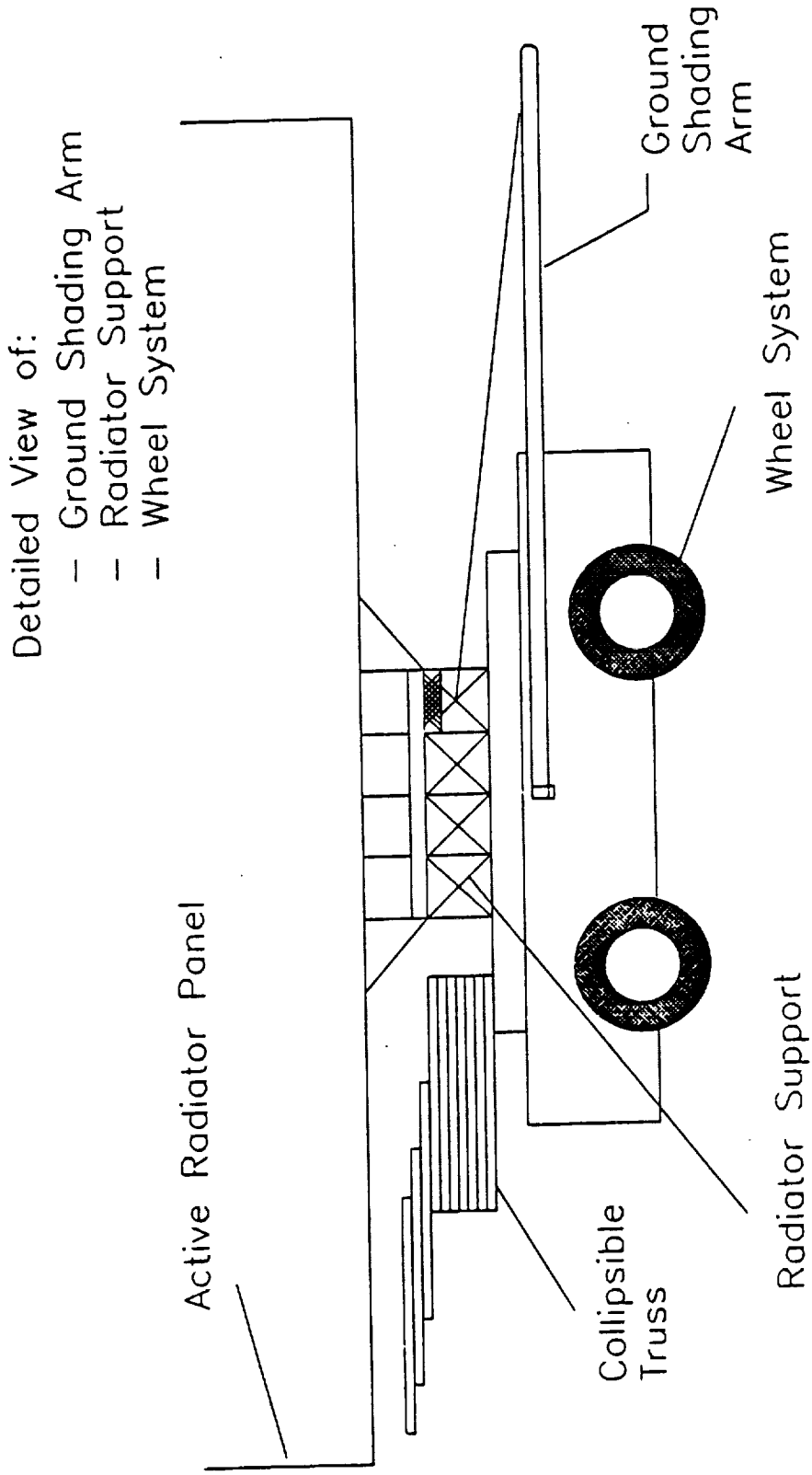


Figure 6.16 Ground Shading System

Since it has not yet been determined what exact position the lunar operation will be on the moon, it has been decided that the refrigerant must be able to operate in the worst case situation of placement at the equator. There are many "cryogenic" refrigerants that would function well in the lower temperature range of the moon, but these refrigerants have low boiling points. There are also refrigerants that would function well in the higher temperature range, but these refrigerants have high freezing points. Thus, one range was chosen to work with. Since it would seem to be easier to keep a fluid from freezing than from boiling, it was decided to choose a working fluid that could withstand the high temperature limit and then heat the fluid when needed to prevent freezing.

One conceptual idea for heating the working fluid is to drain the fluid into a heated reservoir when the temperature falls below an acceptable level. Thus, there would be no great risk of the fluid freezing and damaging the piping system.

There were two fluids found that could withstand the maximum temperature of 102°C. These two fluids are the inhibited glycols, ethylene glycol, and propylene glycol. Ethylene glycol's temperature characteristics are listed in Table 6.4 along with propylene glycol's (Reference 34).

Although ethylene glycol has a freezing point of -12.7°C, "lower operation below -51°C is not recommended". But, propylene glycol sets to glass below -60°C (Reference 36). Both are commonly used refrigerants, so computer analysis was done to determine which would minimize the radiator size. From Figures 6.2 and 6.3, there seems to be little difference in radiator size between the two fluids for the chosen coating of zinc oxide. However, ethylene glycol does have slightly better results. Also, ethylene glycol is said to have better physical properties than propylene glycol, especially at lower temperatures (Reference 36). Thus, due to these previous factors, and the fact that propylene glycol does set to glass below -60°C, ethylene glycol has been chosen as the heat rejection system's working fluid.

6.11 POWER SUPPLY

Another area of concern for this project is the need for a power supply which is independent of that of the LCUV. If the heat rejection unit has the ability to be self-propelled, it can possibly assist the LCUV if it gets stuck, or return to base in case of malfunction with the LCUV. Some possible power supplies include fuel cells and the previously discussed solar cells. Since the power system is to be housed on the heat rejection unit, it could be utilized in case of emergency to power the heat rejection unit. Also, there is a possibility of solar cell placement on the

radiator shading system which could be used in the event of the failure of the fuel cells. This is a large area where much future work could progress.

6.12 PUMP AND PIPING SYSTEM DESIGN

The pump and piping system design serves the purpose of circulating coolant from various LCUV components to an Active Radiator. The primary LCUV components which must be supplied with coolant include the hydrogen-oxygen fuel cells, the two DC motors, and the on-board control system. The device which transports this heat energy to the active radiator is the pump. Other important components considered within the design of the pumping system include the piping, piping material, fluid connections between the radiator and the pump, and possible lubricants for the pump.

Most pumps can be classified into two main categories; positive displacement and kinetic (Reference 39). In each of the two categories, one simple pump was chosen as a possible design for the Daytime Heat Rejection Unit. The first design considered was the piston pump, which lies in the positive displacement category (Figure 6.17). The piston pump was ideal for heat dissipation if the system required a high flow rate of coolant, or a high pressure differential. The type of piston pump is advantageous because it is double acting where coolant discharges on both the forward and reverse strokes. The disadvantage of the piston pump was that it has a relatively short service life because of its high power output (Reference 39).

The second design considered was the centrifugal pump, which lies in the kinetic category (Figure 6.18). The centrifugal pump is used regularly on liquids of moderate viscosity, approximately 1000 Saybolt Universal Seconds (Reference 39). The centrifugal pump operates in a manner that changes the direction of coolant flow, and converts this flow from velocity energy to pressure (Reference 439). Centrifugal pumps generally have a longer service life and have a much wider range of application as compared to piston pumps.

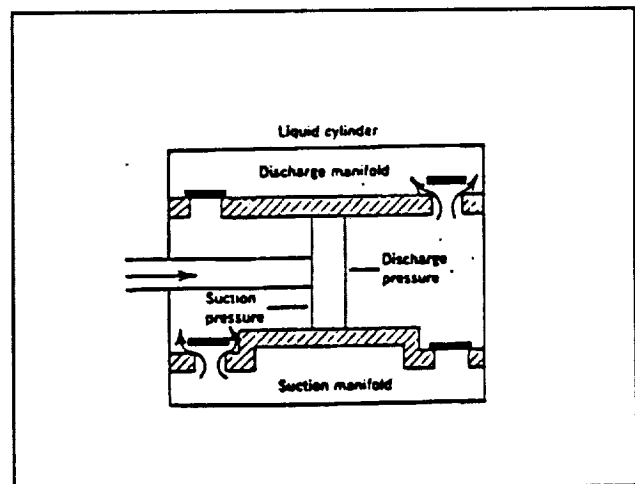


Figure 6.17 Double Acting Piston Pump

The selection of either of the pump designs discussed above depend on five factors (Reference 40). These factors include:

1. The chemical identity of the coolant.

2. The absolute viscosity of the coolant at the pumping temperature.
3. The specific gravity of the coolant at the pumping temperature.
4. The pumping temperature at normal operation.
5. The vapor pressure of the coolant.

Many coolants were researched for the Daytime Heat Rejection Unit. The most likely choice considered for the active radiator sizing was ethylene glycol. The pump must meet two important design criteria. The first design criteria is that the pump must be able to operate with a viscous fluid such as ethylene glycol (Reference 40). The second design criteria is that the pump must be able to withstand the operating temperatures of the coolant. The supply coolant to the LCUV has a temperature of approximately 373°K. The return coolant from the LCUV has a temperature of approximately 440°K. Of the many types of pumps researched, the Piston Pump and the Centrifugal Pump were selected based upon the five factors and two design criteria previously described.

Another important factor for determining the pump size and type is the amount of pressure needed in the overall system. The LCUV components in which the coolant must travel to include the hydrogen-oxygen fuel cells, the two DC Motors, and the On-board Control System (Reference 1). As determined in the NASA/USRA Summer Report, the minimum pipe diameter (for a coolant flow rate of 0.54 kg/sec) is 2.54 centimeters. With the conduction of a thorough fluids analysis, it would be possible to determine the frictional head losses across these LCUV components. Once these head losses are determined, a true differential pressure can be computed through Bernoulli's Equation (Reference 41). The present analysis revealed that the differential pressure was a direct function of the coolant properties:

- density
- flow rate
- kinetic energy
- potential energy
- flow of coolant through pipes, valves, fittings, and nozzles

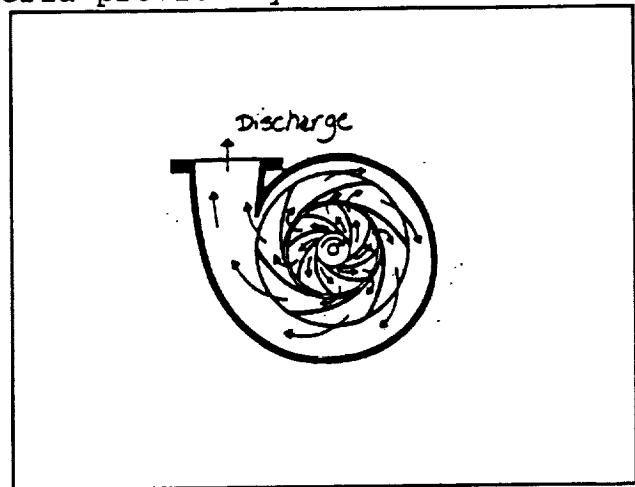


Figure 6.18 In Line Axial Flow Centrifugal Pump

Neglecting any elevation of the coolant, and considering ethylene glycol at an operating temperature of 373°K, the assumed differential pressure for the system is 700 Pascals. This value may change once the frictional head losses have been calculated within the LCUV. This type of analysis can be performed by future design groups. A piping design to reveal in detail how the coolant will remove heat energy from the LCUV components is yet to be determined. Once this piping schematic inside the LCUV is determined, the differential pressure can be computed, and a pump can be sized accordingly.

The conceptual design for the mounting and placement of the pump is shown in Figure 6.19. The major components of this design include the pump itself, the piping system, the coolant reservoir, and at least one swivel joint connection. During LCUV operation,

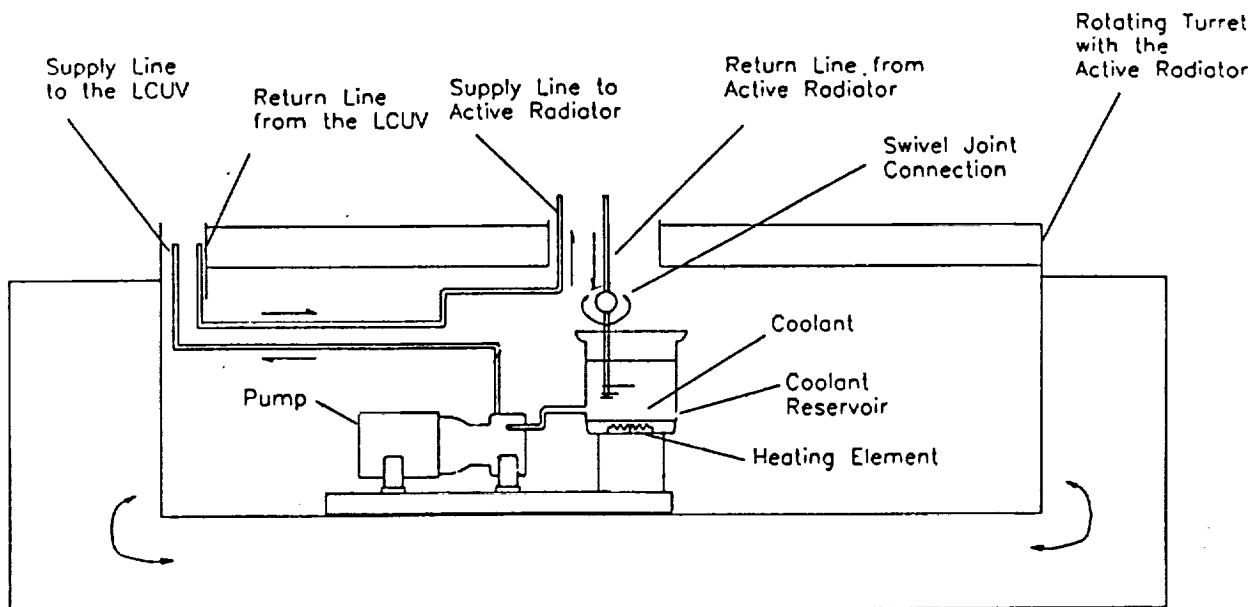


Figure 6.19 Conceptual Pump Design

the coolant travels through several cycles. Starting with the pump, coolant is drawn from the storage reservoir and forced through the collapsible truss to various LCUV components. Once the heat energy is removed from these components, the coolant returns through the collapsible truss, to the active radiator. The active radiator removes the heat energy from the coolant. The coolant then drains back into the storage reservoir and the process begins again. The storage reservoir is utilized when the heat rejection unit is not in use. The storage reservoir includes an interior

heating element. At night, the coolant is drained into the storage reservoir before the lunar surface temperature reaches the freezing point of the coolant. The heating element heats the coolant to prevent it from freezing. The pump is placed inside the Heat Rejection Unit to avoid being exposed to lunar dust and radiation bombardment.

The piping for the Daytime Heat Rejection Unit is important for the transportation of coolant. The conceptual design first considered a dynamic piping system. The pump and reservoir were to remain stationary while the piping was to rotate with the active radiator. Keeping the pump and reservoir stationary meant that the piping system would require more degrees of freedom. More swivel joint connections would then be added to insure a piping system with a higher degree of freedom. Even with the swivel joints dynamically sealed, adding more joints would increase the likelihood of a leak in the overall system. To compensate for this design, an alternative design was chosen. It was agreed that the pump and reservoir should rotate with the active radiator. The coolant return line acts as the central pivot point with one swivel joint connection. The pump and reservoir would be mounted in an enclosed turret that will rotate about the coolant return line, with the active radiator and the collapsible truss. This type of design is advantageous since it cuts down on the amount of swivel joints needed in the piping system. The chance of a leak occurring would then be decreased.

The fluid connections are threaded, male to female, and dynamically sealed. If necessary, this type of swivel joint may also be considered for piping connections to the pump, the active radiator, and the collapsible truss. It is imperative that all connections be sealed completely to prevent any leakage of coolant. Due to the vacuum environment on the lunar surface, any loss of coolant in the piping system, the active radiator, or the collapsible truss would be fatal. As a result, the entire heat rejection unit would ultimately shut down.

There were three types of material considered for the piping system. The first type of material considered was flexible rubber-hosing. After further analysis, it was discovered that the flexible rubber-hosing could not withstand the varying lunar temperatures. The second type of material considered was steel. Also after further analysis, it was discovered that steel was too heavy for space based structures. The material best suited for our application was Aluminum. Aluminum was a lightweight and high strength material. It does not suffer appreciable evaporative losses and was considered an effective deterrent of harmful gamma rays (Reference 1).

Many components of the pump, such as the pistons, rings, and bearings must be kept lubricated. The environment of the lunar surface is varied and harsh. Not only is the environment a vacuum,

but it is also subject to oxidizing agents which reduce chemicals and certain metals. A special lubricant was required for the pump to operate in this type of environment. Frigid lunar surface temperatures were enough to rule out liquid lubricants. High levels of abrasive dust on the lunar surface ruled out the use of dry, thin film lubricants. What was left was a solid type of lubricant, such as Polytetrafluoroethylene or teflon. Teflon can tolerate temperatures from -254°C to $+140^{\circ}\text{C}$ (Reference 42). Teflon was considered applicable as a lubricant for the pump. There is a further need for more testing of how lubricants react in a vacuum state (Reference 42). Without more testing, the pump could have a relatively short life.

7.0 CONCLUSIONS

A 35 kW lunar construction utility vehicle (LCUV) design has been studied. The vehicle is intended for unmanned, heavy construction operations which will occur during the construction of permanent lunar facilities and during many types of mining activities. The LCUV design study assumed continuous vehicle operation for 30 terrestrial days between refueling. Hydrogen-oxygen fuel cells were chosen as the 30 day power source, assuming a central solar cell or nuclear power plant system is available to collect water (produced by the fuel cells) and to resupply the vehicle with liquid hydrogen and oxygen.

A three-point coupling system was designed which could enable autonomous coupling of heavy construction implements without requiring precise positioning. An estimated mating tolerance of 10 cm in all directions appears feasible.

A continuous, elastic loop track design has progressed to the preliminary testing phase. Individual components have been subjected to pre-prototype design and testing as they have been developed. The track system continues to show desirable attributes for heavy construction operations. Interactions between the track system and control system teams produced the conclusion that only one drive motor should be used per track, rather than the original assumption of two. A control system design has evolved which utilizes a joy-stick to generate digital signals which can simulate the command stream that will occur during lunar operations. Successful control of two motors has been demonstrated.

The heat rejection system was designed under a worst case scenario. It was determined that the LCUV could generate 100 kW of heat on the moon's equator. A radiator that could reject this heat would have to be approximately 50 feet long by 50 feet high. A separate logistics trailer has been conceptualized to house the heat rejection unit because the radiator's large size would restrict the LCUV's capabilities. A truss type of structure was incorporated in the design to support the power and coolant lines between the trailer and the LCUV.

More research is needed in the power and heat rejection systems. The large size of the fuel tanks and radiator require an independent, self-sufficient vehicle to support the LCUV. One way to reduce the size would be to use a solar power system, operated during lunar day, instead of fuel cells. This would reduce the weight of the vehicle by eliminating the large fuel tanks. However, a solar panel of the same magnitude as the radiator would probably be needed. This area of the design needs further investigation.

8.0 REFERENCES

1. NASA/USRA Summer Report, Lunar Construction Utility Vehicle, Old Dominion University, Department of Mechanical Engineering and Mechanics, July 1989.
2. Shigley and Mitchell. Mechanical Engineering and Design, 4th Ed., McGraw-Hill Book Company, New York, 1983.
3. O'Leary, Brian. Space Industrialization Vol. II, CRC Press, Inc., Boca Raton, FL, 1982, pp. 68-75.
4. Thompson and Gatland. Materials in Space Technology, Chapel-River Press, England, 1963, pp. 36-46, 135-150.
5. Ravichandran, K.S.; Dwarkadasa, E.S.. "Advanced Aerospace Alloys", Journal of Materials, v.39, May 05, 1987, pp. 28-32.
6. Paine, Thomas, Allan McDougal, and Douglas Davis. "Quick-Disconnect Coupling", US Patent No. 3,656,781, Apr. 18, 1972.
7. Davidson, W.L., et al. "Lunar Surface Construction and Assembly Equipment Study", NASA contract No. NAS9-17878, Eagle Engineering, Inc. Report No. 88-194, Sept. 1, 1988.
8. Martin, J.W., T.J. Martin, T.P. Bennett, and K.M. Martin. Surface Mining Equipment, 1st Ed. Martin Consultants, Inc., Golden Colorado, 1982.
9. Trautwein, W. "Design, Fabrication, and Delivery of an Improved Single Elastic Loop Mobility System (ELMS)", Lockheed Missiles and Space Co., July 1972.
10. Coulson, T. and P. Stiles. "Composite Elastic Loop Mobility System", Old Dominion University Topics Paper, December 1989.
11. Kay Gee Plastics. Technical Consultation, Norfolk Virginia, March 1990.
12. Alberts, Dr. Thomas, and Lonnie Love. Technical Consultation, Old Dominion University, Mar. 1990.
13. Angrist, Stanley W., Direct Energy Conversion, Allyn and Bacon Inc., 1982.
14. Parrish, M.A.. "Fuel Cells-A Survey", Materials in Engineering. Scientific and Technology Press, Surrey, England, vol. 2, No. 2, Dec. 1980.
15. Linden, David, Handbook of Batteries and Fuel cells, McGraw-Hill Book Company, New York, 1984.

16. Jackson, William D. 24th Intersociety Energy Conversion Engineering Conference, vol. 3, 1989.
17. Zdenek, Kopal. The Moon, Academic Press Inc., New York 1960.
18. Incropera, Frank P., and David P. Dewitt. Fundamentals of Heat and Mass Transfer, John Wiley and Sons, New York, 1985.
19. Laquer, Henry L. Cryogenics the Uncommon Cold, U.S. Atomic Energy Commission-Office of Information Services, 1967
20. Vance, Robert W. Applications of Cryogenic Technology, Tinnon-Brown, Inc., 1970 .
21. Gupta, Jai Prakash. Fundamentals of Heat Exchanger and Pressure Vessel Technology, Hemisphere Publishing Corporation, Washington, D.C., 1986.
22. Todd, James P., and Herbert B. Ellis. Applied Heat Transfer, Harper and Row, New York, 1982.
23. Saunders, E.A.D. Heat Exchangers: Selection, Design, and Construction, Longman Scientific & Technical, New York, 1988.
24. Frost, Walter. Heat Transfer at Low Temperatures, Plenum Press, New York, 1975.
25. Minnick, Elbert, Pyramidal Truss Core Panel Compared to Corrugated Core (Navtruss) Panel, For Dr. R.L. Ash, MEM 435 Senior Seminar, October 25, 1988.
26. Alred, Dr. John, et al. Lunar Outpost. Systems Definition Branch, Advanced Programs Office, Johnson Space Center, Houston, Tx. 1989.
27. Craighead, N.D. and R.J.Preliasco. "Design, Development of a Precision Deployable Truss With Optimized Structural Efficiency for Spaceborn Applications", NASA Sixteenth Aerospace Symposium, 1982, pp. 315-328.
28. Aiken, Jeff, Project Engineer, Emergency-One Inc., Personal Interview, March 30, 1990.
29. Fluorocarbon Mechanical Seal Division, Seal Selection Guide.
30. Yeaple, Frank. Fluid Power Design Handbook, Marcel Decker, Inc., 1984, pp.466-486.
31. Dallas, Thomas, Anthony J. Diaguila, and James F. Saltsman, "Design Studies on the Effects of Orientation, Lunation, and Location on the Performance of Lunar Radiators", Lewis Research Center, Cleveland, Ohio, March 1971.

32. Goetzel, Claus. Space Materials Handbook, Addison-Wesley Publishing Company, Inc., Reading Mass. 1965, pp. 426-430.
33. Touloukian, V.S.. Thermal Radiative Properties v.9, Coatings, IFI/Plenum Publishing Corp., New York, 1972, p. 359.
34. Mossman, D.L. et al. "Ultraviolet Electron Irradiating of DC 704 Siloxane Oil on Zinc Orthotitanate Paint", Spacecraft Thermal Control, Design, and Operation; Progress in Astronautics and Aeronautics, vol. 86, AIAA, New York, 1983, pp. 254-266.
35. Hitchcock, Michael, F. "A Review of Polymeric Satellite Thermal Control Material Considerations", SAMPE Journal, Sept/Oct 1983, pp. 15-19.
36. Grant, T, and W. Pence. "Measurements of Thermal Control Coatings on Navstar Global Positioning System Spacecraft", Spacecraft Thermal Control, Design, and Operation; Progress in Astronautics and Aeronautics, vol. 86, AIAA, New York, 1983, pp. 234-247.
37. Taylor, Dr. Arthur. Professor of Mechanical Engineering, Old Dominion University, Personal Interview, February 1990.
38. ASHRAE Handbook, 1985 Fundamentals, SI Edition, ASHRAE Atlanta, GA, 1985, pp. 16.3-18.10.
39. Neerken, Richard F. "Selecting the Right Pump," Fluid Movers, Pumps, Compressors, Fans, and Blowers, Chemical Engineering, McGraw Hill Company, New York, pp.122-133.
40. Stindt, W. H., "Keys to Pump Selection," Fluid Movers, Pumps, Compressors, Fans, and Blowers, Chemical Engineering, McGraw Hill Company, New York, pp. 115-121.
41. Fox, R. W., and A.T. McDonald. Introduction to Fluid Mechanics, Third Edition, John Wiley and Sons, New York, 1985.
42. Howard, J., and A. Kimzey. "Lubrication in Space," Aerospace America, vol. 26, August 1988, pp. 36-37.

9.0 APPENDICIES

- Appendix A** Joystick Algorithm
- Appendix B** Proportional Controller Algorithm
- Appendix C** Proportional and Integral Controller Algorithm
- Appendix D** Multi-Layer Insulation Program
- Appendix E** Program to Determine Deflection and Stress of
Beam Structures
- Appendix F** Program to Size Radiator

Appendix A

Joystick Algorithm

Joystick Algorithm

```
#include <dos.h>
#include <stdio.h>
/*
 * The reason for the three masks is the long time for a zero bit
 * to be returned for an unplugged in joystick
 */
#define STICKA_MASK 0x03
#define STICKB_MASK 0x0C
#define STICK_MASK 0x0F

#define STICKBUFSIZE 150

typedef struct {
    short a1, a2, b1, b2, ax, ay, bx, by;
} JOYSTICK;

typedef struct {
    float axml, axmh, aym1, aymh;
    short axmid, aymid;
} STICK_CHAR;

void joystick(JOYSTICK *);
void calibrate(STICK_CHAR *);
void no_button();

void joystick(JOYSTICK *j){
    unsigned char stickbuf[STICKBUFSIZE];
    unsigned char *sbp, *sbpl;
    short i;
    unsigned char jval;

    sbp = sbpl = stickbuf;

    i = STICKBUFSIZE;

    outp(0x201, 0);

LOOP:
    *sbp = inp(0x201);
    if((*sbp & STICKA_MASK) == 0) goto DONE;
#ifdef DEBUG
    if(--i) sbp++;
    else goto DONE;
#else
    sbp++;
#endif
    goto LOOP;
```

DONE:

```
/*
 * If the following print statement gets too close to zero,
increase
 * the "STICKBUFSIZE" macro
 * NOTE: with DEBUG not defined, STICKBUFSIZE
 * must be roughly twice as great.
 */
#ifdef DEBUG
    if(i) printf("%d ", i);
    else printf("0x%2X ", *sbp);
#endif

    i = (short)(sbp - sbp1);

    do(
        sbp1 = sbp--;
        if(*sbp1 != *sbp){
            jval = (*sbp | *sbp1) ^ (*sbp & *sbp1);
#ifdef DEBUG
                printf("(%d-%d%d%d)", i, ((jval & 1) == 1), ((jval & 2) ==
2),
                    ((jval & 4) == 4), ((jval & 8) == 8));
#endif
                if(jval & 0x01) j->ax = i;
                if(jval & 0x02) j->ay = i;
                if(jval & 0x04) j->bx = i;
                if(jval & 0x08) j->by = i;
            }
        } while(--i);

#ifdef DEBUG
        printf("<d%d%d>", ((*stickbuf & 0x80) == 0x80),
            ((*stickbuf & 0x40) == 0x40), ((*stickbuf & 0x20) ==
0x20),
            ((*stickbuf & 0x10) == 0x10));
#endif
        j->b2 = ((*stickbuf & 0x80) == 0);
        j->b1 = ((*stickbuf & 0x40) == 0);
        j->a2 = ((*stickbuf & 0x20) == 0);
        j->a1 = ((*stickbuf & 0x10) == 0);

        return;
    }

void calibrate(STICK_CHAR *j) {
    short i,xmin,xmid,xmax,ymin,ymid,ymax;
    JOYSTICK x;

    printf(" CALIBRATION PROCEDURE:\n\n");
```

```

printf("\n      Move stick all the way to the left, press button
A\n");
do joystick(&x);
while (x.a1==0);
xmin=x.ax;
no_button();
printf("\n      Move stick all the way to the right, press button
A\n");
do joystick(&x);
while (x.a1==0);
xmax=x.ax;
no_button();
printf("\n      Allow stick to center, then press button A\n");
do joystick(&x);
while (x.a1==0);
xmid=x.ax;
ymid=x.ay;
no_button();
printf("\n      Move stick all the way to the top, press button
B\n");
do joystick(&x);
while (x.a2==0);
ymin=x.ay;
no_button();
printf("\n      Move stick all the way to the bottom, press button
B\n");
do joystick(&x);
while (x.a2==0);
ymax=x.ay;
no_button();
printf("\n\n      CALIBRATION PROCESS COMPLETE.\n\n\n");
j->axmid = xmid;
j->axml = ((float)((xmid-xmin))/100.0);
j->axmh = ((float)((xmax-xmid))/100.0);
j->aymid = ymid;
j->ayml = ((float)((ymid-ymin))/100.0);
j->aymh = ((float)((ymax-ymid))/100.0);
printf("xmid=%d, xmin=%d, xmax=%d\n",xmid,xmin,xmax);
printf("axml=%f, axmh=%f, axmid=%d\n",j->axml,j->axmh,j->axmid);
printf("ymid=%d, ymin=%d, ymax=%d\n",ymid,ymin,ymax);
printf("ayml=%f, aymh=%f, aymid=%d\n",j->ayml,j->aymh,j->aymid);
return;
}
void no_button() {
JOYSTICK x;

do joystick(&x);
while (x.a1 || x.a2 || x.b1 || x.b2);
return;

```

Appendix B

Proportional Controller Algorithm

PROPORTIONAL CONTROLLER ALGORITHM

```
#include <conio.h>
#include <stdio.h>
#include <graph.h>
#include <math.h>

#define true 1
#define false 0

typedef struct { short a1,a2,b1,b2,ax,ay,bx,by;} JOYSTICK;

typedef struct { float axml, axmh, ayml, aymh;
               short axmid, aymid;
               } STICK_CHAR;

extern double a2d(int);
extern void d2a(int, double);
extern void joystick(JOYSTICK *);
extern void calibrate(STICK_CHAR *);
extern void io_init();

void reset(JOYSTICK, STICK_CHAR);
float error(float, float);

main()
{
    JOYSTICK j;
    STICK_CHAR sc;

    int channel_1 = 0
        ,channel_2 = 1;

    int motr_rat_l, motr_rat_r, counter;

    /* @ Vmax out = 20 Volts */
    float ki = 0.2
        ,km_l=.1836 /* Volts/rad per sec === SNAFU */
        ,km_r=.1730 /* Volts/rad per sec === FUBAR */
        ,kt_l=.0143 /* Volts/rad per sec === SNAFU */
        ,kt_r=.0148; /* Volts/rad per sec === FUBAR */

    float v_keithley_l, v_keithley_r, w_max, kp;
    float error_1, error_2, omega_desired_l, omega_desired_r;
    float omega_actual_r, omega_actual_l, error_l, error_r;
```

```

float effort_l, effort_r, effort_volts_l, effort_volts_r;
float control_input_l, control_input_r;

io_init();
calibrate(&sc);
counter=1;

printf("\n\n\n\nEnter Kp and Wmax of the system");
scanf("%f %f",&kp,&w_max);

while (j.a1!=1)
    {
        joystick(&j);

        i f      ( j . a x < s c . a x m i d )
j.ax=((short)((float)(j.ax-sc.axmid))/sc.axml);
        else j.ax=((short)((float)(j.ax-sc.axmid))/sc.axmh);

        i f      ( j . a y < s c . a y m i d )
j.ay=-((short)((float)(j.ay-sc.aymid))/sc.ayml);
        else j.ay=-((short)((float)(j.ay-sc.aymid))/sc.aymh);

        if (abs(j.ax)+abs(j.ay)>100)
            {
                if (j.ax>0) j.ax=100-abs(j.ay);
                else j.ax=-100+abs(j.ay);
            }

        motr_rat_l = j.ax+j.ay;
        motr_rat_r=j.ay-j.ax;

        if(abs(motr_rat_l)<20)
            {
                motr_rat_l=0;
            }
        if(abs(motr_rat_r)<20)
            {
                motr_rat_r=0;
            }

        printf("                Left:%d    %%                Right:%d    %%
\r",motr_rat_l,motr_rat_r);

        omega_desired_l=w_max*motr_rat_l/100;
        omega_desired_r=w_max*motr_rat_r/100;

        omega_actual_l = a2d(channel_1)/kt_l;
        omega_actual_r = a2d(channel_2)/kt_r;

```

```

        if(omega_actual_l<0) omega_actual_l=omega_actual_l-.18;
        else omega_actual_l=omega_actual_l+.18;

        if(omega_actual_r<0) omega_actual_r=omega_actual_r-.17;
        else omega_actual_r=omega_actual_r+.18;

error_l = omega_desired_l - omega_actual_l;
error_r = omega_desired_r - omega_actual_r;

effort_l = error_l*kp;    /* P type control */
effort_r = error_r*kp;    /* P type control */

/*
 *   input signal after p type control
 *
 *   if(effort_l < 0) effort_l=effort_l-3;
 *   else effort_l=effort_l+3;
 */

control_input_l = ((effort_l)*km_l);

        if(effort_r<0) effort_r=effort_r-2.2;
        else effort_r=effort_r+2.2;

control_input_r = ((effort_r)*km_r);

/* VL*1.5737=VR */

if(abs(motr_rat_l)<20)
    {
        control_input_l=0;
    }
if(abs(motr_rat_r)<20)
    {
        control_input_r=0;
    }

control_input_l = control_input_l*(1.9652);    /* /3.612 */
control_input_r = control_input_r*(.6622);    /* /5.02 */

if(control_input_l>9.5) control_input_l=9.0;
if(control_input_l<-9.5) control_input_l=-9.0;
if(control_input_r>9.5) control_input_r=9.0;
if(control_input_r<-9.5) control_input_r=-9.0;
d2a(channel_1,control_input_l);
d2a(channel_2,control_input_r);
    } /* end of while loop */
io_init();
} /* end of main */

```

Appendix C

Proportional and Integral Controller Algorithm

PROPORTIONAL-INTEGRAL CONTROL ALGORITHM

```
#include <conio.h>
#include <stdio.h>
#include <graph.h>
#include <math.h>
#include <time.h>

#define true 1
#define false 0

typedef struct { short a1,a2,b1,b2,ax,ay,bx,by;} JOYSTICK;

typedef struct { float axml, axmh, ayml, aymh;
                short axmid, aymid;
                } STICK_CHAR;

extern double a2d(int);
extern void d2a(int, double);
extern void joystick(JOYSTICK *);
extern void calibrate(STICK_CHAR *);
extern void io_init();

void reset(JOYSTICK, STICK_CHAR);

main()
{
    JOYSTICK j;
    STICK_CHAR sc;

    int channel_1 = 0
        ,channel_2 = 1;

    int motr_rat_1, motr_rat_r, counter;

        /* @ Vmax out = 20 Volts */

    float ki=.02
        ,kp=.08
        ,w_max=130
        ,km_l=.225 /* Volts/rad per sec === SNAFU */
        ,km_r=.225 /* Volts/rad per sec */
        ,kt_l=.014 /* Volts/rad per sec === SNAFU */
        ,kt_r=.014; /* Volts/rad per sec */
```

```

float v_keithley_l, v_keithley_r;
float error_1, error_2, omega_desired_l, omega_desired_r;
float omega_actual_r, omega_actual_l, error_l, error_r;
float effort_l, effort_r, effort_volts_l, effort_volts_r;
float control_input_l, control_input_r, sum_l, sum_r, old_error_l;
float old_error_r;

time_t tstart, tstop;

double tused;

io_init();
calibrate(&sc);
counter=1;

sum_l=0;
sum_r=0;

time(&tstart);

while (j.a1!=1)
{
    time(&tstop);

    tused=difftime(tstop,tstart);

    time(&tstart);

    joystick(&j);

    if ( j . a x < s c . a x m i d )
j.ax=((short)((float)(j.ax-sc.axmid))/sc.axml);
        else j.ax=((short)((float)(j.ax-sc.axmid))/sc.axmh);

    if ( j . a y < s c . a y m i d )
j.ay=-((short)((float)(j.ay-sc.aymid))/sc.ayml);
        else j.ay=-((short)((float)(j.ay-sc.aymid))/sc.aymh);

    if (abs(j.ax)+abs(j.ay)>100)
    {
        if (j.ax>0) j.ax=100-abs(j.ay);
        else j.ax=-100+abs(j.ay);
    }

    motr_rat_l = j.ax+j.ay;
    motr_rat_r=j.ay-j.ax;

    printf("%d /*      ==   */
Left:%d  %%      Right:%d  %%

```

```

\r",counter,motr_rat_l,motr_rat_r);

    omega_desired_l=w_max*motr_rat_l/100;
    omega_desired_r=w_max*motr_rat_r/100;

    omega_actual_l = a2d(channel_1)/kt_l;
    omega_actual_r = a2d(channel_2)/kt_r;

    error_l = omega_desired_l - omega_actual_l;
    error_r = omega_desired_r - omega_actual_r;

sum_l=sum_l+(tused*error_l)-(.5*tused*(error_l-old_error_l));
sum_r=sum_r+(tused*error_r)-(.5*tused*(error_r-old_error_r));
*/
    effort_l = error_l*kp;      /* PI type control */
    effort_r = error_r*kp;

/* if(error_l/omega_desired_l<.05)
    {
        effort_l=effort_l+ki*sum_l;
    }

if(error_r/omega_desired_r<.05)
    {
        effort_r=effort_r+ki*sum_r;
    }
*/

if(control_input_l<0) control_input_l = ((effort_l)*km_l-1);
else control_input_l=((effort_l)*km_l+1);

if(control_input_r<0) control_input_r = ((effort_r)*km_r-1);
else control_input_r=((effort_r)*km_r+1);

if(abs(motr_rat_l) < 10)
    {
        control_input_l=0;
    }

if(abs(motr_rat_r)<10)
    {
        control_input_r=0;
    }

```

```
    d2a(channel_1,control_input_l);
    d2a(channel_2,control_input_r);

    old_error_l=error_l;
    old_error_r=error_r;

    counter++;

}    /* end of while loop */
io_init();
}    /* end of main    */
```

Appendix D

Multi-Layer Insulation Program

```

10 REM This program estimates the amount of heat flow into a cryogenic fluid
20 REM (Hydrogen) located in a cylindrical tank with multi-layered shielding.
30 REM
40 K= .13
50 RR=0' RM1=0; RM2=0
60 SIG=5.67E-08
70 PI=3.1415
80 D1=1.07
90 L=5
100 TNK=21
110 TOUT=383
120 EM1=.021
130 DIM SR(400), EM(400)
140 DEF FNEMC(T)=.0001*T+.01
150 INPUT "ENTER THE NUMBER OF LAYERS NEEDED";NS
160 INPUT "ENTER THE SPACING OF LAYERS (M)";SPA
170 LPRINT "NUMBER OF LAYERS= ";NS
180 LPRINT "SPACING= ";SPA
190 DI=D1
200 FOR N=1 TO NS
210   DI=DI+SPA
220   SR(N)=PI*DI*L
230 NEXT N
240 RO=(Q-FNEMC(TOUT))/(FNEMC(TOUT)*SR(NS))
250 RI=(Q-FNEMC(TNK))/(FNEMC(TNK)*(PI*D1*L))
260 RI=RI+1/(PI*D1*L)
270 FOR N=1 TO NS-1
280   TAP=(N*(TOUT-TNK)/NS)+TNK
290   RM1=RM1 + (1/SR(N))+(1/SR(N+1))
300   RM2=RM2 + 2*((1-FNEMC(TAP))/(FNEMC(TAP)*SR(N+1)))
310   RM=RM1+RM2
320   QIN=(SIG*(TNK^4-TOUT^4)/(RI+RM+RO))
330   HFG=898300!
340   M=ABS((QIN*86397.9)/HFG)
350   REM
360   LPRINT "BOIL OFF AT NUMBER OF SHIELDING = ";N;"IS EQUAL TO ";M"KG/DAY"
370   LPRINT "HEAT FLOW(W/m)=";QIN
380 NEXT N
390 END

```

Appendix E

Program to Determine Deflection and
Stress of Beam Structure

```

10 '          Program To Calculate The
20 '          Deflection, Bending Stress And Shear Stress
30 '          In A Beam Of Round Or Square Cross Section
40 '          Simply Supported At Both Ends
50 '          Subjected To A Specified Distributed Load
60 '
70 '
80 ' Variables
90 '
100 ' C = Distance to Maximum Fiber
110 ' Din = Inside Diameter of Round Beam
120 ' Dout = Outside Diameter of Round Beam
130 ' E = Young's Modulus for Aluminum Alloy
140 ' I = Moment of Inertia
150 ' Inside = Inside Dimension of Square Beam
160 ' L = Maximum Length of Beam
170 ' Large = Dimension of Large End of Beam
180 ' Long = Length of Each Beam Section
190 ' M = Bending Moment
200 ' Outside = Outside Dimension of Square Beam
210 ' Rarea = Area of Round Beam
220 ' Rin = Inside Radius of Round Beam
230 ' Rout = Outside Radius of Round Beam
240 ' Rtao = Shear Stress in Round Beam
250 ' Sect = Number of Beam Sections
260 ' Shear = Shear Stress
270 ' Sigma = Bending Stress
280 ' Small = Dimension at Small End of Beam
290 ' Stao = Shear Stress in Square Beam
300 ' T = Thickness of Round Beam
310 ' Thick = Thickness of Square Beam
320 ' V = Volume
330 ' W = Distributed Load
340 ' X = Position Along Beam
350 ' Y = Deflection Along Beam
360 ' Yallow = Allowable Deflection
370 ' Yards = Maximum Length in Yards
380 ' Ymax = Maximum Deflection
390 KEY OFF
400 COLOR 7,1
410 CLS
420 '
430 ' Selection of Beam Type
440 '
450 INPUT "Round (R) or Square (S) Beam ";ANSS
460 PRINT
470 INPUT "Maximum Allowable Deflection in Inches";YELLOW
480 PRINT
490 IF ANSS ="R" OR ANSS="r" THEN 540
500 IF ANSS="S" OR ANSS="s" THEN 600
510 '
520 ' Round Beam Main Program
530 '
540 GOSUB 700
550 GOSUB 1370
560 GOSUB 1540
570 GOSUB 1720
580 END
590 '
600 ' Square Beam Main Program

```

```

510 '
520 GOSUB 1050
530 GOSUB 1370
540 GOSUB 1540
550 GOSUB 1900
560 END
570 '
580 ' Round Beam Subroutine
590 '
600 INPUT "Outer Diameter of Round Beam";DOUT
610 PRINT
620 INPUT "Inner Diameter of Round Beam";DIN
630 PRINT
640 T=DOUT-DIN
650 ROUT=DOUT/2
660 C=ROUT
670 RIN=DIN/2
680 PI=3.1415
690 RAREA=PI*(ROUT^2-RIN^2)
700 LONG=120
710 E=1.03E+07
720 I=(PI/64)*(DOUT^4-DIN^4)
730 FOR L= 12 TO 2400 STEP 12
740 V=PI*L*(ROUT^2-RIN^2)
750 W=((.1*V)/(6*L))+.0624/6
760 YMAX=(5*W*L^4)/(384*E*I)
770 YARDS=L/36
780 IF YMAX>YALLOW THEN 900
790 NEXT L
800 SECT=L/LONG
810 SMALL=DOUT
820 LARGE=DOUT+(2*T*SECT)
830 COLOR 20,3
840 PRINT "Maximum Length = ";YARDS "yards"
850 COLOR 7,1
860 PRINT
870 PRINT "Diameter at small end = ";SMALL "inches"
880 PRINT
890 PRINT "Diameter at Large End = ";LARGE "inches"
900 PRINT
910 RETURN
920 '
930 ' Square Beam Subroutine
940 '
950 INPUT "Outer Dimension of Square Beam in Inches";OUTSIDE
960 PRINT
970 INPUT "Thickness of Square Beam in Inches";THICK
980 PRINT
990 INSIDE=OUTSIDE-2*THICK
1000 C=OUTSIDE/2
1010 SAREA=OUTSIDE^2-INSIDE^2
1020 LONG=120
1030 E=1.03E+07
1040 I=(OUTSIDE^4-INSIDE^4)/12
1050 FOR L=12 TO 2400 STEP 12
1060 V=L*(OUTSIDE^2-INSIDE^2)
1070 W=((.1*V)/(6*L))+.0624/6
1080 YMAX=(5*W*L^4)/(384*E*I)
1090 YARDS=L/36
1100 IF YMAX>YALLOW THEN 1220

```

```
1810 RTAO=(2*SHEAR)/RAREA
1820 WRITE#1,X/36,SHEAR,RTAO
1830 PRINT X/36,SHEAR,RTAO
1840 NEXT X
1850 CLOSE 1
1860 RETURN
1870 '
1880 ' Square Beam Shear Force/Stress Subroutine
1890 '
1900 INPUT "Save the Shear Data Points";ANSS
1910 PRINT
1920 IF ANSS="Y" OR ANSS="y" THEN 1940
1930 GOTO 2040
1940 INPUT "Input the Filename";OUTFILES
1950 PRINT
1960 OPEN "o",#1,OUTFILES
1970 FOR X=0 TO L STEP 12
1980 SHEAR=((W*L)/2)-W*X
1990 STAO=(1.5*SHEAR)/SAREA
2000 WRITE#1,X/36,SHEAR,STAO
2010 PRINT X/36,SHEAR,STAO
2020 NEXT X
2030 CLOSE 1
2040 RETURN
```

Appendix F

Program to Size Radiator

```

10 '
20 ' *****
30 ' ***** Daytime Heat Rejection System for the Lunar *****
40 ' ***** Construction Utility Vehicle *****
50 ' *****
60 ' ***** "Computer Program To Size Active Radiator" *****
70 ' *****
80 ' ***** Revised from previous Senior Design Group *****
90 ' *****
100 ' ***** REVISED as of 2/6/90 *****
110 ' *****
120 ' ***** program name "PRGRAD" *****
130 ' *****

```

DESCRIPTION OF VARIABLES

```

170 ' COOL :NAME OF THE COOLING FLUID BEING ANALYZED
180 ' D :DIAMETER OF PIPE USED TO CARRY COOLING FLUID (METERS)
190 ' W :MASS FLOW RATE OF THE COOLING FLUID (KG/SEC)
200 ' CP :SPECIFIC HEAT OF THE COOLING FLUID (KJ/(KG)(K))
210 ' VIS :DYNAMIC VISCOSITY OF COOLING FLUID ((N)(SEC)/SQ METERS)
220 ' PR :PRANTL NUMBER OF COOLING FLUID
230 ' K :THERMAL CONDUCTIVITY OF COOLING FLUID (KW/(METERS)(K))
240 ' HR :CONVECTIVE HEAT TRANSFER COEFFICIENT (KW/(SQ METERS)(K))
250 ' RE :REYNOLDS NUMBER
260 ' NU :NUSSELT NUMBER
270 ' TFI :TEMPERATURE OF COOLING FLUID AT THE RADIATOR INLET (K)
280 ' TFO :TEMPERATURE OF COOLING FLUID AT THE RADIATOR OUTLET (K)
290 ' DELTATF :TEMPERATURE DIFFERENCE OF COOLING FLUID AT THE RADIATOR INL
300 ' AND OUTLET (K)
310 ' TM :LUNAR SURFACE TEMPERATURE (K)
320 ' ANGLE :ANGLE BETWEEN SUN AND NORMAL TO RADIATOR SURFACE (DEGREES)
330 ' GS :SOLAR CONSTANT (KW/SQ METERS)
340 ' SBC :STEPHAN-BOLTMANN CONSTANT (KW/(SQ METERS)(K^4))
350 ' Q :TOTAL HEAT REJECTION FLOW RATE (KW)
360 ' A :SOLAR ABSORPTANCE OF RADIATOR COATING
370 ' E :EMITTANCE OF RADIATOR COATING
380 ' TS :EFFECTIVE SINK TEMPERATURE (K)
390 ' TWI :INLET RADIATOR WALL TEMPERATURE (K)
400 ' TWO :OUTLET RADIATOR WALL TEMPERATURE (K)
410 ' TWAV :RADIATOR AVERAGE WALL TEMPERATURE (K)
420 ' AREA :PRIME RADIATOR AREA (SQ METERS)
430 ' SQRAREA :DEMENSIONS OF RADIATOR IN METERS
440 ' SQRARFT :DEMENSIONS OF RADIATOR IN FEET

```

SUBROUTINES

```

480 GOSUB 590 ' INPUT VALUES
490 GOSUB 810 ' RATE OF HEAT REJECTION
500 GOSUB 860 ' TEMPERATURE OF COOLING FLUID AT THE RADIATOR OUTLET
510 GOSUB 920 ' EFFECTIVE SINK TEMPERATURE
520 GOSUB 990 ' CONVECTIVE HEAT TRANSFER COEFFICIENT
530 GOSUB 1390 ' RADIATOR WALL TEMPERATURES
540 GOSUB 1920 ' RADIATOR AVERAGE WALL TEMPERATURE
550 GOSUB 2020 ' PRIME RADIATOR AREA
560 GOSUB 2100 ' PROGRAM OUTPUT
570 END
580 '

```

```

590      INPUT VALUES
600
610  CLS
620  PRINT "***** INPUT VALUES *****"
*":PRINT
630  INPUT "COOLING FLUID BEING TESTED ";COOL$
640  INPUT "OPERATING CONDITION OF LCUV ";OPER$
650  INPUT "SURFACE COATING OF RADIATOR SURFACE ";COAT$
660  INPUT "TOTAL HEAT REJECTION NEEDED FOR ENTIRE LCUV (KW) =" ;QTOTAL
670  INPUT "DIAMETER OF PIPE USED TO CARRY COOLING FLUID (meters) =" ;D
680  INPUT "MASS FLOW RATE OF THE COOLING FLUID (KG/SEC) =" ;W
690  INPUT "SPECIFIC HEAT OF THE COOLING FLUID (KJ/(KG*K)) =" ;CP
700  INPUT "TEMPERATURE OF COOLING FLUID AT THE RADIATOR OUTLET (K) =" ;TFO
710  INPUT "SOLAR ABSORPTANCE =" ;A
720  INPUT "EMITTANCE OF RADIATOR =" ;E
730  INPUT "LUNAR SURFACE TEMPERATURE (K) =" ;TM
740  INPUT "ANGLE BETWEEN SUN AND NORMAL TO RADIATOR SURFACE (DEGREES) =" ;ANG
750      "SOLAR CONSTANT (KW/SQ METERS) =" ;GS
760  LET          GS = 1.356
770      "STEPHAN-BOLTZMANN CONSTANT (KW/(SQ METERS)(K^4)) =" ;SBC
780  LET          SBC = 5.6671E-11
790  RETURN
800
810      RATE OF HEAT REJECTION
820
830  Q=QTOTAL
840  RETURN
850
860      TEMPERATURE OF COOLING FLUID AT THE RADIATOR OUTLET
870
880  DELTATF=Q/(W*CP)
890  TFI=TFO+DELTATF
900  RETURN
910
920      EFFECTIVE SINK TEMPERATURE
930
940  PI=3.14159
950  ANGLE=ANGLE*(PI/180)
960  TS=(TM^4/2+(GS/(2*SBC))*(A/E)*COS(ANGLE))^2.25
970  RETURN
980
990      CONVECTIVE HEAT TRANSFER COEFFICIENT
1000
1010  MEANTF=(TFO+TFI)/2
1020  CLS
1030  PRINT "***** Calculation of Convection Heat Transfer Coefficient *****"
1040  PRINT
1050  PRINT
1060  PRINT ">TEMPERATURE OF COOLING FLUID AT RADIATOR INLET =" TFI "K"
1070  PRINT
1080  PRINT ">TEMPERATURE OF COOLING FLUID AT RADIATOR OUTLET =" TFO "K"
1090  PRINT
1100  PRINT ">MEAN TEMPERATURE OF COOLING FLUID =" MEANTF "K"
1110  PRINT
1120  PRINT "***** NOTE: *****"
1130  PRINT "THE PROPERTIES REQUIRED TO CALCULATE THE CONVECTIVE HEAT"
1140  PRINT "TRANSFER COEFFICIENT SHOULD BE EVALUATED AT THE MEAN"
1150  SQRAREA = SQR(AREA/2)

```

```

1160 PRINT " TEMPERATURE OF THE COOLING FLUID."
1170 PRINT "*****"
1180 PRINT
1190 PRINT "DYNAMIC VISCOSITY.... "
1200 INPUT " OF THE COOLING FLUID ((N)(SEC)/SQ METERS)=";VIS
1210 INPUT "THERMAL CONDUCTIVITY OF COOLING FLUID (KW/(METERS)(K)) =" ;K
1220 INPUT "SPECIFIC HEAT OF COOLING FLUID (KJ/(KG K))";CP
1230 PR=((CP)*(VIS)/K)
1240 IF PR <= .7 OR PR >= 160 THEN 1250 ELSE 1280
1250 BEEP:CLS:BEEP:PRINT "*****IMPROPER PRANTL NUMBER!!!!!!!!!!!"
1260 PRINT
1270 GOTO 1030
1280 RE=(4*W)/(PI*D*VIS)
1290 IF RE <= 10000 THEN 1300 ELSE 1350
1300 BEEP:CLS:BEEP:PRINT "*****Reynold number approaching Laminar!!!"
1310 PRINT:PRINT "**** Must change pipe Diameter and/or Mass flow Rate,"
1320 PRINT " to get turbulent fluid flow."
1330 PRINT
1340 FOR XXX=1 TO 20000: NEXT XXX:GOTO 10
1350 NU=.023*(RE^.8)*(PR^.3)
1360 HR=(NU*K)/D
1370 RETURN
1380 '
1390 ' RADIATOR WALL TEMPERATURES
1400 '
1410 TWI=TFI
1420 CHECK1=1
1430 WHILE (CHECK1>.0001)
1440 F1=TFI-(SBC*E/HR)*(TWI^4-TS^4)-TWI
1450 DF1=4*(SBC*E/HR)*TWI^3-1
1460 TWI=TWI-F1/DF1
1470 CHECK1=ABS(F1/DF1)
1480 WEND
1490 TWO=TFO
1500 CHECK2=1
1510 WHILE (CHECK2>.0001)
1520 F2=TFO-(SBC*E/HR)*(TWO^4-TS^4)-TWO
1530 DF2=4*(SBC*E/HR)*(TWO^4-TS^4)-TWO
1540 TWO=TWO-F2/DF2
1550 CHECK2=ABS(F2/DF2)
1560 WEND
1570 IF TWI>TS AND TWO>TS GOTO 1900
1580 CLS
1590 PRINT "***** PROGRAM OUTPUT *****"
1600 PRINT
1610 PRINT
1620 PRINT ">COOLING FLUID USED IN THIS ANALYSIS : " COOL$
1630 PRINT
1640 PRINT
1650 PRINT ">OPERATING CONDITIONS OF LCUV : " OPER$
1660 PRINT
1670 PRINT
1680 PRINT " PROPERTIES OF THE FLUID USED FOR COOLING"
1690 PRINT
1700 PRINT ">MASS FLOW RATE =" W "KG/SEC"
1710 PRINT ">SPECIFIC HEAT =" CP "KJ/(KG)(K)"
1720 PRINT ">DYNAMIC VISCOSITY =" VIS "(N)(SEC)/SQ METERS"
1730 PRINT ">REYNOLDS NUMBER =" RE

```

```

1740 PRINT ">PRANTL NUMBER =" PR
1750 PRINT ">THERMAL CONDUCTIVITY =" K "KW/(METERS)(K)"
1760 PRINT ">CONVECTIVE HEAT TRANSFER COEFFICIENT =" HR "KW(SQ METERS)(K)"
1770 PRINT ">TEMPERATURE OF COOLING FLUID AT RADIATOR INLET =" TFI "K"
1780 PRINT ">TEMPERATURE OF COOLING FLUID AT RADIATOR OUTLET =" TFO "K"
1790 PRINT
1800 PRINT
1810 PRINT "INVALID RESULTS: THE EFFECTIVE SINK TEMPERATURE CANNOT BE"
1820 PRINT "          GREATER THAN THE INLET OR OUTLET RADIATOR"
1830 PRINT "          WALL TEMPERATURE."
1840 PRINT
1850 PRINT "> The Effective Sink Temperature =" TS "K"
1860 INPUT "DO YOU WANT TO CONTINUE PROGRAM (0=NO:1=YES) ";ANSWER
1870 PRINT
1880 IF ANSWER=0 GOTO 2500
1890 IF ANSWER=1 GOTO 480
1900 RETURN
1910 '
1920 '          RADIATOR AVERAGE WALL TEMPERATURE
1930 '
1940 NUM=TWI-TWO+(E*SBC/HR)*(TWI^4-TWO^4)
1950 DEN1=(1/HR)*LOG((TWI^4-TS^4)/(TWO^4-TS^4))
1960 DEN2=LOG(((TWI-TS)*(TWO+TS))/((TWO-TS)*(TWI+TS)))
1970 DEN3=2*(ATN(TWI/TS)-ATN(TWO/TS))
1980 DEN=E*SBC*(DEN1+(1/(4*E*SBC*TS^3))*(DEN2-DEN3))
1990 TWAV=((NUM/DEN)+TS^4)^.25
2000 RETURN
2010 '
2020 '          PRIME RADIATOR AREA
2030 '
2040 AREA=Q/(E*SBC*(TWAV^4-TS^4))
2050 SQRAREA = SQR(AREA/2)
2060 '   CONVERT TO FEET
2070 SQRARFT = SQRAREA*3.28084
2080 RETURN
2090 '
2100 '          PROGRAM OUTPUT
2110 '
2120 BEEP:FOR XXX=1 TO 2000:NEXT XXX:BEEP:FOR XXX=1 TO 2000:NEXT XXX:BEEP
2130 CLS
2140 PRINT "*****          PROGRAM OUTPUT          *****"
2150 PRINT
2160 PRINT
2170 PRINT ">COOLING FLUID USED IN THIS ANALYSIS : " COOL$
2180 PRINT
2190 PRINT
2200 PRINT ">OPERATING CONDITIONS OF LCUV : " OPER$
2210 PRINT
2220 PRINT
2230 PRINT "          PROPERTIES OF THE FLUID USED FOR COOLING"
2240 PRINT
2250 PRINT ">MASS FLOW RATE =" W "KG/SEC"
2260 PRINT ">SPECIFIC HEAT =" CP "KJ/(KG)(K)"
2270 PRINT ">DYNAMIC VISCOSITY =" VIS "(N)(SEC)/SQ METERS"
2280 PRINT ">REYNOLDS NUMBER =" RE
2290 PRINT ">PRANTL NUMBER =" PR
2300 PRINT ">THERMAL CONDUCTIVITY =" K "KW/(METERS)(K)"
2310 PRINT ">CONVECTIVE HEAT TRANSFER COEFFICIENT =" HR "KW(SQ METERS)(K)"

```

```
2320 PRINT ">TEMPERATURE OF COOLING FLUID AT RADIATOR INLET =" TFI "K"
2330 PRINT ">TEMPERATURE OF COOLING FLUID AT RADIATOR OUTLET =" TFO "K"
2340 PRINT
2350 PRINT
2360 PRINT "                PROPERTIES OF THE RADIATOR "
2370 PRINT
2380 PRINT ">TOTAL HEAT REJECTION RATE =" Q "KW"
2390 PRINT ">SOLAR ABSORPTANCE =" A
2400 PRINT ">EMITTANCE =" E
2410 PRINT ">LUNAR SURFACE TEMPERATURE =" TM "K"
2420 PRINT ">EFFECTIVE SINK TEMPERATURE =" TS "K"
2430 PRINT ">INLET RADIATOR WALL TEMPERATURE =" TWI "K"
2440 PRINT ">OUTLET RADIATOR WALL TEMPERATURE =" TWO "K"
2450 PRINT ">RADIATOR AVERAGE WALL TEMPERATURE =" TWAV "K"
2460 PRINT ">PRIME RADIATOR AREA =" AREA "SQ METERS"
2470 PRINT ">TWO ACTIVE SIDES, each ";SQRAREA "by";SQRAREA "METER"
2480 PRINT ">TWO ACTIVE SIDES, each ";SQRARFT "by";SQRARFT "FEET"
2490 RETURN
2500 END
```